CHEMICAL REVIEWS

REVIEW

pubs.acs.org/CR

Catalytic NO_x Abatement Systems for Mobile Sources: From Three-Way to Lean Burn after-Treatment Technologies

Pascal Granger*[,†] and Vasile I. Parvulescu*[,‡]

[†]Unité de Catalyse et de Chimie du Solide, UMR CNRS 8181, University of Lille 1, 59655 Villeneuve d'Ascq, France

[‡]Department of Organic Chemistry, Biochemistry and Catalysis, University of Bucharest, Romania, 4 − 12 Regina Elisabeta Boulevard, Bucharest 030016, Romania

CONTENTS

Received: June 1, 2010
Published: March 18, 2011

1. GENERAL CONTEXT

Up to now heterogeneous catalytic processes for environmental issues have probably been the most efficient solution because of their high efficiency and selectivity toward the removal of undesired side products, such as atmospheric pollutants from automotive exhaust gas. Several sets of standards have already been defined in the past two decades for different types of vehicles.[1] Tier 1 standards were published in 1991 in the U.S. and progressively phased-in between 1994 and 1997. Then, Tier 2 standards were adopted in 1999 with a phase-in implementation schedule from 2004 to 2009. Tier 1 standards were applied to light-duty vehicles, while Tier 2 regulation introduced more stringent numerical emission limits relative to the previous Tier 1 requirements, and a number of additional changes were made that are more stringent for larger vehicles.[2] Similar emission limits were adopted for all vehicles regardless of the fuel consumption including gasoline, diesel, or alternative fuels. The sulfur levels in gasoline were required to be reduced by 30 ppm with an 80 ppm sulfur cap in 2006. Diesel fuel of maximum sulfur level of 15 ppm was made available for highway use beginning in 2006. Tier 4 standards designed for the period of 2008−2015 require that emissions of particulate matter and NO_x be further reduced by about 90%. Sulfur was recommended to be reduced to 15 ppm (ultralow sulfur diesel) as of June 2010 for nonroad fuel and in June 2012 for locomotive and marine fuels. Such emission reductions can be achieved only through the use of control technologies—including advanced exhaust gas after-treatment systems, catalytic particulate filters, and NO_x adsorbers.[3] As shown in Table 1, progress in European standard regulations also highlights more stringent emission limits especially for NO_x emissions within the Euro 6 standard regulations.

Actually, the performances of commercial catalytic post-treatment systems are not optimized to fulfill the forthcoming U.S. standard legislation and those that will be implemented in Europe near 2014, particularly the low limit of NO_x emissions from diesel engines. The lean-burn engine is actually the most attractive solution combining low consumption and low CO_2 emission, recognized for its greenhouse gas behavior. There are also apparent advantages in Europe that might explain a continuous expansion of the diesel car market related to the implementation of a favorable tax system. However, the suitability of this technology, from an environmental point of view implies the minimization of atmospheric pollutants, particularly nitric oxide emissions, which actually represent a serious drawback with no practical solution commercially available. Hence, while CO and unburned hydrocarbons can be easily removed, the simultaneous abatement of NO_x and particulates from diesel exhaust gas represents an outstanding issue. The current three-way technology used near stoichiometric conditions is unable to meet upcoming regulations in Europe, United States, and Japan. The existing technical solutions (see Figure 1) involving an exhaust gas recirculation to get an optimal NO_x/particulates compromise[4] by controlling the recirculated gas rate or modifying the distribution channel will likely be unable to fulfill the next Euro 6 standard regulation. As illustrated in Figure 2, the implementation of an optimal strategy is not an easy task because a reduction of NO_x induces an increase in particulate emission (point A in Figure 2) and reversibly subsequent reduction of particulate matter will induce an increase in NO_x emission (point B in Figure 2). Consequently such a situation implies to reconsider the actual end-of-pipe technologies commercially available combining diesel particulate filter (DPF) and DeNO$_x$ catalysts.

Commercial NO_x abatement technologies are actually available. They are essentially developed for heavy-duty vehicles such as the urea selective catalytic reduction (SCR). On the other hand, a more confusing context characterizes light vehicles with a competition between SCR and NO_x storage and reduction after-treatment systems. Both technologies suffer from strong kinetic and thermodynamic limitations, which make a suitable solution difficult. In addition, the main challenge is the reduction of the catalyst volume and the automatic control of urea injection in the particular case of urea SCR systems. In this complex technological context, the development of noble-metal free catalysts represents an important breakthrough that stimulates car and catalyst manufacturers to develop new conceptual ideas and original systems capable of fulfilling future requirements.

A wide number of reviews have already been written on the subject in the past two decades[6−15] dealing with various macroscopic aspects related to previous achievements in three-way catalysis, future challenges, and prospects to find out novel catalytic formulations for diesel engines. Microscopic aspects have also been reviewed separately concerning reaction mechanisms and possible intermediates stabilized in various operating conditions. Most of those reviews offer the state of the art with an overview of the catalyst formulations currently classified in three varieties: (i) supported noble metals, (ii) oxides, mixed oxides, and (iii) zeoliths. Obviously, no significant breaktrough has been put forward regarding the catalyst

Table 1. Evolution of Standard Regulation of Atmospheric Pollutants from Mobile Sources in the European Community

	gasoline engine				diesel engine			
standard regulation[a]	CO	HC	NO_x	HC + NO_x	CO	NO_x	HC + NO_x	particulates
Euro 1 (1993)	2.72			0.97	2.72		0.97	0.14
Euro 2 (1996)	2.20			0.5	1.00		0.90	0.10
Euro 3 (2000)	2.30	0.20	0.15		0.64	0.50	0.56	0.05
Euro 4 (2005)	1.00	0.10	0.08		0.50	0.25	0.30	0.025
Euro 5 (2009)	1.00	0.10	0.06		0.50	0.18	0.25	0.005
Euro 6 (2014)	1.00	0.10	0.06		0.50	0.08	0.17	0.005

[a] Measured from New European Driving Cycle (g/km).

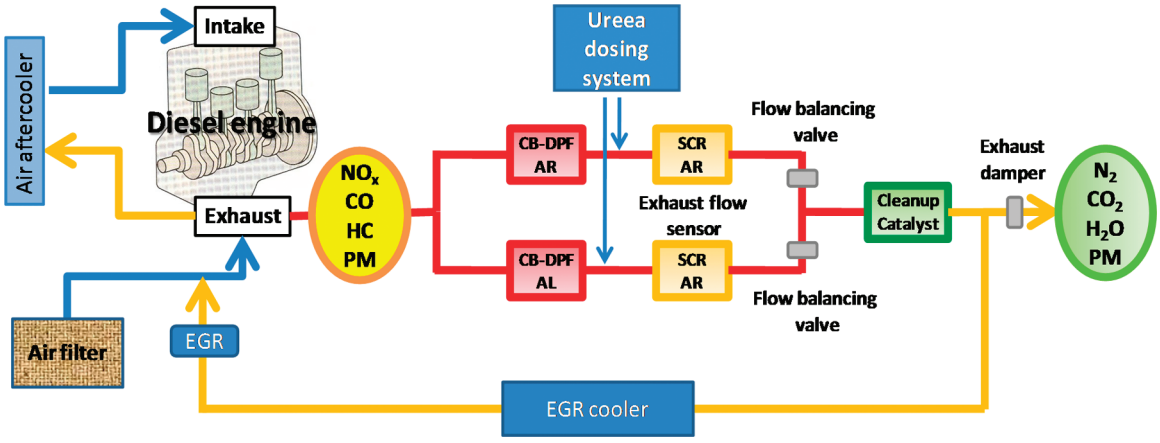

Figure 1. System integrating exhaust gas recirculation.

design for gasoline and diesel powered vehicles since the emergence of three-way catalysts. By way of illustration, NO_x storage reduction catalysts consist of three-way catalysts modified by barium addition.[16] The most significant improvements essentially concern the implementation of advance catalysts to convert efficiently atmospheric pollutants during the cold start engines, high thermal stability and durability up to 160 000 km, and high oxygen storage properties for gasoline engines. Despite huge efforts being dedicated to lean-DeNO_x systems, it is obvious that we are still far from the above-mentioned requirements. Unfortunately, such a situation persists at the dawn of the emergence of more restrictive standards for NO_x emissions. This statement could be a provocation for the academic community and catalyst manufacturers. Unfortunately, it is worthwhile to note that catalyst formulations for advanced NO_x storage reduction systems mimic those of conventional three-way catalysts. Even though we can claim that further improvements will imply an integrated approach involving significant feedback to engine design and control, it seems also obvious that the catalyst plays a key role in the core of this technology. Presently the development of novel catalytic materials specifically designed for the various functions needed for NO_x removal might be considered as an important point. By way of illustration, the precursor work earlier proposed by Djega-Mariadassou et al.[15] dealing with the requirement of three functions as described in Figure 3 for DeNO_x only represents a starting point, which suggests at least two main questions: which optimal interaction between active elements is needed to get significant enhancements in NO_x conversion and how can we get such an interaction by developing alternative catalyst synthesis routes? Probably, this strategy needs a better understanding of the catalyst working under realistic conditions via the development of *operando* spectroscopic studies.

In this sense, the main objective of this review is to deliver the state of the art in the field of DeNO_x catalysis, which could help academia and industry to discover new guidelines to favor the emergence of original conceptual ideas and systems in order to fulfill future requirements. This review resumes important results reported on three-way and lean-burn DeNO_x catalysts, demonstrating the added value of surface science and molecular modeling investigations. Some illustrations emphasize the fact that these comparisons may help in determining the nature of the catalytic active sites and building predictive tools for simulations under running conditions. Non-steady-state investigations and the implementation of powerful *in situ* spectroscopic techniques is of fundamental interest for kinetic modeling and could provide molecular information that could drive improvements in the performances of the existing technologies or development of alternative systems running under lean-burn conditions.

2. THREE-WAY CATALYSTS AND RELATED SYSTEMS

2.1. Role of the Composition and the Preparation Methods

The implementation of exhaust gas after-treatment systems provided remarkable results in the past three decades in terms of atmospheric pollutant abatement under complex running conditions due to the occurrence of transient regimes and the need

dx.doi.org/10.1021/cr100168g |*Chem. Rev.* 2011, 111, 3155–3207

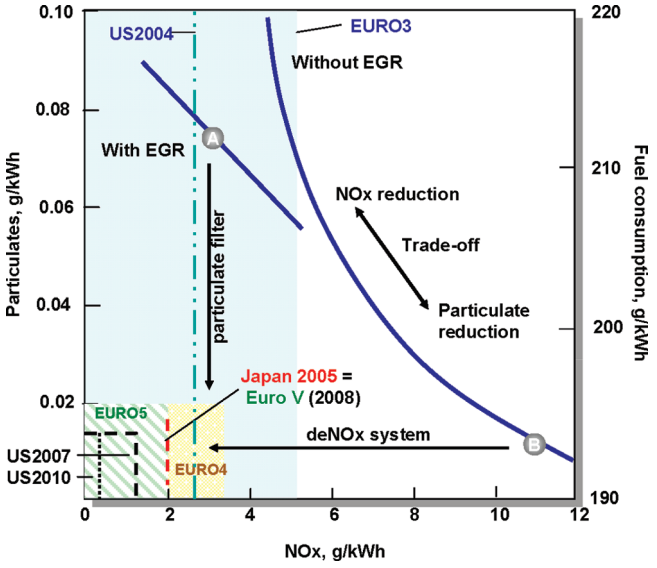

Figure 2. General trend of the NO_x and particulate emissions in Europe, Japan, and U.S. for light- and medium-duty engines (ESC test cycle) and effect of engine tuning on NO_x/particulate emissions and fuel consumption. Reprinted with permission from ref 5. Copyright 2007 Elsevier B.V.

to achieve a complete conversion. Probably, the adoption of three-way converters corresponded to a first breakthrough among the conventional technological solutions available. As illustrated in Figure 4, they usually operate under oscillating conditions induced by the feedback lambda control maintaining the air-to-fuel (A/F) ratio near the stoichiometry. Accordingly, conversions higher than 95% for CO, unburned hydrocarbons (HC), and NO_x can be obtained.[10]

TWC composition is currently optimized to promote the following competitive oxidation and reduction reactions for NO_x, CO, and unburned hydrocarbon abatement.

Oxidation

$$CO + \frac{1}{2}\,O_2 \rightarrow CO_2 \quad (1)$$

$$C_xH_y + (x + y/4)O_2 \rightarrow xCO_2 + \frac{y}{2}H_2O \quad (2)$$

Reduction

$$NO + H_2 \rightarrow \frac{1}{2}N_2 + H_2O \quad (3)$$

$$NO + CO \rightarrow \frac{1}{2}N_2 + CO_2 \quad (4)$$

$$(2x + y/2)NO + C_xH_y \rightarrow (x + y/4)N_2 + xCO_2 + \frac{y}{2}H_2O \quad (5)$$

The combination of Pt and Rh ensures a quasi-complete removal of NO_x, CO, and HC.[13,16−18] There is also a growing interest in partly replacing Pt with less-expensive Pd.[19] However it is important that those noble metals occupy a particular position in the monolith to operate properly, which requires the development of advanced impregnation techniques in order to avoid alloying effect during three-way operating conditions.[20] By way of illustration, it is usual that Pd forms alloyed particles with Rh inducing a loss of the intrinsic properties of Pd and Rh in

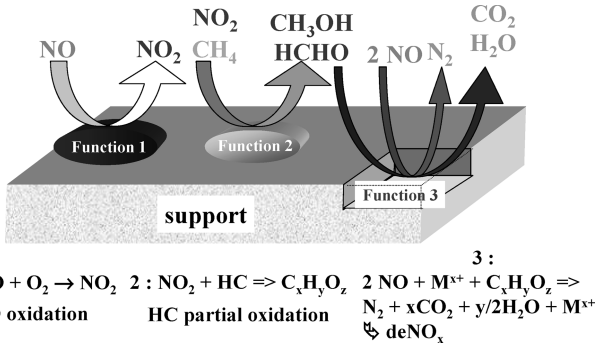

Figure 3. The three-way function model for designing $DeNO_x$ catalysts in the presence of methane as reductant. Reprinted with permission from ref 15. Copyright 2007 Elsevier B.V.

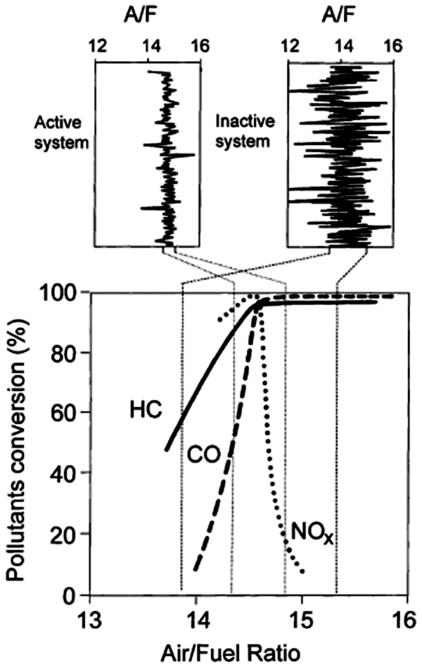

Figure 4. Influence of the A/F ratio on the catalytic efficiency of three-way catalysts. Reprinted with permission from ref 10. Copyright 2003 Elsevier B.V.

the reaction involved in three-way conditions.[21] Typically, noble metals are well-dispersed after impregnation of highly porous alumina wash-coat (20−40 μm) on ceramic honeycomb structures or monoliths. Particular attention is paid to textural properties of the alumina support in order to minimize heat and mass transfer limitations. The wash-coat is essentially composed of alumina with specific surface areas in the range 100−200 $m^2\,g^{-1}$, which represents approximately 5−15 wt % of the monolith. Due to exposure to high temperature up to 1273 K in full load operation, subsequent incorporation of lanthana and barium additives is needed, acting as stabilizers to prevent the formation of α-Al_2O_3 exhibiting maximum specific area of approximately 10 $m^2\,g^{-1}$.[22,23] It was found that the thermal resistance depends on the mode of incorporation according to sol−gel or coprecipitation procedure.[18] Subsequent improvements essentially concerned oxygen storage capacity (OSC) in order to enlarge the

dx.doi.org/10.1021/cr100168g |*Chem. Rev.* 2011, 111, 3155–3207

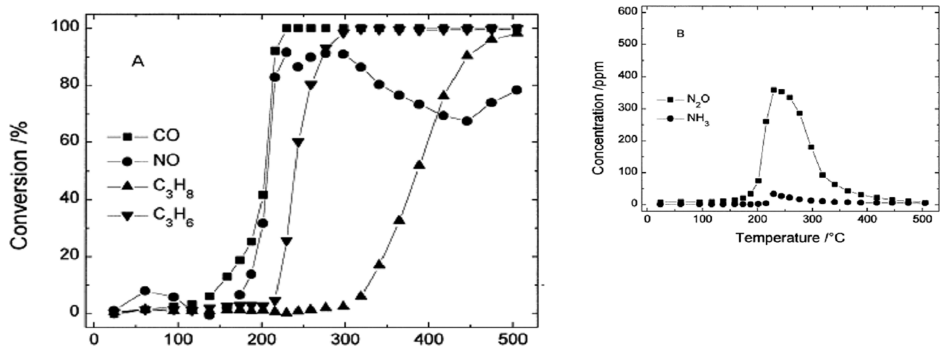

Figure 5. Light-off curves for the reaction of the standard mixtures (R = 0.98, 5000 ppm H_2O) over Rh/Al_2O_3: (A) conversions of CO, NO, C_3H_6, and C_3H_8; (B) production of N_2O and NH_3. Reprinted with permission from ref 29. Copyright 1998 Elsevier B.V.

operating window near the stoichiometry to convert simultaneously NO_x, CO, and unburned hydrocarbons.[24−28] The development of ceria−zirconia mixed oxides led to significant improvements of the OSC performance and ensure a quasi-complete conversion of NO to N_2 in three-way conditions. Those mixed oxides also enhance the efficiency of noble metals at low temperature particularly during the cold start engine. In such conditions, the low conversion level on unpromoted Rh-based catalysts is usually accompanied with a significant production of nitrous oxide (N_2O) as illustrated in Figure 5.[29]

2.1.1. Importance of the Support Properties in TWC. Bulk cerium oxide is known to provide excellent refractory oxide support for platinum group metals other than rhodium and enables the attainment of highly dispersed small crystallites of platinum on the ceria particles and that the bulk ceria may be stabilized by impregnation with a solution of an aluminum compound followed by calcinations.[30,31] The nature of the platinum precursor is also very important to provide an active catalyst.[32]

Cerium oxide improves the performance of these catalysts by discharging or storing oxygen and by controlling the oxidation of CO and HC and the reduction of NO_x. Reaction 6 occurs on the surface of cerium oxide particles:

$$CeO_2 \leftrightarrows CeO_{2-x} + (x/2)O_2 \qquad (6)$$

Direct relationship between the reducibility and the specific surface area suggested that OSC properties are restricted to the surface on ceria.[33] At elevated temperature (ca 1073 K), the total surface area is reduced by the growth of the cerium oxide particles, which deteriorates the oxygen storage capacity. The incorporation of lanthanides diminishes this detrimental effect due to the formation of mixed oxides characterized by the formula $Ce_{1-x}La_xO_{2-(x/2)}$ (with $0.3 \leq x \leq 0.5$).[34] Several combinations have been further proposed as effective supports for noble metals. By way of illustration, mixed powders of zirconium oxide with alumina−magnesia spinel and cerium oxide were successfully developed.[35] Alternative solutions involving the impregnation of CeO_2 mixed with ZrO_2 with 10 wt % Fe_2O_3 and physical mixtures composed of the respective cerium, zirconium, and iron oxides were also proposed.[36] Subsequent strontium incorporation was found to improve the properties of those combinations.[37] Other poison-resistant supports are based on metal−zirconium phosphate components to prevent the formation of sulfates.[38]

As described in Table 2, the development of ceria−zirconia mixed oxides led to significant improvements of OSC performance and specific surface area in comparison with CeO_2. Correlatively, it was found that a greater stabilization of the noble metal dispersion could be obtained in three-way conditions leading to promotional effects in the water−gas-shift reaction and CO removal by oxidation.

Further studies demonstrated that several rare earth oxides can be used as promoters of ceria−zirconia. Praseodymium, neodymium or yttrium can be added to the ceria−zirconia composite to modify the resultant oxide properties.[39,40] Many of the reported patents suggested the utility of alkaline earth metals in combination with ceria and zirconia. This is stated to enhance the catalysts stability after exposure for a long period of time to high temperatures (1173−1373 K).

It is obvious that significant improvements in TWC were essentially obtained on the chemical composition of the support materials. On the other hand, one has to mention that most of the attempts to replace rhodium failed. Subsequent replacement of platinum by palladium did not lead to commercial application due to a lower sulfur tolerance. In fact, while TWC technology is nowadays consolidated, further developments for improving catalyst composition by reducing the noble metal content or developing noble metal-free catalysts is still a challenging issue that is of interest for academia and industry. Indeed, recent developments of compressed natural gas engines emphasize the development of efficient after-treatment systems for the simultaneous removal of NO_x and methane at low temperature but also for lean-burn applications since noble metals exhibit a poor selectivity in the presence of an excess of oxygen. The low efficiency of TWC during the cold start engine also represents an important issue. Additional parameters have to be taken into account to model automotive post-treatment systems under realistic conditions. As exemplified in Figure 6, under typical three-way conditions, mass transport phenomena taking place above the light-off temperature overlap the kinetic limitations.

Santos and Costa[41] concluded that in the absence of internal mass transfer phenomena, the efficiency of TWC conversion would be strongly enhanced. As observed in Figure 6, TWC operates in a mixed regime with internal and external mass transfer.[41] Despite internal mass transfer seeming to be more important to control the conversion, the current generation of TWCs are designed on the basis external mass transport characteristics, which suggests that a large unexploited domain should be considered in the future regarding the development mesoporous material stable at high temperature. It is obvious that those developments would improve the resistance to internal mass transfer phenomena under typical three-way operating conditions. Up to

dx.doi.org/10.1021/cr100168g |*Chem. Rev.* 2011, 111, 3155–3207

Table 2. OSC Values of Ceria and $Ce_xZr_{1-x}O_2$ Oxides[a]

			O storage		OSC μmol O		
catalyst	tox (K)	BET area ($m^2\ g^{-1}$)	red.	°C	g^{-1}	m^{-2}	ref
CeO_2	1173 (6 h)	22	CO	400	71	3.2	Cuif et al.[25]
$Ce_{0.6}Zr_{0.4}O_2$	1173 (6 h)	52	CO	400	232	4.5	Cuif et al.[25]
CeO_2 NP[b]	1173 (4 h)	13	CO	400	64	4.9	Rossignol et al.[26]
$Ce_{0.9}Zr_{0.1}O_2$ NP[b]	1173 (4 h)	18	CO	400	125	6.9	Rossignol et al.[26]
$Ce_{0.9}Zr_{0.1}O_2$ SG[c]	1173 (4 h)	43	CO	400	252	5.9	Rossignol et al.[26]
$Ce_{0.75}Zr_{0.25}O_2$ SG[c]	1173 (4 h)	32	CO	400	217	6.8	Rossignol et al.[26]
Pt/CeO_2	773 (1 h)	49	CO	600	250	5.1	Kacimi et al.[27]
$Pt/Ce_{0.75}Zr_{0.25}O_2$	773 (1 h)	72	CO	600	723	10	Kacimi et al.[27]

[a] Data reported in the literature. [b] Prepared by nitrate precipitation. [c] Sol−gel technique (Zr propoxide).

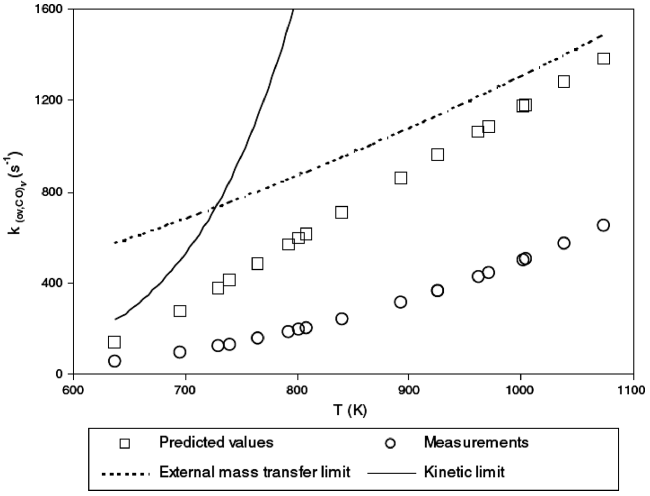

Figure 6. Predicted values of $k_{(ov,CO)_v}$ versus the operating temperature in the TWC with no internal mass transfer limitation. Reprinted with permission from ref 41. Copyright 2008 Elsevier B.V.

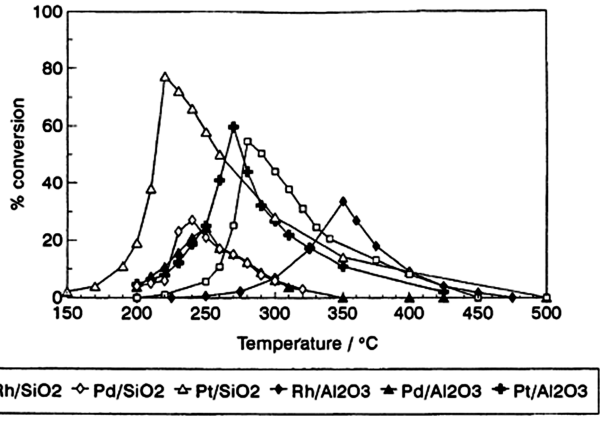

Figure 7. Reduction of NO by propene under lean conditions vs temperature on monometallic Pt, Rh, and Pd based catalysts supported on SiO_2 and Al_2O_3 (500 ppm NO, 1000 ppm C_3H_6, and 5% O_2, space velocity 60 000 h^{-1}). Reprinted with permission from ref 43. Copyright 1995 Elsevier B.V.

now, several attempts using mesoporous silica templates led to highly ordered mesoporous cerium oxides, composed of nanocrystalline pores walls exhibiting high thermal stability.[26] More recently, Li et al.[42] reported the synthesis of ceria−zirconia solid solutions exhibiting unique physicochemical properties associated with the coexistence of three-dimensionally ordered macroporous and mesoporous walls that could be potential candidates for three-way applications. It is obvious that those previous findings might be considered as a starting point to improve the performances of automotive exhaust catalysts particularly under lean conditions with the use of unburned heavy hydrocarbons. However, the thermal stability of those materials has not been demonstrated under wet atmosphere.

2.1.2. Noble Metal Substitution and Related Systems under Lean Conditions. NO_x reduction to nitrogen strongly attenuates over noble metals under lean conditions[43] with a narrower conversion range as illustrated in Figure 7. In addition, the loss of NO conversion is usually correlated to an increase in N_2O production which might be considered as a serious drawback with the forthcoming regulation integrating the reduction of greenhouse gas emissions.

A high-throughput approach, aided by multiobjective design of experiments based on a genetic algorithm, was reported to optimize the combinations and concentrations of a noble metal-free catalyst active in the selective reduction of NO with C_3H_6.[44] Using adequate variation operators and constraint handling techniques the investigation checked a multiobjective approach to test the ability not only to find the best catalyst formulation but also to find multiple best catalysts with respect to several goals. One of the important questions addressed by these studies was whether binary combinations can provide enough active catalysts or the use of multicomponent systems is required. The experimental design was composed of 11 elements in different combinations and concentrations that can be classified into three groups: (i) elements acting as support, (ii) the main elements with likely a major contribution to the catalytic efficiency, and (iii) elements acting as promoter. Al was chosen as element for the support, Cu, Ni, Co, Fe, Mn, La, Ce, and Sm were chosen as active elements, and K and Sr were chosen as promoters. The best noble metal free catalysts found by this method are combinations of Cu or Ni with Al. Other active catalysts at low temperature included Co and Fe. Several catalysts based on transition metals (Cu, Co, Fe) and different supports (ZSM-5, activated carbon, Al_2O_3) have been tested in the selective catalytic reduction of NO_x with propene in the presence of an excess of oxygen, simulating lean-burn conditions from diesel

dx.doi.org/10.1021/cr100168g |Chem. Rev. 2011, 111, 3155–3207

engines.[45] The efficiency order with respect to the metal was Cu ~ Fe > Co with ZSM-5-based catalysts having superior behavior over Al_2O_3. The application of activated carbon as a support is not practical due to its degradation in the course of the reaction. The selectivity for N_2 was independent of the support, being higher than 95%. Various kinds of metal oxide supported Cu catalysts have been thoroughly investigated in the HC-SCR such as Cu/SiO_2,[46] Cu/Al_2O_3,[47] and Cu/ZrO_2.[48] However, the deactivating effect of SO_2 on the selective catalytic reduction over CuO/Al_2O_3 catalysts has been reported and assigned to the formation of ammonium and copper sulfates.[49,50] Cerium oxide was also suggested as catalyst support to enhance NO_x removal using copper.[51] The development of zeolite-based catalysts represents an important issue and led to significant improvements in terms of activity and selectivity. However, the stabilization of the active phase seems to be a very challenging task particularly under wet atmosphere. The introduction of iron in zeolites through $FeCl_3$ sublimation was also reported to yield highly active catalysts but with different stability depending on the reductant and on the presence of H_2O and SO_2.[52−54] Interestingly, it has also been shown that high concentrations of water vapor during decane-SCR-NO do not significantly change the conversion of NO to N_2 over Fe/MFI catalysts.[55] While Fe/MFI is more active in oxidation of NO to NO_2 at low temperature, Cu-MFI is significantly more active in the decane-SCR-NO. Although Cu/MFI exhibits a significant reversible deactivation in NO oxidation, the decane-SCR-NO performance is surprisingly enhanced in the presence of water.[56] Co(II,III)/MFI prepared by a precipitation method with NaOCl in alkaline solution exhibits high activity for N_2 at 250 °C in comparison with Co(II)/MFI.[57] The formation of CO does not occur over Co/MFI, which makes these different from the Fe/MFI catalysts. In fact, it was demonstrated that the different synthesis conditions for MFI and the different locations of Co^{2+} on MFI have a strong impact on the catalyst properties for the selective catalytic reduction of NO by alkanes in the presence of excess oxygen.[58] A low degree of Co^{2+} exchange corresponds to higher TOF for NO reduction than that of materials having a higher degree of Co^{2+} exchange indicating that at least two types of Co^{2+} sites coexist in the Co^{2+}-exchanged MFI. The exchange degree and the location of Co^{2+} depend on the alkalinity of the hydrothermal synthesis and on the sodium content of the resulting Co^{2+}-exchanged MFI.

Significant changes observed in the catalytic behavior of Co-MOR powders and monoliths depend essentially on the hydrocarbon nature (carbon number) and the concentration of water in the feed.[59] In the presence of methane, a low concentration of water (2%) decreases the NO to N_2 conversion. On the other hand, the maximum NO conversion increases for both the Co-MOR powder and monolith when butane is used as reducing agent. In fact, the nature of adsorbates changes according the nature of the reducting agent. In the presence of methane, water has a detrimental effect due to stronger adsorption than NO. On the contrary, a beneficial effect of water is discernible when butane is used, because water enhances the removal of surface carbon deposits. The formation of Co_3O_4 was detected in all deactivated powder and monolithic catalysts and resulted from the cobalt ion migration promoted in wet atmosphere.[60]

The stabilization of Co-mordenite catalysts through lanthanum exchange was recently reviewed.[61] The presence of exchanged lanthanum was reported to preserve the integrity of the zeolite structure preventing the migration of cobalt ions with the subsequent formation of cobalt oxide. These CoLa-mordenite catalysts are not affected by the severe hydrothermal treatment showing no sign of Co or La migration out of the exchange positions. The stabilization effect of the active species in zeolite-based catalysts by the lanthanide exchanged ions has also been reported by using samarium and cerium.[62] Despite a huge number of investigations at the laboratory scale for improving the thermal stability of noble metal free catalysts and their sulfur tolerance, it is obvious that no practical solution has arisen yet able to compete efficiently with noble metals except urea-SCR catalyst for heavy duty vehicles.

2.2. Extrapolation of Surface Science Studies to Polycrystalline Catalysts for Single Reactions: Elucidation of Active Sites

A wide number of surface science experiments under ultrahigh vacuum were performed on model catalysts helping to determine the nature of elementary steps involved in postcombustion catalysis. Despite relevant information being obtained on the nature of those elementary steps, it seems obvious that the well-known pressure gap, the involvement of surface reconstruction processes, and the effective role of the support must be taken into account to build up reliable kinetic models capable of simulating the functioning mode of three-way catalysts under transient conditions. In light of the information provided by these investigations, the most relevant observations are probably related to the establishment of useful correlations between kinetic measurements on single crystals and polycrystalline catalysts. Hence, surface science experiments largely contributed to the elucidation of reaction mechanisms, the identification of limiting steps, and the structure sensitivity of reactions involving noble metals. Useful guidelines to design future efficient supported catalysts based on the fact that each plan is characterized by its own intrinsic efficiency can be derived from such experiments.

Preliminary experiments of the NO/CO reaction were essentially focused on Rh surfaces showing that NO readily dissociates at room temperature (RT) on stepped surfaces but strongly chemisorbed or subsurface oxygen desorbing at high temperature might considerably alter their adsorptive properties.[63] On the other hand, NO and CO adsorb molecularly at 300 K on Pt(100), (110), and (111)[64,65] but not on Pt(410)[66] exhibiting unusual behavior predicted by the model proposed by Banholzer et al.[67] for NO decomposition on Pt, which takes into account the symmetry of the orbitals available for the reaction based on the Woodward−Hoffmann rules. The model assumes a complicated structure composed of several atoms with an optimal arrangement to produce a set of surface orbitals that are conducive to the reaction. If such conditions are fulfilled, then NO can dissociate. Gohdrone et al.[68] who also investigated the behavior of Pt(410) and (210) surfaces found that Pt(410) is much more active than (210) surface toward NO dissociation despite Pt(210) exhibiting a higher step density and identical step geometry. Such a comparison emphasizes the fact that the active site is not an individual atom but probably involves more complicated arrangements as postulated in Banholzer's model. Practical applications associated with the development of Pd-only TWCs also stimulated investigations of NO chemisorption on Pd(100), (110), and (111) by auger electron spectroscopy (AES) and ultraviolet and X-ray photoelectron spectroscopy (UPS, XPS) between 300 and 1100 K. Similar tendencies as

those reported on Pt and Rh surfaces characterize Pd surfaces highlighting a structure-sensitive NO dissociation with the observation of partial dissociation on Pd(100), while molecular adsorption takes place on (110) and (111) surfaces. Subsequent O diffusion in the bulk also occurs with back-diffusion taking place at high temperature, above 700 K.

2.2.1. Model vs Polycrystalline Supported Noble Metal Catalysts. Interesting comparisons have been earlier reported on Rh(100), Rh(111), and Rh/Al_2O_3[69,70] for modeling the CO/O_2 and the CO/NO reactions. Basically, the former reaction accounts for a classical Langmuir−Hinshelwood mechanism rather than an Eley−Rideal one in which mobile adsorbed CO species react with immobile oxygen atoms. Molecular O_2 adsorption was previously characterized at 100 K on Rh(111) as a precursor to dissociative adsorption of oxygen.[71] Generally speaking, the following set of elementary steps is usually considered, where * stands for a free adsorption site:

$$CO + * \leftrightarrows CO_{ads} \quad (7)$$

$$O_2 + 2* \rightarrow 2O_{ads} \quad (8)$$

$$CO_{ads} + O_{ads} \rightarrow CO_2 + 2* \quad (9)$$

However, it is worthwhile to note that better agreement was found between calculated and experimental rates by considering the rate of O_2 adsorption proportional to the fraction of vacant sites, θ_v, rather than θ_v^2 according to the above-mentioned sequence, which suggested that the rate-controlling step involves the initial interaction between molecular O_2 on a single Rh site with subsequent dissociation occurring much more readily.[72] Trends such as these were more recently verified on bimetallic $Pt-Rh/Al_2O_3$ with apparent order with respect of O_2 close to 1 emphasizing the fact that a bimolecular reaction between chemisorbed O_2 and CO molecules or O_2 adsorption was the rate-limiting step.[73] Returning to the comparison between Rh(111) and Rh/Al_2O_3, excellent agreement was obtained showing the weak sensibility to the structure of the CO/O_2 reaction in the temperature range 475−515 K under stoichiometric conditions (with $P_{CO} = P_{O_2} = 0.01$ atm). The authors accounted for a linear CO dependency of the activation energy of CO desorption in their model prediction, which can be related to repulsive interactions between chemisorbed CO molecules. Let us mention that those operating conditions were selected to avoid the formation of surface oxide on Rh(111), which would complicate the kinetics. Kinetic oxidation on Pd, Pt, and Ir catalysts shown that a negative order dependence on O_2 partial pressure is obtained under highy oxidizing conditions highlighting the presence of strongly bound oxygen species similar to surface oxide formed by deliberate oxidation.[74] The surface oxidation did not change the activation energy but mainly acts as a simple site blocking effect. Interestingly, those authors also evidenced a negative order dependence on Pt despite that it could not be oxidized under reaction conditions. Now regarding the CO/NO reaction, a strong structure sensitivity was observed contrarily to the CO/O_2 reaction highlighting drastic changes in the kinetic behavior of single and polycristalline catalysts modeled on the basis of the following reaction sequence:

$$CO + * \leftrightarrows CO_{ads} \quad (10)$$

$$NO + * \leftrightarrows NO_{ads} \quad (11)$$

$$NO_{ads} + * \rightarrow N_{ads} + O_{ads} \quad (12)$$

$$NO_{ads} + N_{ads} \rightarrow N_2 + O_{ads} \quad (13)$$

$$2N_{ads} \rightarrow N_2 + * \quad (14)$$

$$CO_{ads} + O_{ads} \rightarrow CO_2 + 2* \quad (15)$$

Two different pathways were initially identified for the formation of nitrogen[69] corresponding to the recombination of two adjacent chemisorbed N atoms and a surface reaction involving chemisorbed NO and N species according to step 13. Recent investigations reported interesting kinetic features from adsorption and reaction of NO on clean and CO-precovered Ir(111).[75] Two NO adsorption states corresponding to fcc-hollow sites and atop sites were characterized. NO adsorbed on hollow sites dissociates above 283 K with subsequent recombination of N_{ads} atoms producing nitrogen above 574 K and a disproportionation reaction, which proceeds between atop-NO and N_{ads} at 471 K. CO was found to inhibit NO adsorption on atop sites, while NO adsorption is not altered on hollow sites, which emphasizes the fact that surface heterogeinity on polycrystalline catalysts plays a key role in determining the kinetic behavior. Oh et al.[69] did not report the formation of N_2O on Rh. The model predicted a surface quasi-completely saturated by N_{ads} at 675 K accounting for N_2 desorption being altered by the presence of repulsive interactions between N_{ads} and CO_{ads} further lowering the activation energy of nitrogen desorption. On the basis of this observation, nitrogen desorption was suggested to be the rate-limiting step. Belton et al.[76] also found that the coadsorption of O and N atoms also favors subsequent N_2 desorption, which has been modeled by an oxygen coverage dependency of the activation energy of N_2 desorption. A strong additional effect due to lateral repulsion has also been observed from molecular beam experiments examining the thermal decomposition on Rh(111).[77] Finally, Belton et al.[76] also demonstrated that the associative desorption of two adjacent N atoms is not inherently rate-limiting because the isolated $N_{ads} + N_{ads}$ reaction on Rh(111) occurs 50 times faster than that measured under reaction conditions. Molecular beam experiments of NO adsorption and dissociation on various Pd cluster sizes (2.8−45 nm) deposited on MgO(100) revealed a comparable behavior to that observed on Rh.[78] It was found that NO physisorbed on the support can diffuse and then chemisorb on Pd. The equilibrium coverage was found to be higher on small particles than on larger ones. The dissociation of NO leads to a quasi-complete production of nitrogen with no detectable N_2O formation. Interestingly, the authors concluded that desorption of strongly N bound adatoms could be the main limiting step rather than the dissociation step of NO, but such an explanation could be debatable according to previous findings on Rh.[77] Those authors also provide interesting arguments for further extrapolations in case of supported polycrystalline catalysts showing that in their operating conditions between 423 and 673 K at low pressure ($10^{-9}-10^{-6}$ Torr), the turnover number is not an appropriate parameter to determine the intrinsic activity depending on the particle size and the particle shape. They found that medium sized particles having preferentially (111) facets are more active than the biggest particles exhibiting (100) facets.

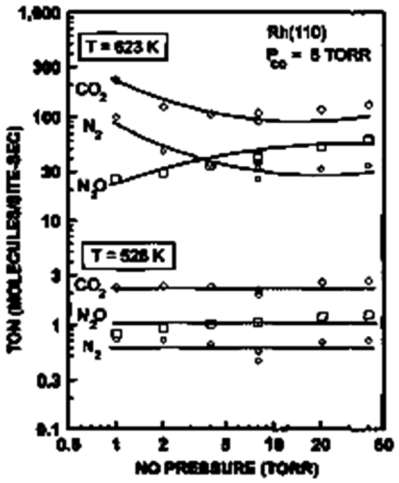

Figure 8. The CO_2, N_2O, and N_2 TONs as a function of NO pressure with a fixed CO pressure of 8 Torr at 623 and 528 K over Rh(110). Reprinted with permission from ref 83. Copyright 1995 Elsevier B.V.

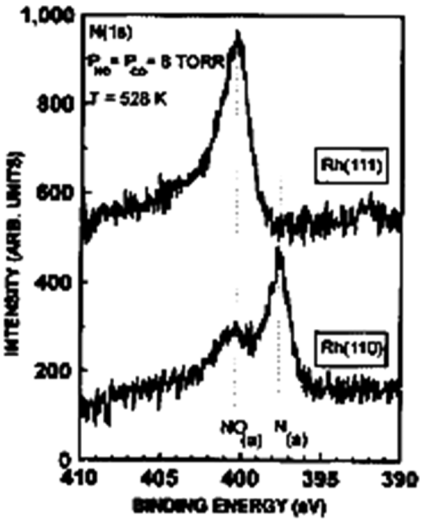

Figure 9. N 1s XPS spectra obtained after NO−CO reaction at 500 K in 8 Torr of each reactant. The crystals were cooled in the gas mixture after reaction, products were analyzed by GC, and the gas mixture was pumped out of the reactor prior to introduction into the UHV surface analysis chamber. Reprinted with permission from ref 83. Copyright 1995 Elevier B.V.

It is obvious that UHV experiments brought new insight into the nature of elementary steps for the NO/CO reaction.[79] Simulation of the kinetics on the basis of Monte Carlo approaches offered the advantage that lateral repulsive interactions can be considered in the calculation of activation energies. From those experiments, it was found that NO displaced chemisorbed CO molecules, which implies that the dissociation of NO is not significantly hindered by CO on Rh(100). At low coverage (<0.3 ML), NO is totally converted to N_2, whereas NO coadsorbed with atomic O and N atoms strongly inhibits the dissociation. A result such as this is of interest because it offers some guidelines to model kinetic measurements at high pressure in particular to select elementary steps that would likely occur for the production of nitrogen.[64,66,80−82] Conversely, Pt exhibits a different behavior essentially because CO adsorbs more strongly and displaces NO on Pt(111) and (110).[82] Formally, these observations clearly suggest that the beneficial behavior of Rh characterized in stoichiometric or rich conditions will probably disappear under lean conditions with subsequent changes in the adsorptive properties of Rh due to surface oxide formation that might alter competitive adsorptions and the CO/NO reaction. These arguments would emphasize the fact that structural properties have to be optimized for enhancing the structure sensitive NO/CO reaction and preventing the parallel CO/O_2 reaction under lean conditions. Interestingly, kinetic measurements on Rh(110) and Rh(111) provide evidence of this structure sensitivity and the influence of the partial pressure and temperature conditions on the catalytic properties summarized in Figures 8 and 9.[83,84] It was found that Rh(111) only produces N_2O contrary to previous observations from electron beam experiments under UHV with surface N coverage varying in the range 0.05−0.5. Those experiments suggested an additional step corresponding to a reaction between NO_{ads} and N_{ads} leading to the formation of nitrous oxide in agreement with further observations on Ir(111):[76]

$$NO_{ads} + N_{ads} \rightarrow N_2O + 2* \qquad (16)$$

These authors modeled thermo-programmed NO desorption based on the following set of assumptions: (i) the requirements of two types of vacant sites, atop and hollow sites; (ii) a linear surface NO coverage dependency of the activation energy of NO dissociation, which emphasizes the fact that NO dissociation strongly depends on the adsorption/desorption equilibrium, that is, on the value of the equilibrium adsorption constant. Simulations showed a strong NO inhibiting effect with NO dissociation rates 500 lower than that calculated at low coverage. As illustrated in Figure 8, kinetic measurements performed on Rh(110) and (111) at different temperatures, 528 and 623 K, and high pressure in the range 1−100 Torr[84] provide interesting information because at low temperature (T < 600 K), the selectivity for the production of N_2O is insensitive to the partial pressure of NO whereas at high temperature (T > 600 K) it becomes dependent on the pressure conditions as illustrated in Figure 8. Previous explanations based on the involvement of a common "N_2O"-like intermediate for the simultaneous production of N_2 and N_2O[76,85] have not been considered. The authors explained this selectivity behavior based on the fact that NO dissociation as rate-limiting step is strongly inhibited at low temperature corresponding to surface saturated by NO_{ads}. Hence, the adsorption/desorption equilibrium has been ascribed as the primary determining factor on the selectivity. Further, increase in temperature favors a partial NO desorption thus liberating free vacant sites for NO dissociation. Such tendencies can be quantitatively rationalized on the basis of steps 13 and 14 for the production of N_2 and step 16 for the formation of N_2O. Changes in selectivity for the production of N_2O vs the partial pressure of NO can be quantitatively explained by eqs 17 and 18:

$$\frac{r_{N_2}}{r_{N_2O}} = \frac{k_{14}}{k_{16}}\frac{\theta_N}{\theta_{NO}} + \frac{k_{13}}{k_{16}} \qquad (17)$$

Subsequent calculation of θ_N/θ_{NO} from steady-state approximation leads to eq 18.

$$\frac{4r_{N_2}}{r_{N_2O}} = \left(1 + \frac{k_{13}}{k_{16}}\right)\sqrt{1 + \frac{8k_{12}k_{14}}{(k_{13}+k_{16})^2 K_{NO}P_{NO}}} + \frac{3k_{13}}{k_{16}} - 1 \qquad (18)$$

Examination of eq 18 reveals that for high K_{NO} values the relative rate of nitrogen will become independent of NO partial

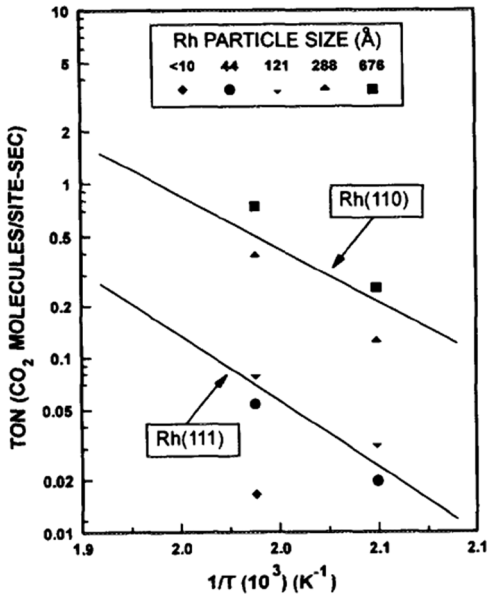

Figure 10. A comparison of CO_2 TONs from the CO−NO reaction over Rh(110), Rh(111), and several Rh/Al_2O_3 supported catalysts with varying particle sizes. Reprinted with permission from ref 83. Copyright 1995 Elsevier B.V.

pressures, Rh sites will be essentially covered by NO_{ads}, and the probability of finding two adjacent chemisorbed N atoms becomes very low (experiments at 528 K in Figure 8). On the other hand, the reverse tendency will take place when K_{NO} becomes very low, that is, when the temperature increases accompanied with subsequent NO desorption. Such a situation leads to a significant increase in θ_N.[85−87] Subsequent XPS observations illustrated in Figure 9 also reveal that NO dissociates more readily on Rh(110) than on Rh(111) with a greater contribution of the N 1s photopeak near 397 eV for the former single crystal.

The influence of alkali on the dissociation of NO over noble metals represented an important issue in order to promote the dissociation of NO and subsequently its selectivity toward the formation of nitrogen. Previous catalytic experiments at "high pressure" revealed a beneficial effect on the catalysts' selectivity for the production of N_2. Subsequent experiments on model surfaces under UHV conditions revealed an increase of the total amount of dissociated products correlated to lower activation energy for NO dissociation and presumably a higher rate constant. Interestingly, Whitman and Ho[81] demonstrated on preadsorbed Rh(100) surface a significant reduction of the activation energy of NO dissociation in the presence of 0.17 ML at 100 K but correlatively a decrease in the rate constant due to a large concomitant decrease in the pre-exponential factor.

In some particular cases, comparative kinetic and spectroscopic measurements at atmospheric pressure and UHV conditions were useful to rule out hypotheses related to the involvement of isocyanate species as a possible intermediate for the production of nitrogen. In fact, such species are unstable on noble metals above 573 K.[88,89] As a general conclusion, there is some evidence that single crystals can mimic the kinetic behavior of supported polycrystalline catalysts. However, there are also some differences, which have been earlier discussed.[83] Subsequent comparisons are sometimes not easy because turnover number values are not frequently reported for supported catalysts. Additionally, kinetics measurements are usually performed in different reactors (batch for UHV experiments and fixed bed flow reactor). Nevertheless, Peden et al.[83] draw interesting extrapolations with respect to previous experiments on low and highly loaded supported Rh based catalysts.[90−92] Comparable behavior between highly loaded silica Rh based catalysts and Rh(111) suggests that large Rh particles would be mainly populated by Rh(111). In contrast, small particles would be essentially modeled by (110) surface even if more complex surface structure usually characterizes small particles.

Subsequent comparisons in Figure 10 differ from the abovementioned expectation because large particles (>20 nm) exhibit a (110)-like behavior whereas supported catalysts having intermediate particle size behave like a (111) surface. Of course, surface reconstructions under reactive conditions might partly explain such changes on supported catalysts. Nevertheless, as mentioned earlier, this tendency has to be compared with previous investigations on Pd/MgO(100) showing that turnover number might not be an appropriate parameter to determine the intrinsic activity depending on the particle size and the morphology of the metallic particles.

2.2.2. Surface Characterization of Polycrystalline Catalysts on Reducible Surfaces and Related Catalytic Performances. Significant developments were achieved when noble metals have been dispersed on support materials inducing stronger interactions than on conventional alumina and silica supports. Such interactions may change the particle morphology,[93,94] the oxidation state of the noble metal,[95] the metal dispersion,[96] and the electronic properties of noble metal through electron transfer with reduced Ce species.[97] Different approaches were implemented to characterize the microstructures formed when noble metals interact with ceria. Comparative HRTEM observations and computer simulation led to the conclusion that Rh microcrystals can be depicted according to truncated cuboctahedron morphology as seen in Figure 11. The same authors also characterized epititaxially orientated-Rh(111) planes with respect to (111) ceria planes.[98]

Golunski et al.[100] investigated surface modifications induced by ceria modification on Pt/CeO_2 and rationalized their observations in terms of strong metal support interaction (SMSI) effect accompanied with a partial migration over the surface of platinum particles. The most important consequences are related to a partial blocking of conventional metallic Pt sites and the creation of new sites involving the participation of oxygen vacancies on the ceria surface. Interestingly, such structural modifications at the surface are reversible under oxidative atmosphere associated with the coalescence of ceria and the restoration of Pt particles.

All those modifications have an impact on the catalytic properties generally associated with further improvement of oxygen storage properties[101] and correlatively an enhancement of the rates of the CO/NO and CO/O_2 reactions.[91,102−107] The influence of the surrounding atmosphere is well-known to play a key role. Typically structural changes occur under cycling conditions with reductive/oxidative atmospheres. They affect the metal/support interface and related catalytic performances as explained. By way of illustration, NO adsorption and dissociation were investigated on Rh supported over ceria films exhibiting variable Ce^{3+}/Ce^{4+} ratio by thermal desorption and soft X-ray photoemission spectroscopy of Rh 3d photopeaks.[80] Through these experiments, an enhancement in NO dissociation related to an increase of the Ce^{3+}/Ce^{4+} ratio has been evidenced.

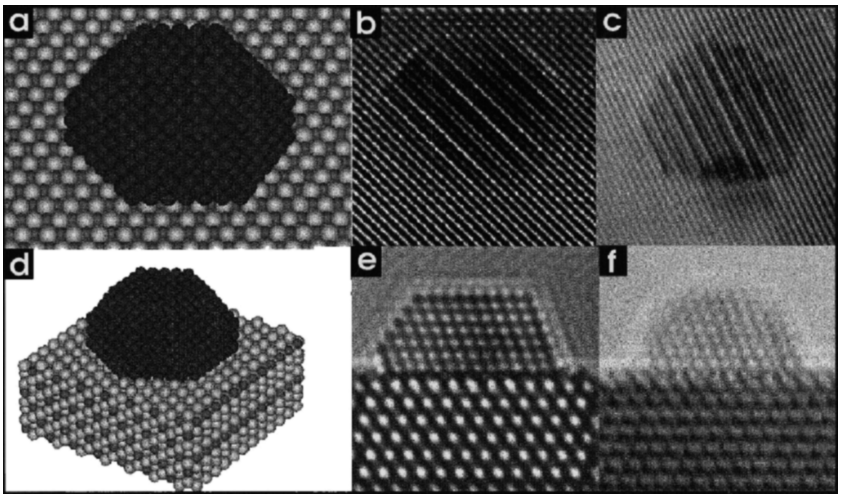

Figure 11. Comparison between experimental (c, f) and computer simulated (b, e) HRTEM images for Rh/CeO_2 in planar (c, d) and profile (f, e) views. The supercell structural model used as the input for the computer calculations is shown in panels a (Rh zone axis [100]) and d (Rh zone axis 99). Reprinted with permission from ref 96. Copyright 1998 Elsevier B.V.

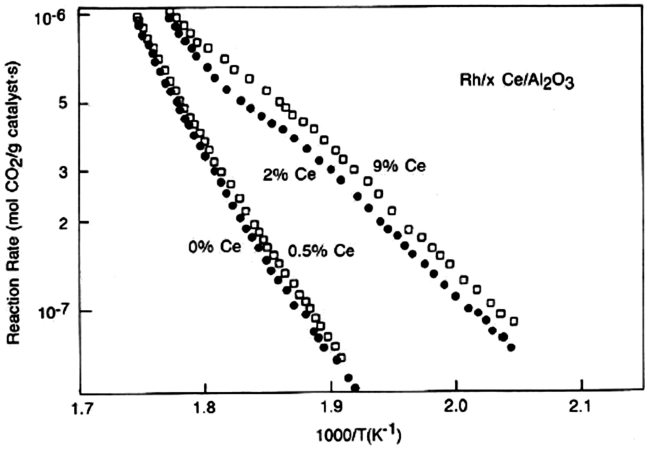

Figure 12. Arrhenius plots for CO_2 production rates over 0.014 wt % Rh/Al_2O_3 containing variable levels of Ce in a reactant mixture containing 1 vol % CO and 0.5 vol % NO. Reprinted with permission from ref 91. Copyright 1990 Elsevier B.V.

Preliminary temperature-programmed NO desorption is consistent with this finding showing an enhancement in nitrogen production at the expense of N_2O.[108] The authors also concluded that ceria slow the usual oxygen inhibiting effect on the rate of NO conversion due to spillover from noble metals to reduced ceria. Regarding the relative impact of ceria on the kinetics of the CO/NO reaction, the most important features are mainly related to the suppression of the N_2O formation, a decrease in the apparent activation energy well-illustrated in Figure 12, and a shift to a positive order dependence of the rate of NO reduction essentially at low temperature.[100,108]

Electronic modifications of noble metals have also been characterized by ESR and infrared spectroscopy, which underlined a higher reactivity of surface oxygen vacancies at the ceria−RhO_x boundary than on pure CeO_2 and a parallel stabilization of Rh^{2+}.[94] As explained for the CO/O_2 reaction on $Pd/CeO_x/Al_2O_3$, the presence of Pd^0 sites is needed to activate CO through electron transfer into the antibonding $2\pi^*$ orbital and then weakening the C−O bond.[102] Electronic requirements would be greatly facilitated in the presence of ceria. Generally speaking the usual beneficial effect of ceria can be explained by considering the same elementary steps previously proposed over noble metals considering that the presence of ceria would drastically change the relative rates of the elementary steps involved in the CO/O_2 and CO/NO reactions. Alternately, different reaction sequences can be proposed that account for the formation of new active sites involving the cooperation of noble metals and anionic vacancies from ceria.[91,105−107]

2.3. New Achievements in Catalyst Synthesis and Related Structural and Catalytic Characterizations

2.3.1. Changes in Structural Properties under Three-Way Conditions. As mentioned the individual adsorptive properties of noble metals can be profitably used for the simultaneous removal of NO, CO, and unburned hydrocarbons especially during the warm-up period.[109] Typically the presence of Rh is needed for the reduction of NO_x, whereas the catalytic properties of Pt and Pd are useful to oxidize CO and HC. However, there is also some evidence for the formation of bimetallic Pt−Rh particles in freshly prepared and engine-aged catalysts, which might create significant modifications in the kinetic properties.[20,109,110] For instance, Ng et al.[85] who investigated the CO/NO reaction on $Pt_{10}Rh_{90}$ (111) surface found that Pt and Rh would preserve their individual adsorptive properties. They interpreted the loss of performance compared with Rh(111) to a dilution effect of Pt. However, they did not completely rule out possible electronic modifications. Significant variations in the surface composition of $Pt_{10}Rh_{90}$ (111) were also reported after annealing at 1273 K with surface Rh enrichment as Rh_2O_3 under oxidizing conditions.[111] Sometimes the formation of alloyed particles is reported in the case of bimetallic catalysts, which has been associated with a beneficial effect on the catalyst properties, particularly those of Rh in the conversion of NO_x, CO, and HC.[112,113] Particular attention was paid in the past to the effect of thermal aging on the catalytic properties of Rh.[112,114,115] It is obvious that a detrimental effect is usually observed ascribed to extensive oxidation into orthorhombic Rh_2O_3 and subsequent diffusion of Rh^{3+} into the bulk alumina

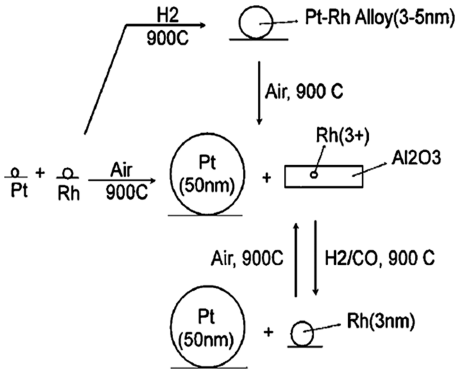

Figure 13. Structural transformation of Pt−Rh catalysts according to various thermal treatments. Reprinted with permission from ref 112. Copyright 1998 Elsevier B.V.

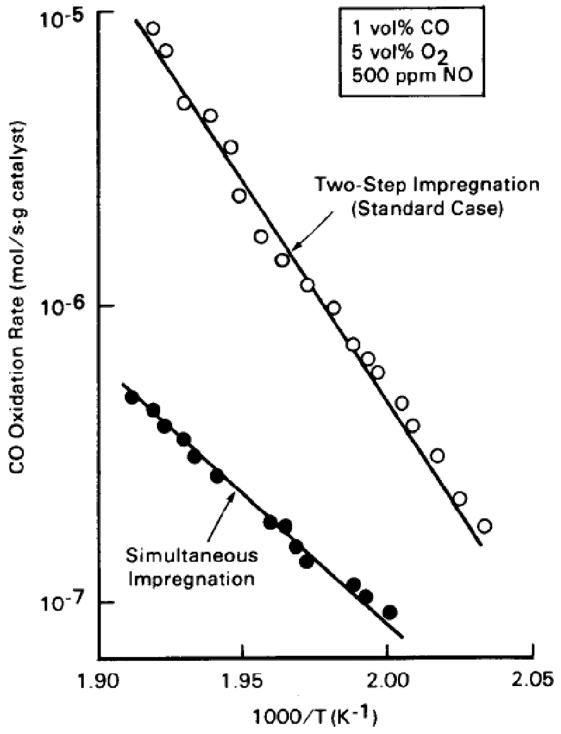

Figure 14. Arrhenius plot for CO oxidation over the fresh bimetallic catalysts prepared by stepwise and simultaneous impregnations. Reprinted with permission from ref 117. Copyright 1986 Elsevier B.V.

support producing nonreducible Rh aluminate species.[116] Hu et al.[112] reported interesting trends on structural transformation occurring during thermal aging under simulated and real exhaust conditions on a monolithic catalyst with a Pt−Rh catalyst, which consisted of a physical mixture of Pt/Al_2O_3 and Rh/Al_2O_3. Structural changes observed in reductive or oxidative conditions are illustrated in Figure 13.

In fact, they found that Rh is the main active component responsible of the catalyst activity. While a significant detrimental effect is observed on Rh/Al_2O_3 inherent to the formation of Rh aluminate species, it seems obvious that the presence of Pt considerably limits this phenomena keeping Rh as metallic particles. Tentative experiments with Pt and Rh incorporated on the same substrate according to a two-step impregnation procedure led to significant enhancement in the CO/O_2 reaction with a residual activity higher than that simply resulting from the combination of the intrinsic properties of the individual noble metals (Figure 14).[117] According to the experimental procedure, the authors explained this rate enhancement on the basis of a statistical mixture of Pt and Rh sites that exist on the support as separate entities. Generally Pt catalysts are inhibited by a strong CO adsorption, which suppresses subsequent O_2 adsorption. It will no longer be the case in a bimetallic catalyst with the occurrence of noncompetitive adsorptions with preferential CO adsorption on Pt whereas oxygen adsorbs on Rh. However, these authors did not rule out the possibility that Pt preserves the metallic character of Rh as postulated by Hu et al.[112] Simultaneous impregnation leads to different surface properties with lower activity related to the formation of surface Rh enriched bimetallic catalyst with relative inactive Rh_2O_3.

Advanced synthesis methods were developed to bring the two metals in bimetallic catalysts in close contact. They involved surface redox reaction using preadsorbed hydrogen on a parent monometallic catalyst, which reduces the second metal. This procedure has been successfully developed for the preparation of $Pt−Rh/Al_2O_3−CeO_2$.[118−120] Let us mention that kinetic and thermodynamic limitations have to be considered to get optimal interaction between Pt and Rh particularly on $Pt/Al_2O_3−CeO_2$ because of surface reduction of ceria during the prereductive pretreatment.

2.3.2. Surface Characterization. Among the physicochemical techniques implemented for surface characterization of the topmost surface of three-way catalysts, the use of FTIR spectroscopy is widespread particularly to investigate the adsorption of CO as probe molecule. From those studies, a number of correlations were tentatively achieved with microcalorimetric and theoretical studies.[121−123] Also thermal aging of $Pt−Rh/Al_2O_3$ was found to induce significant changes in the topmost surface of bimetallic Pt−Rh catalysts with a significant surface Rh enrichment. Surface modifications were correlated to change in kinetic behavior in connection with a drastic decrease in the low coordination site number and a loss of the metallic character of rhodium.[124] Interestingly, subsequent correlations between spectroscopic and kinetic data found for the first time that the experimental adsorption constant of NO and CO can reflect changes in surface Rh composition in Pt−Rh based catalysts.

On the basis of those previous infrared observations showing drastic changes in spectral features of CO and NO adsorption on Rh and Pt, FTIR spectroscopy was used to characterize the surface composition of commercial and reference bimetallic $1Pt−02Rh/CeO_2−Al_2O_3$ based on successive NO and CO adsorptions.[125] Interestingly, this methodology led to different conclusions regarding the impact of thermal aging previously reported on $Pt−Rh/Al_2O_3$ because the presence of Rh is practically undetected after thermal aging at 1273 K under N_2 + 10% H_2O, while the surface composition of freshly prepared catalyst reflects the bulk composition on the fresh catalyst. This means that oxygen storage materials strongly influence surface reconstructions, which occur under simulated conditions. Generally speaking, the generalization of classical methods involving CO adsorption are currently criticized because of the huge capacity of ceria-based support materials to store CO. Methods using low-energy ion scattering (LEIS) for determining the cluster size of $Pt/Rh/CeO_2/\gamma\text{-}Al_2O_3$ have been profitably used. The potential of this technique seems to be related to an increase

Table 3. Calculated Enthalpies (ΔH) and Activation Barriers (ΔE) in kJ mol^{-1} for Various Elementary Steps Suggested in the NO/H_2 Reaction on Pt(111) and Pd(111)

	Pt(111)		Pd(111)	
elementary step	ΔH	ΔE	ΔH	ΔE
$NO_g + * \rightarrow NO_{ads}$	−109	0	−134	0
$H_{2g} + 2* \rightarrow 2H_{ads}$	−75	13	−84	9
$O_{2g} + 2* \rightarrow 2O_{ads}$	−213	0	−232	0
$NO_{ads} + * \rightarrow N_{ads} + O_{ads}$	−100	53	−143	38
$NO_{ads} + H_{ads} \rightarrow N_{ads} + OH_{ads}$	−78	22	−114	7
$NO_{ads} + H_{ads} \rightarrow NH_{ads} + O_{ads}$	32	96	1	89
$2N_{ads} \rightarrow N_{2g} + 2*$	25	111	142	179
$NO_{ads} + N_{ads} \rightarrow N_{2g} + O_{ads} + *$	−75	7	−1	53
$NO_{ads} + N_{ads} \rightarrow N_2O_g + 2*$	113	113	197	197
$NO_{ads} + N_{ads} \rightarrow N_2O_{ads} + *$	72	81	142	142
$N_2O_{ads} \rightarrow N_2O_g + *$	41	41	55	55
$N_2O_{ads} \rightarrow N_{2g} + O_{ads}$	−132.3	0	−287.4	0
$NO_{ads} + NH_{ads} \rightarrow N_{2g} + OH_{ads}$	−185	0	−116	0
$NO_{ads} + NH_{ads} \rightarrow N_2O_g + H_{ads}$	−19	30	52	74
$N_{ads} + H_{ads} \rightarrow NH_{ads} + *$	132	150	143	159
$N_{ads} + H_{2ads} \rightarrow NH_{ads} + H_{ads}$	83	110	88	118
$NH_{ads} + H_{ads} \rightarrow NH_{2\ ads} + *$	−41	48	−25	61
$NH_{2ads} + H_{ads} \rightarrow NH_3 + 2*$	−7	23	36	44
$O_{ads} + H_{ads} \rightarrow OH_{ads} + *$	22	85	29	91
$OH_{ads} + H_{ads} \rightarrow H_2O_g + 2*$	−77	0	−66	0
$O_{ads} + H_{2ads} \rightarrow OH_{ads} + H_{ads}$	−26	139	−27	137

of the accuracy for very small clusters while microscopic methods need a minimum cluster size.[126]

3. A MOLECULAR APPROACH TO DETERMINE THE DESIGN OF ACTIVE SITES?

3.1. Theoretical Approach: Phenomenological Vs Theoretical Calculation

Combined experimental and theoretical approaches provide useful information that might help to get a better representation of the architecture of the active sites, particularly in the case of bimetallic particles where different configurations can be envisioned from alloyed to segregated active elements on inert supports. In fact, two different bordeline cases can be considered with active elements keeping unchanged their electronic properties, that is, their adsorptive properties, or conversely, the occurrence of charge transfer which may drastically alter the electronic density of noble metal atoms leading to synergy effects on the catalytic properties.[86,124,127−130] A concept has been previously explored when cheaper transition metals are incorporated with noble metals.[127,129] The real impact of additives is explained by either structural or electronic effects. In this sense, theoretical calculations might provide additional arguments to build up decisive conclusions. It is obvious that theoretical investigations were initially essentially focused on single crystals. Before the development of DFT calculations in the particular case of $DeNO_x$ reactions, different approaches were examined. The bond order conservation−Morse potential and its generalization as the unity bond index−quadratic exponential potential (UBI−QEP), previously developed by Shustorovich et al.[130−132] was a precursor mathematical model, which provides in a straightforward manner the heat of adsorption for molecular and radical species and the activation barrier for elementary reactions. Calculations on close-packed Pt(111) and Pd(111) surfaces were achieved by examining different scenarios concerning the dissociation step of NO as exemplified in Table 3. It is well-accepted that NO dissociates on a nearest-neighbor vacant site. This hypothesis has been widely considered but could be questionable in the case of the NO/H_2 reaction because in that case chemisorbed H atoms would assist the dissociation of NO according to step ($NO_{ads} + H_{ads} \rightarrow N_{ads} + OH_{ads}$).[133−135] Earlier investigations regarding the kinetics of the NO/H_2 reactions did not consider this elementary step,[136] except Hecker and Bell[137] who suggested this hypothesis on polycrystalline Rh-based catalysts. Recently, investigations on supported Pt and Pd polycrystalline catalysts showed a better agreement taking into account the effective role of hydrogen in the dissociation of NO. As a matter of fact, those trends open the discussion on the possible involvement of adsorbed NOH species. Up to now theoretical treatment has not extensively considered such an assumption even though the issue might have some repercussions particularly for explaining the beneficial effect of hydrogen on silver-based catalysts for the reduction of NO_x by hydrocarbons. By way of illustration, Backman et al.[138] suggested on silver catalysts a fast elementary step inducing a bimolecular reaction between two adsorbed NOH molecules leading to the production of nitrogen. Probably, the use of hydrogen will represent in the near future a growing interest in the particular case of NO_x storage/reduction systems with a possible injection of reformate during rich exposure to ensure a complete restoration of the NO_x trap efficiency but also to produce ammonia subsequently converted according to a dual system coupling a NSR system with an ammonia SCR catalyst.[139]

Clearly, the development of the DFT calculation provided new insight into the nature of elementary steps involved in $DeNO_x$ reactions. Particular attention was paid to the structure sensitivity of NO dissociation over noble metals.[140] A wide number of investigations dealt with NO adsorption on Rh and Pd, for instance, to solve controversial assignments from infrared spectroscopic observations regarding NO adsorption on Pd sites.[141] Calculations on Rh(100), (110), and (111) lead to the conclusion that both electronic and geometrical effects alter the dissociation of NO, but geometrical effects were found to exceed the electronic ones. NO dissociation is currently assumed as the rate-limiting step and can explain the highest intrinsic activity of Rh in comparison with Pt and Pd. As above-mentioned, surface science investigations concluded that the presence of defect sites, typically steps and kinks corresponding to higher intrinsic activities, is currently associated with lower activation barriers. However, earlier investigations demonstrated that electronic effects might greatly influence the catalytic properties in the reduction of NO by CO. By way of illustration, Renouprez et al.[129] provided a significant example on Pd−Mn/SiO_2 catalysts because they found an increase of activity for alloyed Pd/Mn particles, while Mn occupied low coordination sites decreasing the number of Pt atoms located on edges and corners. Similar synergy effects were found on Pd−Mo/Al_2O_3 and, interestingly, the conclusion drawn by these authors also accounted for two possible explanations taking into account either the specific behavior of electronically modified Pd sites or the peculiar role played by MnO_x or MoO_x. Hence, Schmal et al.[128] explained the enhancement observed on the selective conversion of NO to N_2 by the creation of new active sites where Pd and Mo would participate. They suggest a reaction sequence involving CO adsorption on Pd^0 that would promote the reduction of Mo^{6+} to $Mo^{\delta+}$, while NO would induce the

dx.doi.org/10.1021/cr100168g |Chem. Rev. 2011, 111, 3155–3207

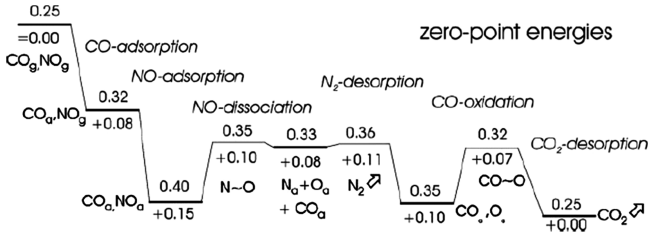

Figure 15. Relevant zero-point energies (in eV) during the reaction. Values below the profile are wrt to gas-phase molecules NO and CO. Reprinted with permission from ref 144. Copyright 2001 Elsevier B.V.

reoxidation of $Mo^{\delta+}$. On the basis of the extended Hückel theory on Pd(111), Pd(100), and Pd_3Mn alloy, a charge transfer from Mn to Pd was demonstrated that takes into account four nearest neighbor Mn atoms.[142] Subsequent calculations also showed that NO dissociation on Pd corresponds to a large barrier of 1.9 eV, whereas a lower value of 1.0 eV characterizes Pd_3Mn.[142] In this latter case, lying down NO molecules would be the precursor state of NO dissociation. The potential of DFT calculation is certainly related to the precise characterization of the transition states, which allow the determination of reaction pathways. Clearly such an approach has been profitably used for $DeNO_x$ reactions over noble metals. Comparative calculations showed that the structure sensitivity can be correlated to the rate constant of NO dissociation, the geometry of the dissociation precursor state and the stability of the final dissociated state on various Pd and Rh surfaces. For instance, Tian et al.[140] found that Rh(111) is less active than (110) and (100) surfaces because of a higher activation barrier correlated to a vertical precursor state and a weakly stable final product. Comparative DFT calculations on Rh and Pd surfaces demonstrated a beneficial effect on stepped Rh and Pd(511) surfaces formed with (100) terrace and (111) step facets. It was found that the optimal pathway for NO dissociation implies the step of the Pd(511) surface in agreement with experimental studies.[143] The very small rate constants lead to the conclusion that NO does not dissociate at 300 K irrespective of the surface structure. Different trends characterize Rh because the rate constant is strongly lowered on the steps of the (511) surface in comparison with (100), but the high rate constant value on the Rh surface is fully compatible with a dissociative adsorption of NO on Rh whereas the associative one predominates on Pd. DFT calculations might also provide evidence to discriminate different mechanism proposals as earlier suggested in the literature. Previous steady state rate measurements on supported Pt shown that a bimolecular reaction between chemisorbed NO and CO for yielding nitrogen disagrees with rate measurements, the most likely step being the dissociation of NO on a nearest neighbor vacant site.[84] Subsequent rate calculations assumed that this step is rate-determining. Eichler and Hafner[144] calculated activation barrier in all subprocesses taking place on Pt(100) during the NO/CO reaction leading ultimately to the production of N_2 and CO_2. They found a mixed NO/CO island rather than two separate islands. Nevertheless, they demonstrated that a bimolecular $NO_{ads} + CO_{ads}$ leads to a barrier much higher than that obtained for the dissociation of chemisorbed NO on a vacant site under the assumption that one of the neighboring CO molecules desorbs. The energy profile in Figure 15 vs reaction coordinates clearly indicates that once formed weakly bound N_2 and CO_2 at the surface desorb.

Now regarding the role of additive, the incorporation of alkali metals represents an important issue particularly for developing the selective conversion of NO at low temperature during the cold start engine. Unfortunately, it seems difficult to rationalize the real effect of alkali on the catalytic properties of noble metals because the usual methods by co-impregnation implemented for alkali incorporation to noble metals do not lead to optimal interactions and do not allow any control of such interactions.

Interestingly Machida and Watanabe[145] observed a promotional effect in NO conversion to nitrogen despite Na incorporation inducing a loss of metal dispersion. They ascribed this rate enhancement to a possible stabilization of nitrite species as intermediates. SSITKA of the NO/H_2 reaction also revealed a beneficial effect correlated to an increasing concentration of N_2 precursor.[146] Hence, preferential interactions with Na surrounding Pt sites would favor charge transfer from K to Pt.[147] It is well accepted that alkali metals alter the electronic properties of noble metals[148] having some consequences on their intrinsic adsorptive properties and their ability to dissociate chemisorbed NO molecules. Nevertheless, such a picture does not offer a detailed description on the real impact of K at a molecular level. In this sense, DFT calculation is able to provide robust arguments supporting IRAS and TPD of NO on Pd(111), Pd(100) showing molecular and reversible adsorption of NO, while NO decomposition prevails on stepped Pd(311) and K-modified Pd(111) surfaces emphasizing the beneficial effect of K on the dissociation of NO.[149,150] From these previous observations, no conclusion was drawn to explain the distinct effect of steps and K. DFT calculations showed a stronger NO adsorption with a lower NO stretching frequency for a tilted atop species as a dissociation precursor. Interestingly the adsorption energy of that species stabilized on a K-doped surface becomes similar to that calculated on Pd(311).[151]

3.2. *In situ* and *Operando* Investigations of $DeNO_x$ Reactions: From Qualitative to Quantitative Information

The development of *in situ* or *operando* spectroscopic investigations probably represents a significant advance in heterogeneous catalysis for a better elucidation of the reaction intermediates and the design of active sites because those ones probably only exist during the catalysis.[152−154] Catalytic reactors were previously mostly considered as a black box and *ex situ* analysis allowed tentative correlations leading sometimes to conflicting kinetic models particularly in $DeNO_x$ catalysis. This type of experiment also offers alternative explanations to those provided by surface science investigations typically performed on single crystals under UHV. As previously exemplified, these conditions provide significant information on the nature of the elementary step particularly over noble metals to explain the structure sensitivity of NO dissociation. However, such experiments fail to describe the kinetics under realistic operating conditions far from UHV conditions unable to mimic surface reconstructions and deactivation effects. Hence, it is nowadays possible to gain new insight into atomic scale on the functioning mode of heterogeneous catalysis and to develop rational strategies in catalyst synthesis to optimize the interactions between the active elements. It is also obvious that the contribution of DFT theory combined with such *operando* spectroscopic approaches strengthen the relevance of the microkinetic formalism. Practically, *operando* investigations consist of correlating physicochemical characterization in the course of the reaction and simultaneous activity and selectivity data. Strictly speaking, it is possible to evaluate the impact of surface reconstructions to changes in catalytic properties, which allows more relevant structure/activity relationships. Probably one of the most

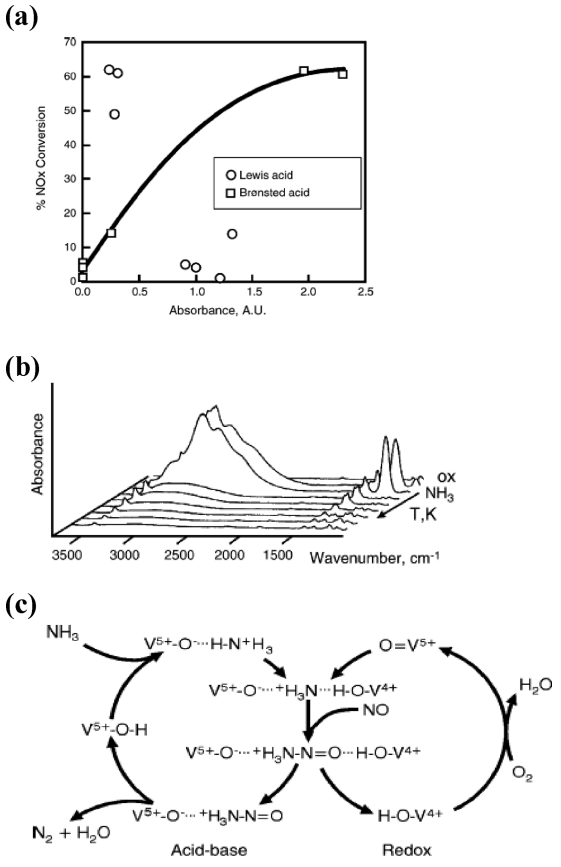

Figure 16. In situ investigation of the SCR of nitric oxide by ammonia on 6 wt % V_2O_5/TiO_2: (a) percent NO_x conversion vs absorbance of NH_4^+ band (BA) (~1420 cm^{-1}) and band due to coordinated NH_3 (LA) (~1605 cm^{-1}); (b) changes in spectral features of NH_3 preadsorbed surface subsequently exposed to flowing NO from 373 to 623 K; (c) proposed scheme for the catalytic removal. Reprinted with permission from ref 154. Copyright 2006 Elsevier B.V.

significant results, which illustrates the above-mentioned comments, was provided by the comparative microkinetic spectroscopic studies earlier reported by Topsøe[153,154] for the selective reduction of NO_x by ammonia over vanadia-based catalysts, 6 wt % V_2O_5/TiO_2. Previous microkinetic investigations revealed for this reaction a quite simple reaction scheme involving a strong adsorption of ammonia on acidic sites (M) and the activation of ammonia by reaction with gaseous NO via the involvement of sites (S) emphasizing the redox chemistry.

$$NH_3 + M \leftrightarrows M{-}NH_3 \quad (19)$$

$$M{-}NH_3 + S \leftrightarrows S{-}NH_3 + M \quad (20)$$

$$S{-}NH_3 + NO \leftrightarrows \text{products} + S \quad (21)$$

FTIR spectroscopy observations reported in Figure 16 showed that ammonia adsorbs preferentially on Brønsted sites associated with ($V^{5+}-OH$) (Figure 16a) whereas vanadyl groups $O{=}V^{5+}$ reduce to $HO-V^{4+}$ during the reduction of NO by chemisorbed ammonia (Figure 16b). This study elucidated the beneficial role of oxygen related to the restoration of $O{=}V^{5+}$ by oxidation and offered a detailed description of the active sites leading subsequently to the proposal of a mechanism scheme that accounts for the impact of oxygen usually considered as an inhibitor mostly on noble metal based catalysts (Figure 16c). This microkinetic model has been profitably used for industrial applications.[155] We will return to this application with a growing interest in postcombustion catalysis with the development of urea SCR processes on heavy-duty vehicles. More recently it was found that an optimal molar $NO_2/NO \approx 0.7$ is needed on copper-based catalysts.[156] Such a finding seems to be in line with the fact that the reoxidation step of $HO-V^{4+}$ to $O{=}V^{5+}$ on vanadia-based catalysts occurs more readily with NO_2 than oxygen. Hence, similar behavior would be involved on copper-based catalysts involving the participation of oxidic Cu(II) and Cu(I) species.

Returning to three-way applications, a great number of publications were dedicated to *in situ* and *operando* characterizations of supported noble metal based catalysts with a particular attention paid to the adsorptive properties of noble metals, changes occurring in real exhaust conditions, and the elucidation of reactive intermediate corresponding to both quantitative and qualitative approaches.[123,157−163] Probably, the study of NO adsorption on Rh/Al_2O_3 by Arai and Tominaga[163] was a precursor study associated with the identification of a cationic $Rh-NO^+$ species resulting from transfer of an electron from antibonding π^*_{2pz} molecular orbital to d orbitals of the metal, leading to a strengthening of the N−O bond, and an anionic $Rh-NO^-$ species corresponding to a weakening of the N−O bond. $Rh-NO^-$ species are usually assigned as precursors of nitrogen production. Changes in spectral features were previously reported on Rh supported on W^{6+}-doped TiO_2 with the observation of $Rh-NO^-$ at lower wavenumber (1680 vs 1750 cm^{-1} on Rh/TiO_2) emphasizing some modifications in the electronic state of Rh via electronic interactions at the metal/support interface.[164] In the absence of Rh^0 sites, the dissociation of NO leading to nitride Rh−N species, generally from Rh-NO^-, stops and more stable $Rh-NO^+$ species develop. On the other hand, there is no consensus on the nature of intermediates involved in the production of N_2O probably because the characteristic IR bands of both intermediates overlap. Dinitrosyl NO species, $Rh(NO)_2$, as well as $Rh-NO^+$ species, have been previously assigned as possible intermediates.[123,162−165] In fact, both assignments can be reconciled by the arguments developed by Unland[166] emphasizing the existence of an equilibrium between $Rh(NO)_2$ and $Rh-NO^+$. The formation of isocyanate species was also reported supporting previous observations on Pt.[166] This adsorbed species currently forms more readily on Rh than on Pt and has been previously ascribed to Rh(NO)(CO) species characterized by twin bands at 2108 and 2040 cm^{-1} on Rh/Al_2O_3.[167,168] It was postulated that the N−O bond breaking would occur via an electron transfer from CO ligand to the antibonding molecular orbital of chemisorbed NO molecules. Interestingly, they observed correlatively the formation of N_2O, which would form according to a subsequent reaction between Rh−N and NO, whereas NCO species would result from a direct interaction between Rh−N and CO. Generally speaking, the formation of isocyanate on Rh has been preferentially ascribed to spectator rather than intermediate in the overall NO/CO reaction in three-way conditions. NCO decomposition might occur, but it seems obvious that the rate of diffusion of this species on the support seems to be higher than those of subsequent surface reaction over noble metals. On the other hand, such a species could be a predominant intermediate under lean conditions showing in those conditions a complex chemistry where the hydrolysis of isocyanate species would release ammonia and then

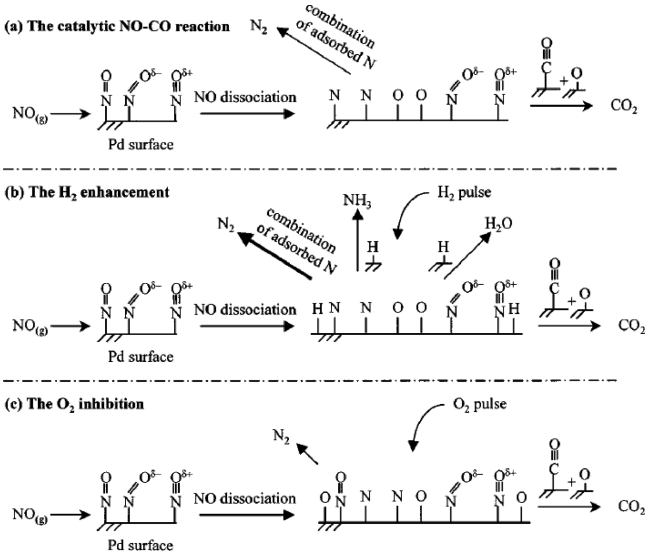

Figure 17. (a) The proposed NO−CO reaction pathway. (b) Selective enhancement causes a decrease in the concentration of active adsorbate. (c) Selective poisoning causes an increase in the concentration of active adsorbate. Reprinted with permission from ref 165. Copyright 1998 Elsevier B.V.

promote the SCR transformation. More recent investigations provided by Chafik et al.[162] threw the debate back concerning the real impact of NCO in the production of N_2O. They succeeded in the stabilization of isocyanate species on Rh particles dispersed on W^{6+}-doped TiO_2. Accordingly, they found a correlation between the population of surface isocyanate and the formation of N_2O, which led the authors to the conclusion that it is reasonable to suggest an additional route for the production of N_2O involving a bimolecular reaction between adsorbed NCO and gaseous NO. Let us mention that such a comparison could not be obvious according to the methodology developed in this above-mentioned study because more reactive intermediates are generally related to a decrease of the surface concentration from transient experiments. The implementation of transient experiments with selective enhancement and poisoning techniques is probably more appropriate to elucidate the nature of intermediates.[165] This methodology is described in Figure 17.

As shown, under steady state under NO/CO flow, H_2 pulses were found to accelerate the specific reaction that depletes the reactive adsorbate. Conversely oxygen species poisoned the surface with further accumulation of active intermediates. Among the different NO adsorbates intermediate indentified by FTIR, Pd−$NO^{\delta+}$, PdN═O, and bent Pd−$NO^{\delta-}$, it was suggested that the dissociation of Pd−N═O species would likely occur during the NO/CO reaction. A similar approach was implemented for investigating the nature of rhodium dicarbonyl species, $Rh^+(CO)_2$, and their reactivity. Previous SSITKA demonstrated rapid exchanges between ^{13}CO and $Rh^+(^{12}CO)_2$ but fail to describe the effective role of *gem*-dicarbonyl species.[169] Selective enhancements showed the involvement of such a species during the NO/CO reaction.

According to these transient approaches, the influence of W additive on Rh/TiO_2 was found to weaken the N−O bond of the $Rh-NO^-$ resulting in a higher rate of NO dissociation and N_2 production in the gas phase.[162] Hence, the authors explained that W incorporation would alter the electronic properties of Rh.

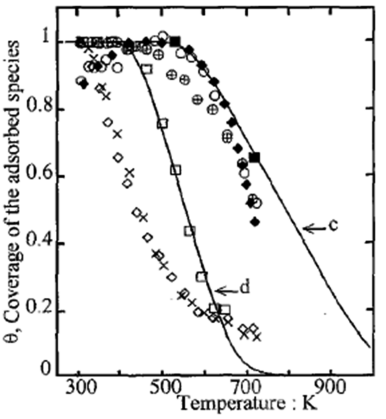

Figure 18. Evolution of the coverages of the linear and bridged CO species with adsorption temperature on 3% Rh/Al_2O_3. Reprinted with permission from ref 157. Copyright 2001 Elsevier B.V.

However, they completely ruled out possible structural changes suggested by DFT calculations, which might also participate. *In situ* infrared spectroscopy was also developed for quantitative approaches[157,159] in order to estimate the heat of adsorption of different CO and NO chemisorbed species on supported Pt and Rh catalysts. The plot of the coverage of the adsorbed species versus temperature calculated from IR spectra (Figure 18) can be modeled assuming a linear relationship between the heat of adsorption and the coverage θ according to a Temkin formalism.

This quantitative approach is suitable to estimate the surface coverage dependency of the heat of adsorption of linear and bridged CO species and to evaluate their intrinsic activity in realistic pressure conditions. Hence, it is possible to identify the most probable geometry of the intermediates involved in the CO/O_2 reaction but also to depict surface reconstructions occurring on supported polycrystalline Pt catalysts under reactive conditions. By way of illustration Bourane et Bianchi[170] found two different kinetic regimes modeled by Langmuir−Hishelwood mechanisms (M1 and M2) involving linearly coordinated CO species on Pt^0 reacting with weakly adsorbed oxygen species (M1) or strongly adsorbed oxygen species (M2). A switch for M1 to M2 has been interpreted on the basis of similar observations over Pt single crystals corresponding to surface reconstruction from a Pt surface predominantly covered by CO to a surface mainly covered by strongly chemisorbed O atoms. Hence, *in situ* and *operando* FTIR technique is a useful tool to characterize in detail the nature of adsorbate and then to identifiy the most reactive ones and ultimately to probe surface changes that might bring about significant modifications in the kinetic behavior.

Now, regarding the use of this methodology for lean burn catalysts, a huge number of publications demonstrate the potential of *in situ* and *operando* approaches.[171−177] Nevertheless they mostly showed the complexity of the chemistry in which some difficulties arise for discrimining between adsorbate spectator and reactive intermediate particularly for the HC-SCR on silver-based catalysts (see section 4).[171,177] Indeed various stable species were identified such as nitrate and nitrite species, which would be capable of reacting with oxygenates produced from the partial oxidation of hydrocarbons then inducing the formation organonitro compounds, which might further decompose to release nitrogen. Bion et al.[177] demonstrated the reactivity of chemisorbed intermediate in the presence of water-releasing ammonia as possible reducing agent for NO (Figure 19).[177]

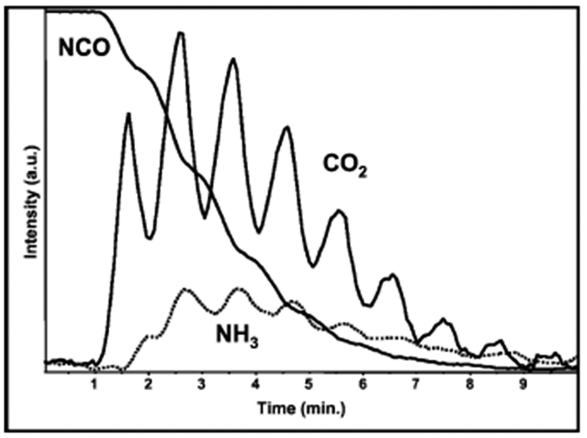

Figure 19. FTIR of NCO consumption and of CO_2 and NH_3 gas species produced during the introduction of H_2O pulses on Ag/Al_2O_3 previously treated under CO + NO at 873 K. Reprinted with permission from ref 177. Copyright 2003 Elsevier B.V.

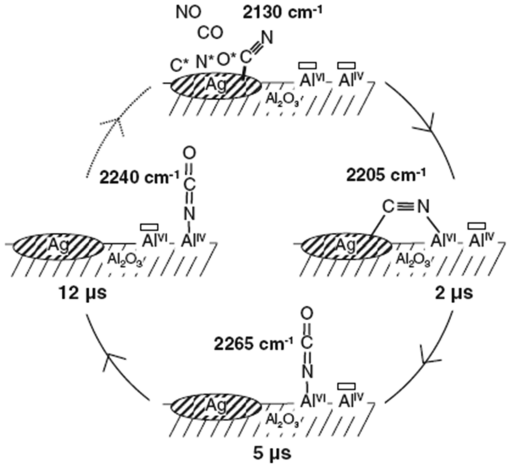

Figure 20. Reaction mechanism for $DeNO_x$ reaction on alumina-supported silver catalyst. Reprinted with permission from ref 171. Copyright 2010 AAAS.

Novel spectroscopic methodologies such as step-scan FTIR provided relevant spectral information. Recent paper found by using femtosecond laser excitation followed by nanosecond time-resolved *in situ* FTIR spectroscopy that the key step in the $DeNO_x$ reaction on silver-based catalysts is the flip of a cyanate group from a silver nanoparticle to the alumina support with a lifetime of 2 μs as exemplified in Figure 20.

The development of *in situ* and *operando* FTIR experiments is also suitable to characterize NO_x storage reduction catalysts (NSR) (Figure 21).[176] A large part of publications is dedicated to spectroscopic investigations of the storage phase highlighting the role on noble metals, which catalyze NO to NO_2 more readily than the barium oxide and the role of barium oxide to stabilize nitrates from NO_2 formation as exemplified in Figure 21. Some of those investigations focus on the switch period from lean to rich conditions.[178] The presence of CO in the gas mixture may be profitably used as probe molecule to visualize the modifications of the surface properties of Pt showing a progressive shift of the linearly coordinated CO species to lower frequencies indicating a restoration of the metallic character of Pt. This observation suggests that during a short period of time, Pt particles recovered by strongly chemisorbed O species will be unable to convert efficiently NO to nitrogen. The information is an important point for optimizing the efficiency of such systems, particularly the concentration of hydrogen admitted during the regenerative step of NSR systems and the duration of the regenerative step.

3.3. Kinetic Modeling of $DeNO_x$ Reactions under Simulated and Real Exhaust Conditions

Mathematical modeling plays an important role in developing monolithic catalysts. The performances of monolith reactors are a complex function of design parameters (channel geometry, length and diameter of the channel, channel wall thickness), operating conditions (temperature, velocity), the properties of the catalyst (active species loading, washcoat loading, etc.), and the reaction mixture. In addition, complexity arises from continuously changing inlet conditions that require a transient description of the monolith reactor. Hence, the experimental investigation of the performance of monolithic reactors is time-consuming and requires a large experimental setup.[179−185] Previous kinetic models simulated step changes in temperature and feedstream composition integrating empirical rate equations on commercial monolith three-way catalysts using a recycle fixed bed flow reactor exhibiting CSTR performances.[186−189] However, it is worthwhile to note that they sometimes provided numerical solutions for the kinetic parameters without real significance from a chemical point of view despite good correlation for the prediction of outlet concentration of atmospheric pollutants. Probably, the most illustrative results were given by Votz et al.[189] who obtained positive values for NO adsorption enthalpy, which points out that the numerical values for the apparent kinetic order have a poor influence on the kinetic modeling. This is consistent with the conclusion drawn by Dubien and Schweich[190] who found a good agreement between experimental and predicted conversions for the light-off curves by simply adjusting the pre-exponential factor and the apparent activation energy of the rate constants in the overall rate equations. However, it is also obvious that they did not reflect with certainty the real chemical processes taking places on TWCs under simulated conditions. More recently some attempts were successfully made for modeling under steady-state conditions a ceria-modified $Pt−Rh/Al_2O_3$ monolith catalyst demonstrating a significant impact of water on the kinetics related to the involvement of steam reforming and the water−gas-shift reactions at high temperature. By neglect of diffusion limitations, the rate expressions were capable of predicting modifications of noble metal behavior at low temperature in the presence of ceria taking into account intrinsic OSC properties.[191] Clearly, on the basis of those previous investigations the set up of rational kinetic models that account accurately for heat and mass transfer phenomena and chemical reactions seemed to be a challenging task despite those studies representing a significant added value from a practical issue. As a matter of fact, the prediction of the outlet concentration during light-off experiments or transient operating conditions typically under cycling conditions could be achieved accurately by measuring modifications in the surface adsorbate concentrations in order to identify the most abundant adsorbate species and the related rate-limiting step. Weak predictions could be also related to incomplete models, which neglect the production and subsequent transformation of N_2O probably because under steady-state conditions only nitrogen is usually produced but the transient production of N_2O has to be taken into account

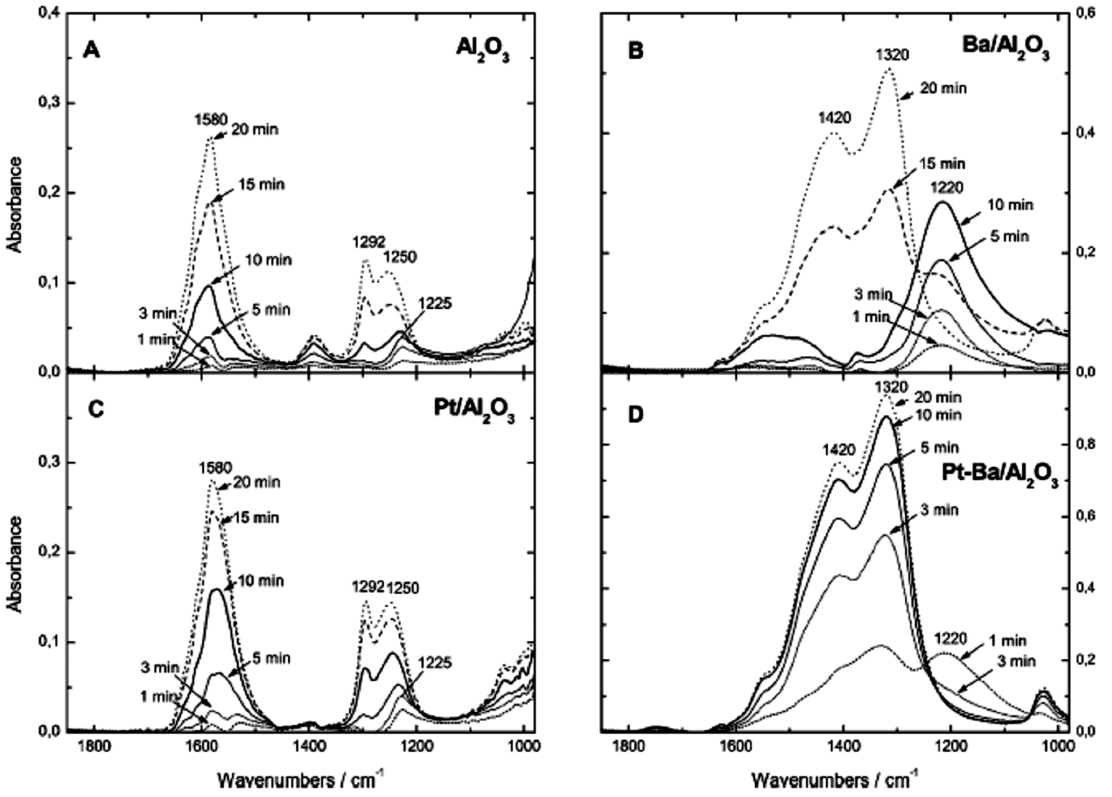

Figure 21. Results of NO/O_2 adsorption FTIR experiments at 623 K over (A) γ-Al_2O_3, (B) Ba/γ-Al_2O_3, (C) Pt/γ-Al_2O_3 and Pt-Ba/γ-Al_2O_3 (NO/O_2 = 1:4; pNO = 5 mbar). Reprinted with permission from ref 176. Copyright 2004 Elsevier B.V.

during the light-off conditions.[192] Controversial arguments were previously reported in the literature regarding the real impact of the CO/N_2O subreaction in the overall CO/NO process over noble metals.[193−197] Previous statements considered two kinetic regimes with the production of N_2O on TWC via step 16; the preferential formation of N_2 via steps 14 and 13 without intermediate formation of N_2O because the rate of the isolated CO/N_2O reaction was found to be substantially lower than that for the CO/NO reaction both on Pt and Rh based catalysts[198,199] In fact, subsequent comparisons between experimental and calculated data on Rh catalysts supported on alumina, ceria, and modified ceria revealed that the suppression of the N_2O production at high temperature during the NO/CO reaction is due to the fast N_2O/CO reaction.[194,195] Detailed kinetic analysis indicates that the sticking coefficient of N_2O under typical reaction conditions is extremely low, $\sim 2 \times 10^{-6}$, which leads to the conclusion that the rate-limiting step of the isolated N_2O/CO reaction is the adsorption of N_2O onto the catalyst surface. In fact, Cho explained his results by a significant lowering of the CO inhibiting effect during the overall CO/NO reaction because of the occurrence of lateral repulsive interactions between CO_{ads} and N_{ads}, from the dissociation of NO enhancing the subsequent desorption of CO. The strong NO adsorption on Rh also prevents the readsorption of N_2O and its subsequent dissociation involving an additional nearest neighbor vacant site. Consequently, the subsequent CO/N_2O reaction on Rh only starts when NO is quasi-completely converted in the gas mixture. This competition is more in favor of N_2O on Pt, which enhances the CO/N_2O reaction below the light-off temperature while a large part of NO is not yet converted. Hence, these observations emphasize the beneficial effect of Rh in the conversion of NO to nitrogen in three-way condition but also underline its detrimental effect particularly during the cold start engine. This is a key point which will probably need particular attention if the emissions of green house gas, such as N_2O having a much higher global warming power than CO_2, will be considered in the forthcoming standard regulations.

3.3.1. Previous Statements in Stoichiometric Conditions: The Detrimental Effect of Oxygen on TWCs. Banse et al.[200] found two different rate-limiting steps for the NO/CO reaction depending on the adsorbate composition when Pt surfaces, preadsorbed with NO or CO, are further exposed to, respectively, gaseous CO and NO. Interestingly the rate expression $r = k\theta_{CO}\theta_O$ predominates for modeling the transient CO_2 production at the onset of the experiment because probably a partial dissociation took place during preadsorption. However, a shift of the rate-determining step is observed from step 15 to step 12 when the reaction is going on with a rate expression $r = k'\theta_{NO}\theta_v$. As exemplified by Cho et al.,[201] it is obvious that the rate-controlling step may change during the cold start engine. At low temperature, the dissociation of NO governs the reaction while above the light-off temperature the oxygen scavenging process controls the reaction. Previous investigations on bimetallic $Pt-Rh/Al_2O_3$ partly agree with the fact that under typical three-way conditions the catalyst surface would be mainly composed of strongly chemisorbed oxygen and subsurface species.[202] Hence, under operating three-way catalysis, with low residual concentrations of CO and NO, the desorption step of oxygen given by the following equation could not be neglected for deriving a rate for CO_2 production:

$$2O_{ads} \rightarrow O_2 + * \qquad (22)$$

dx.doi.org/10.1021/cr100168g |*Chem. Rev.* 2011, 111, 3155–3207

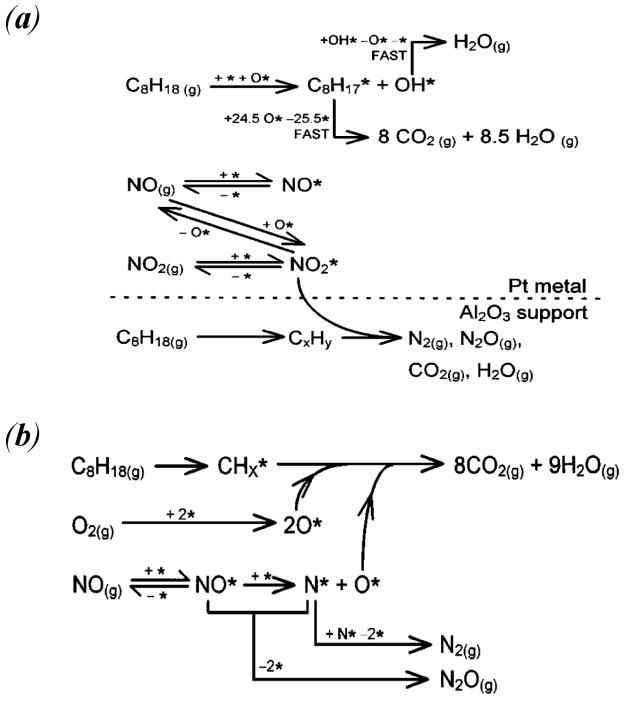

Figure 22. Proposed mechanism for the $C_8H_{18}-NO-O_2$ reaction in the low $[C_8H_{18}]/[O_2]$ (a) and in the high $[C_8H_{18}]/[O_2]$ concentration region (b). Reactions above the dotted line occur on the Pt surface, while reactions below occur on the alumina support. Reprinted with permission from ref 203. Copyright 1999 Elsevier B.V.

Consequently, the rate for the production of CO_2 (r_2) would differ from that established at low temperature and low conversion (r_1), which points out that complicated kinetic features have to be taken into account for modeling accurately the performance of TWC during the cold start engine.

$$r_2 = r_1\left[1 - \frac{2k_{12}k_{22}K_{NO}P_{NO}}{k_{15}K_{CO}P_{CO}}\right] \quad (23)$$

$$r = \frac{kK_{NO}P_{NO}}{(1 + K_{NO}P_{NO} + K_{CO}P_{CO})^2} \quad (24)$$

K_i (with i = CO, NO) represents the equilibrium constant of the reactant i, while k_n stand for the rate constant related to step n.

3.3.2. The Mechanistic Aspect of the Effective Role of Oxygen for Lean Burn Applications: Toward an Integrated Approach. Interestingly, oxygen behaves differently under lean conditions, and this led to different mechanism proposals over noble metals. Burch et al.[203−205] were probably among the first researchers to investigate the reaction mechanism over noble metals under lean conditions and reported complex kinetic features depending on the $[HC]/[O_2]$ ratio and the chemical nature of hydrocarbons, that is, saturated or unsaturated hydrocarbons.

As earlier described, the kinetics of NO reduction by heavy hydrocarbons such as octane, is governed by the competition between O_2 and C_8H_{18} on supported Pt catalysts. Figure 22 shows the reaction scheme according to the $[C_8H_{18}]/[O_2]$ values. At low $[C_8H_{18}]/[O_2]$ ratio, Pt is saturated by oxygen losing its metallic character. Chemisorbed NO_2 molecules from surface NO oxidation, spill-over from Pt onto alumina and react

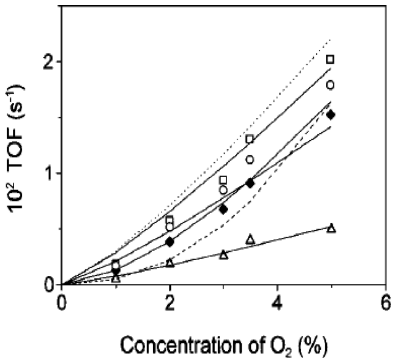

Figure 23. The effect of varying O_2 concentration on the TOF of n-C_8H_{18} (○), total NO_x (□), NO to N_2 (♦), and NO to N_2O (Δ) for reaction at 473 K over Pt/Al_2O_3 showing fits to high $[C_8H_{18}]/[O_2]$ concentration kinetic models for NO_x reduction via NO dissociation (solid lines) and by reaction between adsorbed NO and carbonaceous species (···, NO_x; −−−, n-C_8H_{18}). Reactant feed 1000 ppm n-C_8H_{18} and 500 ppm NO. Reprinted with permission from ref 203. Copyright 1999 Elsevier B.V.

subsequently with C_8H_{18}-derived species at the metal/support interface (mechanism a). At high $[C_8H_{18}]/[O_2]$ the surface is predominantly covered by C_8H_{18}-derived species. The local reduction of Pt surface would preserve the metallic character of Pt and its ability to dissociate NO according to the sequence b. Similar kinetic features characterize the reduction of NO by C_3H_8 and C_3H_6 reaction.[204] Let us mention that the predominance of mechanism a or b will strongly depend on the rate of hydrocarbon adsorption well-recognized as a slow step (Figure 23). Unsaturated hydrocarbons generally adsorb more strongly than their saturated homologues and irreversibly at low temperature on Pt/SiO_2 irrespective of the gas composition.[205]

Most papers dedicated to noble metals for lean burn applications led to unsuccessful results due to a low level of NO conversion correlated to significant production of N_2O and NO_2. Successive investigations also revealed a complex chemistry suggesting the involvement of various intermediates resulting from various recombination between NO_2 and oxygenates produced from the partial oxidation of hydrocarbons with the formation of nitro and isocyanate species. Interestingly, NCO species may act as intermediate contrary to previous statements in three-way conditions. Despite a huge amount of papers that dealt with mechanistic aspects on a wide variety of catalysts, it seems obvious that no detailed reaction scheme has been yet proposed on the basis of experimental evidence. Recent developments of microkinetic models under real exhaust conditions on monolith catalysts might be considered as a starting point. A detailed elementary reaction mechanism is proposed on supported silver-based catalysts using a microkinetic approach rather than a single rate expression, which accounts for a power-law fitting on Langmuir−Hinshelwood kinetics to optimize kinetic parameters.[206] This study refers to previous pulse reaction infrared spectroscopic measurements,[175,207] which provided evidence for the possible participation of isocyanate species (NCO) when silver is incorporated in alumina. Additional spectroscopic observations supported by DFT calculations suggested that those intermediates would come from the decomposition of CH_3NO_2.[208] On the basis of those previous observations Mhadeshwar et al.[206] developed a microkinetic model that accounts for 13 reductants, poisoning effects of aromatics by site-blocking, and interestingly

dx.doi.org/10.1021/cr100168g |Chem. Rev. 2011, 111, 3155–3207

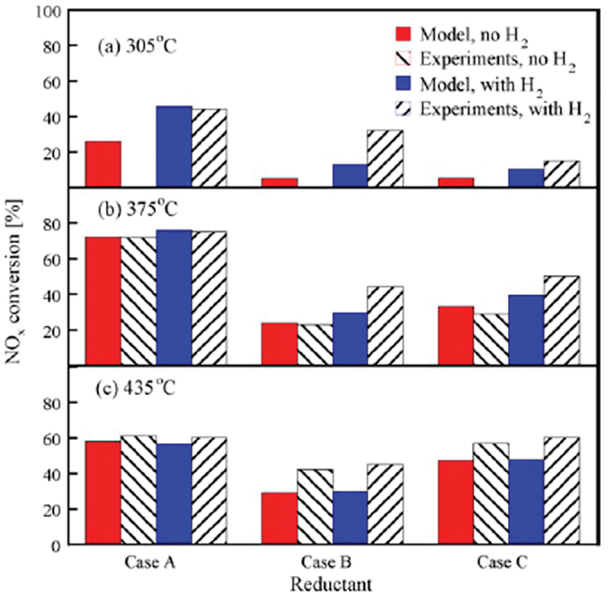

Figure 24. Comparison between experimental and predicted NO_x conversion during the HC-SCR on silver-based monolith catalyst. Case A: pure octane with C_1/NO_x = 5:1. Case B: octane + toluene with C_1/NO_x = 5:1 (equal C_1/NO_x = 2.5:1 for octane and toluene). Case C: octane + toluene with total C_1/NO_x = 10:1 (equal C_1/NO_x = 5:1 for octane and toluene). Effect of 1000 ppm H_2 in feed is also shown. Monolith cell density is 230 cpsi. Reprinted with permission from ref 206. Copyright 2009 Elsevier B.V.

the promoting effect of hydrogen.[209−214] This latter aspect could be considered as an outstanding parameter in lean $DeNO_x$ applications on silver-based catalysts, which will be discussed in detail in section 4. The microkinetic approach developed by Mhadeshwar et al.[206] combines experimental and theoretical calculations using DFT and the semiempirical UBI−QEP method. As previously shown, this latter mathematical model provides the heat of adsorption for molecular and radical species and the activation barrier for elementary reactions. A relatively accurate model can be achieved taking into account the dissociation of chemisorbed NO molecules assisted by hydrogen atoms at the surface on silver (Figure 24). The occurrence of this elementary step has been earlier discussed over noble metals and correctly models the NO/H_2 reactions near stoichiometric conditions.[133−135,137] However, under lean conditions in a large excess of oxygen, this hypothesis became inadequate because the H_2/O_2 reaction usually occurs much more readily than the NO/H_2 reaction and then considerably lowers the hydrogen coverage. This is a strong questioning point underlined by this model that accounts for the following elementary step under lean conditions, which would potentially explain the beneficial effect of hydrogen.

$$NO_{ads} + H_{ads} \rightarrow N_{ads} + OH_{ads} \qquad (25)$$

As a general tendency, the modeling of non-steady-state kinetic regimes for after-treatment technologies represents a growing interest from a fundamental point of view for developing robust mathematical models that account for the chemistry and a practical one for designing and control integrated after-treatment systems.[139,215−217] Particular attention has been initially focused on urea−SCR systems on $V_2O_5−WO_3/TiO_2$.[217] Kinetic parameters previously calculated on powder catalysts were input in the mathemathical model of SCR monolith reactor and provided good correlations between prediction and experimental data. The mathematical model predicts the chemical processes involved at the catalyst surface representing correctly the inhibiting effect of ammonia at low temperature and an optimal surface coverage of ammonia, which is probably a useful finding for designing the ammonia/urea dosage strategies.[215] Nowadays such predictive mathematical tools will develop due to more complex architecture for after-treatment systems combining DOC, DPF, NSR, and SCR catalysts.[218] Recently, Zukerman et al.[139] built up a platform capable of simulating the dynamic behavior of multiple-unit after-treatment systems based on COMSOL Package. Interesting information has been provided concerning the coupling of NSR and SCR catalysts. Kinetic models were developed separately considering the ammonia formation and oxidation during the regenerative step of the NSR catalyst under rich conditions. The balance between stored and reacted NO_x and ammonia has been found to be the key factor in determining the efficiency of the global system (Figure 25).

3.4. Impact of Kinetic Information on the Design of Supported Catalysts: Toward a Reduction of Noble Metal Contents?

Shelef and Graham[18] reported interesting observations related to several attempts for replacing Rh and making combinations of other active components able to behave like Rh. Probably infrared observations were the starting point highlighting the stabilization of *gem*-dinitrosyl NO species on Rh. Theoretical calculations showed a weakening of terminal N−O bond in N_2O_2 molecules compared with NO. By analogy with IR observations, it was concluded that *gem*-dinitrosyl NO species on Rh could be the precursor state for nitrogen production. Subsequently, IR observations provided evidence of such an adsorbate also on Mo-based catalysts, which stimulated further research to develop TWC-like behavior in $Pt(Pd)/MoO_x$-(WO_x).[219,220] Low-level Pd loading catalysts on MoO_x substrate was also investigated at the laboratory scale.[221] However, despite promising results, such a solution was impractical due to the low sulfur tolerance of Mo and a high volatilization of molybdenum and tungsten oxyhydroxides under realistic automotive exhaust conditions.

There are actually strong efforts at the laboratory scale to develop rational methods for controlling the size and the morphology of noble metal particles. According to previous observations, it is obvious that both parameters probably govern the balance between the oxidative and reductive behavior of supported catalysts. Recent developments were also focused on the preparation of well-defined platinum nanocrystals by a colloid method subsequently deposited on alumina.[222] An approach such as this is appropriate for lean burn $DeNO_x$ reactions to favor the structure-sensitive NO/C_3H_6 reaction at the expense of the competitive catalytic combustion of propene. Interestingly the main observation mimics those earlier reported under UHV conditions showing that the catalytic behavior is mainly related to the shape rather than the size of Pt particles. The catalytic performance evaluated after thermal aging showed that cubic Pt particles stabilized up to 673−773 K are slowly converted to round ones correlated to an enhancement of the overall NO conversion but to a simultaneous loss in nitrogen production. It is obvious that such findings might open new

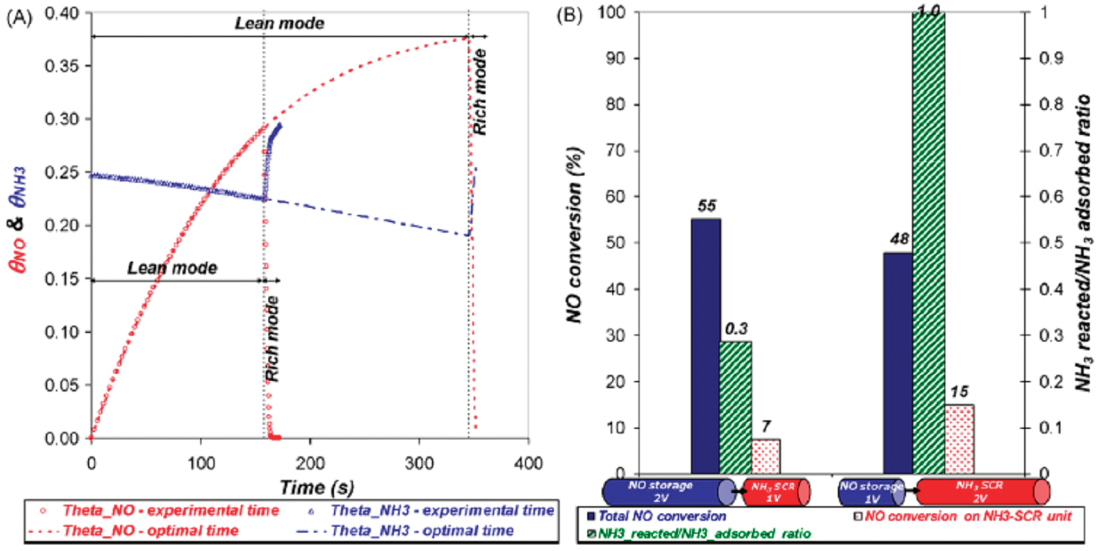

Figure 25. (A) θ_{NO} and θ_{NH_3} (the ratio between NO and NH_3 to catalyst capacity, respectively) in a NO_x storage unit under EC1 conditions as function of time (at experimental time and at optimal time). (B) NO conversion and the ratio between NH_3 and adsorbed (stored) NH_3 for two volume configurations under EC1 conditions. Reprinted with permission from ref 139. Copyright 2009 Elsevier B.V.

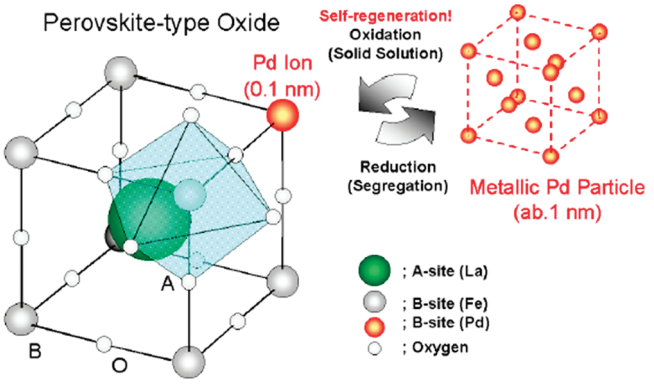

Figure 26. Self-regenerative behavior of $LaFe_{0.95}Pd_{0.05}O_3$ under three-way conditions. Reprinted with permission from ref 228. Copyright 2006 Elsevier B.V.

prospects in the optimization of morphological control of noble metal catalysts particularly for lean burn applications with lower running temperature conditions. The development of sol−gel methods also contributes to improve the resistance to thermal sintering as well as the catalytic performance in terms to N_2 production in comparison with conventional impregnated catalysts.[223−225]

Recent developments have shown that the nature of the support is an important adjustable parameter to control the particle size of noble metals and their morphology. By way of illustration, perovskite-based materials were found to be appropriate for three-way applications.[226−234] It has been found that thermal sintering reactions are inhibited when Pd is incorporated inside a perovskite structure $LaFePdO_x$ (Figure 26). Under oxidative/reductive cycling conditions, reversible changes take place related to the reduction of oxidic palladium species going outside the structure and subsequent oxiditation/diffusion leading to the restoration of isolated Pd^{2+} stabilized in the B sites of the perovskite structure. This behavior promotes the catalytic performances in terms of activity and selectivity under cycling conditions and also the durability. Under reductive conditions, epitaxially orientated Pt particles on the characteristic planes of $LaFeO_3$ were characterized by HRTEM, which might explain the lower sensitivity to thermal sintering particles. Such microstructures are also characterized by an increase in activity and selectivity toward the conversion of NO to nitrogen.[234]

4. RECENT ADVANCED FINDINGS ON ALTERNATIVE SYSTEMS: ADVANTAGES AND DRAWBACKS

4.1. Diesel Exhaust Treatment Concept

Diesel engines run at a high A/F (air to fuel) ratio under very fuel lean conditions. Due to this, they have very low emissions of gas-phase hydrocarbons and carbon monoxide. However, diesel exhaust is characterized by relatively high emissions of nitrogen oxides (NO_x) and particulates as condensed material at 325 K. Particulates are multiple phases composed of solid (insoluble) carbon soot particles, liquid hydrocarbons in the form of lube oil or unburned fuel (the so-called SOF), and the so-called "sulfate" in the form of $SO_3 + H_2O = H_2SO_4$.

Future emissions standards for NO_x and particulates have been recently adopted in the U.S.[2] and Europe (see Table 1) for both heavy duty and light duty diesel powered vehicles, which are expected to reduce these emissions by at least 50% and quite likely by 70−90%.

Several solutions have already been proposed for controlling NO_x emissions from diesel-powered vehicles.[4,5] One set of approaches focuses on the engine. Techniques such as exhaust gas recirculation and partially homogenizing fuel−air mixtures are helpful, but these techniques alone will not eliminate NO_x emissions as discussed elsewhere.[4] Another set of approaches remove NO_x from the vehicle exhaust. These include the use of lean-burn NO_x catalysts, SCR catalysts, and NO_x storage reduction catalysts (NSR).[12,16]

Lean-burn NO_x catalysts promote the reduction of NO_x under oxygen-rich conditions. Reduction of NO_x in an oxidizing atmosphere is a difficult task.[14] It has proven challenging to find a lean-burn NO_x catalyst that has the required efficiency, durability, and

dx.doi.org/10.1021/cr100168g |Chem. Rev. 2011, 111, 3155–3207

operating temperature range. A reductant such as diesel fuel must be steadily supplied to the exhaust for lean NO_x reduction introducing at least a fuel economy penalty of 3%. Currently, peak NO_x conversion efficiencies for lean-burn NO_x catalysts are unacceptably low[43] and usually accompanied with a significant amount of N_2O production.[13,14]

SCR generally refers to selective catalytic reduction of NO_x by ammonia. The reaction takes place even in an oxidizing environment. NO_x can be temporarily stored in an adsorbent, or ammonia can be fed continuously into the exhaust. SCR can achieve high levels of NO_x reduction, but there is a disadvantage in the lack of infrastructure for distributing ammonia or a suitable precursor. Another concern relates to the possible release of ammonia into the environment, which supposes an optimized system for ammonia injection.[215] To clarify the state of a sometime ambiguous nomenclature, it should be noted that in the exhaust after-treatment art, the terms "SCR catalyst" and "lean NO_x catalyst" are occasionally used interchangeably. Where the term "SCR" is used to refer just to ammonia-SCR, as it often is, SCR is a special case of lean NO_x catalysis. Commonly, when both types of catalysts are discussed in one reference, SCR is used with reference to ammonia-SCR and lean NO_x catalysis is used with reference to SCR with reductants other than ammonia such as SCR with hydrocarbons.

Nowadays, primarily due to thermal stability concerns of V-SCR technology during high-temperature diesel particulate filter regeneration, the most common diesel after-treatment configuration for Tier 2 Bin 5 standards is a diesel oxidation catalyst followed by a Cu-SCR catalyst, and then a diesel particulate filter.[235] In this configuration, the diesel oxidation catalyst oxidizes hydrocarbons and carbon monoxide before the Cu-SCR catalyst and serves to create an exotherm during diesel particulate filter regeneration and desulfation. This configuration is not ideal for converting NO_x during the cold start engine. The best-case condition for cold start NO_x performance is to move the SCR catalyst closer to the engine and ahead of the DOC. This exposes the SCR catalyst to engine-out conditions, which can have a detrimental effect on the catalyst performances. In the case of V-SCR technology, higher temperatures may cause thermal durability concerns. For Cu-SCR technology, engine-out hydrocarbon levels may seriously hinder NO_x performance. The lack of upstream diesel oxidation catalyst means a Cu-SCR catalyst will not have an exotherm available for desulfation but at the same time the Cu-SCR catalyst will not be exposed to SO_3, which is more detrimental to Cu-SCR technology than SO_2.[236]

4.2. Catalytic Conversion of NO_x Released by Internal Combustion Engines

The NO_x conversion depends on various controllable and uncontrollable parameters. The catalyst temperature seems to be an important parameter for NO_x conversion. Moreover, controllable parameters such as the cycle time, that is, the reduction cycle containing the NO_x storage period (lean) and the regeneration period (rich), the bypass time, that is, the period when the bypass valve is opened and the catalyst flow reduced, and the injection rate corresponding to the period when diesel fuel is injected into the exhaust stream turned out to be key parameters.[237−239]

As previously mentioned, combustion modifications in the engine design with the implementation of exhaust gas recirculation will be unable to meet ongoing regulations. Due to excess oxygen present in diesel exhaust gases, the opportunity for NO_x reduction under rich or stoichiometric air/fuel is not possible. SCR is a technology that has been shown effective in removing NO_x from oxygen-rich exhaust. A number of SCR systems have been developed that because of infrastructure concerns have used diesel fuel or oil as the reductant source. Unfortunately as of this date, a hydrocarbon reducing catalyst has not yet been developed that has sufficient efficiency and is effective over the entire operating range of the diesel engine.[240]

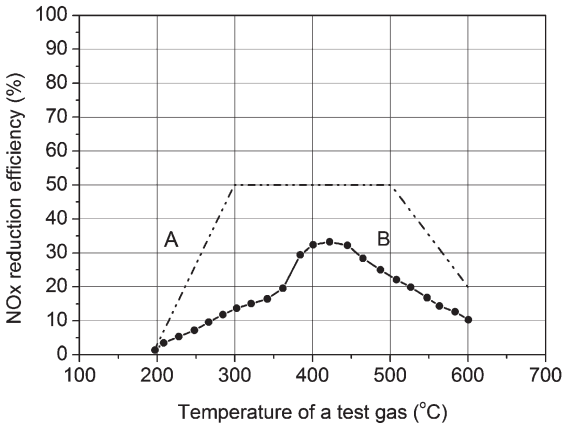

Figure 27. NO_x reduction capability using diesel fuel or light oil as reduction agent (flow rate 4000 h^{-1}, diesel fuel or light oil concentration in the test gas 3000 ppm). Reprinted from ref 250. U.S. Patent 6087298, 2000, to Engelhard Corporation, U.S.A.

The idea of introducing a two-step after-treatment system, first for the removal of the nitrogen oxides and the second for oxidizing hydrocarbons, has been proposed even in the early 1970s.[241] Other technologies suggested a catalytical gas treating method in which the exhaust gas goes through a catalyst layer at a very high space velocity to produce carbon monoxide from the particulates in the exhaust gas, which then reduces the nitrogen oxides. A possible catalyst composition including ruthenium supported on an alumina honeycomb was suggested.[242] Nowadays more complex exhaust treatment devices are proposed in order to fulfill the international regulations.[243−249] Among those proposals, an upstream catalytic zone where several layers containing zirconium and at least one rare earth element (La, Nd, etc.) on which palladium supported on alumina, silica, silica−alumina, alumina−zirconia, or alumina−ceria is deposited is coupled with a downstream catalytic zone stable up to 1173 K, which comprises in addition to palladium an oxygen storage component (ceria, zirconia, neodymia, lanthana) that is not in intimate contact with metallic platinum. The active catalytic species correspond to the three-way composition to which gold or platinum can be added. The second downstream layer contains at least one element of the platinum group metals. This layer also contains an oxygen storage component.[250] In the most convenient mode, direct injection of diesel fuel or light oil as reducing agents upstream of the $DeNO_x$ converter does not provide a sufficiently high $DeNO_x$ reduction efficiency as shown in Figure 27B.[251]

The exhaust temperature of diesel engines for trucks is generally in the range 373 to 473 K during idling operations and about 773 K during full-throttle operations. From the standpoint of the relationship between the operation state of the engine and the NO_x concentration in the exhaust, it is highly desirable or ideal to provide a NO_x reducing characteristics as

shown in Figure 27A. The $DeNO_x$ reduction efficiency in a narrow range of the exhaust temperature around 673 K is only slightly higher than 30%, which is unsatisfactory for practical use. A possibility to improve the $DeNO_x$ reduction efficiency is to decompose the diesel fuel into more reactive lower unsaturated hydrocarbons before the $DeNO_x$ converter using electrical heating and to add the decomposition products to the exhaust that is then supplied to the $DeNO_x$ converter equipped with a metallosilicate catalyst.[251] It is also worth considering that the content of oxygen in the exhaust gas emitted from the diesel engine is generally about 18−20% during idling and as small as about 3−5% during full-throttle operations. Since the content of oxygen is particularly small during half-throttle and full-throttle operations in which a large amount of NO_x is contained in the exhaust gas, only a small amount of lower unsaturated hydrocarbons is produced for effectively reducing NO_x even if the temperature of the decomposition chamber is raised to temperatures as high as 1273 K, resulting in insufficient NO_x reduction efficiency of the $DeNO_x$ catalyst. Also temperatures of 1273 K are disadvantageous in terms of increased consumed electric power.[251] However, the energy balance can be improved by replacing the heated decomposition chamber with a plasma exhaust gas treatment device, which treats the exhaust by a corona-discharging plasma.[252]

With the same scope, the use of an ozone generator coupled with an adsorbent and a main passage leading from ozone generator through the ozone adsorbent to the trapping device has also been proposed, wherein at least part of the ozone generated reacts with particulate matter trapped providing additional energy.[253] Zeolites were suggested as the ozone adsorbent. The silica−alumina ratio, which dictates the pore size of the silica−alumina, determines whether ozone can be adsorbed (trapped) and the adsorption temperature. As adsorbent in addition to zeolites, physical adsorption of ozone on activated charcoal was investigated. However, this solution has no practical interest because activated charcoal gradually burns in contact with ozone.[253]

4.3. Recent Developments in Diesel Engine Exhaust Reduction with Ammonia

4.3.1. Current Technologies. Sufficient NO_x reduction to meet current regulations has been achieved by combustion modifications in the diesel engine. Projected emission levels are such that combustion and engine modifications will not be sufficient to meet the more stringent levels.[254] SCR is a technology that has been shown effective in removing NO_x from oxygen-rich exhausts. A common nitrogen oxide reducing agent, currently used in industrial processes, is ammonia. It is known that ammonia SCR systems can be used effectively to control the emissions produced by vehicles powered by diesel engines, that the NO_x-reducing catalysts adsorb and then store ammonia at low temperatures and desorb the stored ammonia at higher exhaust gas temperatures, and that steady-state NO_x emissions determined from mapped speed and load engine conditions can be readily controlled by metering ammonia in stoichiometric relationship to the NO_x emissions. SCR is currently under development for mobile sources, vehicle applications using urea (e.g., aqueous solution) as the source of NH_3. Early patents controlled ammonia metering by considering the emissions to be controlled at steady-state conditions. It was concluded that since ammonia adsorption occurs below 473 K and desorption in the temperature range 473−1073 K, the SCR system should operate at higher temperatures to achieve complete reaction between ammonia and NO_x.[255] Thus, the fuel mass flow is sensed, and NH_3 is throttled at a percentage of fuel flow provided the temperature of the gases in the catalytic converter are within a set range. Further studies investigating NO_x emissions at various speed ranges concluded that a linear relationship exists between fuel flow and NO_x.[256] This basic control concept is used today in most mobile ammonia SCR systems. For instance, the humidity of intake air and one or more operating parameters of engine power, intake air temperature, fuel consumption, and exhaust gas temperature are considered to optimize an ammonia ratio control valve.[257] The molar ratio of ammonia to NO_x is set at less than one (substoichiometric) to minimize ammonia slip. The system uses a 2 wt % V_2O_5/7 wt % WO_3/TiO_2 honeycomb catalyst operating with a molar NH_3/NO_x ratio of 0.85.

Within the literature, significant numbers of reports have been published by engine investigators using ammonia as reducing agent and control strategies to optimize SCR NO_x systems. Walker and Speronello[258] injected various quantities of ammonia at various engine speeds and loads to obtain optimum NO_x conversions at steady state. The speeds and loads were mapped and stored in a look-up table (specific for each engine and each SCR catalyst), which was then accessed periodically to set an ammonia metering rate. The ratio of injected ammonia to NO_x is strongly dependent on the temperature.[259] Above 623−673 K, a molar NH_3/NO_x ratio greater than 1 leads to substantial improvements in performance without NH_3 slip. At low temperature, steady-state results showed that operation with α less than 1 can lead to reduced NH_3 slip with no measurable loss in NO_x conversion efficiency for an SCR catalyst saturated with NH_3.

S. Lepperhoff[260] analyzed the step load changes to evaluate transient systems showing that the load on the engine changes at constant rpm, the NO_x emissions increase, the temperature increases, and the total exhaust flow increases. Response of the catalyst to step changes in the engine operating conditions are referred to as step load tests. Ammonia slip occurs when engine load increases; the slip is correlated to the ammonia stored on the catalyst. Catalyst porosity was found to be an important parameter with respect to transient emissions,[261] and a stoichiometric injection of ammonia would ensure a maximum efficiency. The effect of the space velocity (intake air mass flow) and of the catalyst temperature was also stressed by Luders et al.[262] Ammonia storage and thermal inertia were noted as factors affecting the conversion, but the control system discussed had no special provisions, other than numerical modeling. Other studies, in full agreement with Koebel et al.,[263] reported that the catalyst is saturated with adsorbed ammonia at lower temperatures.

4.3.2. Vanadia-Based Catalysts: Surface Composition and Related Performance. NO_x-reducing catalysts have been developed that are effective over the operating range of the engine. In this process, NO_x is reduced to N_2 with NH_3 over a catalyst (e.g., zeolite, V/Ti). This technology is capable of NO_x reduction in excess of 90%, and thus it is one of the best candidates for meeting the severe NO_x reduction goals. Usually the V_2O_5/TiO_2 catalyst is promoted by tungsten trioxide. However the use of molybdenum trioxide (MoO_3), sulfates, and combinations of these have been reported as well.[243] V_2O_5/TiO_2 is typically made batchwise by wet-phase chemistry, entailing large amounts of waste solvent. Most procedures to prepare V_2O_5 on TiO_2 start from TiO_2 as the support onto which pentavalent vanadium oxide is deposited by impregnation or

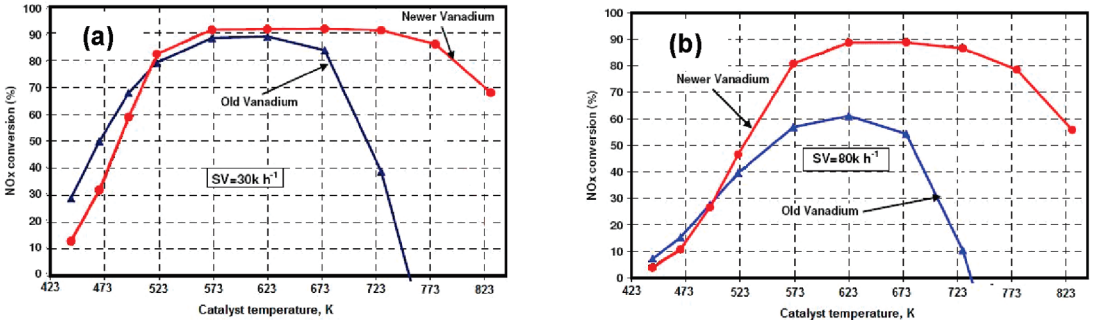

Figure 28. NO_x conversion performance of previous generation vs state of the art vanadium SCR catalyst formulations. Catalysts aged 75 h at 823 K: (a) space velocity of 30 000 h^{-1}, (b) space velocity of 80 000 h^{-1}. Reprinted with permission from SAE 2008-01-1029. Copyright 2008 SAE International.

adsorption using ammonium metavanadate[264−266] and vanadium or vanadyl chloride[267,268] precursors. Adsorption methods[269] using vanadyl acetylacetonate[270,271] and vanadyl triisobutoxide have also been described.[272] Vogt et al.[273] suggested the impregnation of the support with an aqueous solution of NH_4VO_3 that was electrochemically reduced in an acidified suspension (pH about 0.5) of the support material.

Sol−gel procedures have also been implemented[274,275] to prepare one-pot mesoporous $V_2O_5-TiO_2-SiO_2$ catalysts. The high surface, pore volume, and pore diameter of the support coupled with its improved stability allowed an enhancement of the catalytic efficiency in the SCR of NO by NH_3 compared with commercial $WO_3/V_2O_5/TiO_2$. In contrast, to this, a dry, continuous process, flame aerosol synthesis was recently proposed that offers an alternative for synthesis of catalysts with high efficiency.[276] These new catalysts are prepared from mixtures of titanium−tetra-isopropoxide and vanadium−oxo-tri-isopropoxide in flame of iso-octane. Flame aerosol synthesis leads to vanadia on agglomerated titania nanoparticles of regular spherical shape. Compared with catalysts from conventional methods, the texture of flame-made catalysts shows minimal porosity at high specific surface area. No indication for the formation of an interstitial solution of vanadium inside the titania lattice has been reported. Vanadia spreads out well, and homogeneous distributions were obtained. The powders exhibit excellent efficiency for SCR of NO by NH_3, which corresponds to a similar overall behavior to powder catalysts prepared by classical methods.

Replacing the iso-octane flame with a hydrogen flame led to a catalytic efficiency of the pilot-scale-made vanadia/titania for NO removal that was twice as much as the one by a conventionally prepared catalyst.[277] Using this methodology, the product properties can be varied in terms of crystal phase from mainly rutile to pure anatase and specific surface area that can exceed 100 m^2/g. Likewise, the addition of vanadia did not affect the titania phase or the specific surface area.

Recent studies reported that the properties of the commercial vanadia−titania catalysts can be dramatically improved following an aging treatment in an atmosphere of oxygen, water, and carbon dioxide.[278] This vanadium SCR system can survive high-sulfur fuel exposure and can function with low-sulfur fuel. It is thermally durable to 823 or 873 K and is not affected by hydrocarbons or sulfur. The NO_x conversion performance of these vanadium SCR catalysts can fulfill Euro 5 NO_x levels.

Data presented in Figure 28 shows that the previous generation of vanadium-based catalysts suffered from deteriorated performance after the 823 K aging conditions. However, catalysts prepared following the newer technology had very promising performance after long-term aging at this temperature. The difference in performance between the previous generation of vanadium SCR catalysts and the newer technologies is more pronounced at high space velocities, as shown in Figure 28b. The use of promoters is extremely important for both the stabilization of the structure and the increase of the catalyst stability; and the role of tungsten was well proven almost 2 decades ago.[13] In addition to this, to get the low-temperature sulfur-resistant V_2O_5/TiO_2 catalysts, quantum chemical calculations demonstrated that Se, Sb, Cu, S, B, Bi, Pb, and P can be suitable promoters.[279] Among these promoters, Se, Sb, Cu, and S promoted V_2O_5/TiO_2 catalysts showed indeed a higher catalytic efficiency for NH_3 selective catalytic reduction of NO_x at temperatures between 423 and 673 K. Sb has small vapor pressure and exhibits a high tolerance to SO_2 in the presence of water compared with other metal promoters.

Despite discrepancies about the detailed nature of the system, there is general consensus from experimental studies that the reaction involves V−OH groups, V=O species, or both functionalities. Thus in the literature it has been reported that the temperature and the presence of water have significant effects on the selectivity.[280] According to Ciardelli et al.,[216] the main reactions expected when NO, NO_2, NH_3, and O_2 are fed over $V_2O_5-WO_3/TiO_2$ catalyst are described in eqs 26−39.

$$NH_3 \leftrightarrow NH_3^* \qquad NH_3 \text{ adsorption/desorption} \qquad (26)$$

$$NH_3 + \frac{3}{4}O_2 \rightarrow \frac{1}{2}N_2 + \frac{3}{2}H_2O \qquad NH_3 \text{ oxidation} \qquad (27)$$

$$NH_3 + NO + \frac{1}{4}O_2 \rightarrow N_2 + \frac{3}{2}H_2O \qquad \text{standard SCR} \qquad (28)$$

$$2NH_3 + NO + NO_2 \rightarrow 2N_2 + 3H_2O \qquad \text{fast SCR} \qquad (29)$$

$$4NH_3 + 3NO_2 \rightarrow \frac{7}{2}N_2 + 6H_2O \qquad NO_2 \text{ SCR} \qquad (30)$$

$$2NH_3 + 2NO_2 \rightarrow N_2 + NH_4NO_3 + H_2O$$
ammonium nitrate formation (31)

$$NH_4NO_3 \rightarrow NH_3 + HNO_3$$
ammonium nitrate equilibrium (32)

Scheme 1. Redox Catalytic Cycles of the Standard and Fast SCR Reactions over $V_2O_5-WO_3/TiO_2$ Catalysts[a]

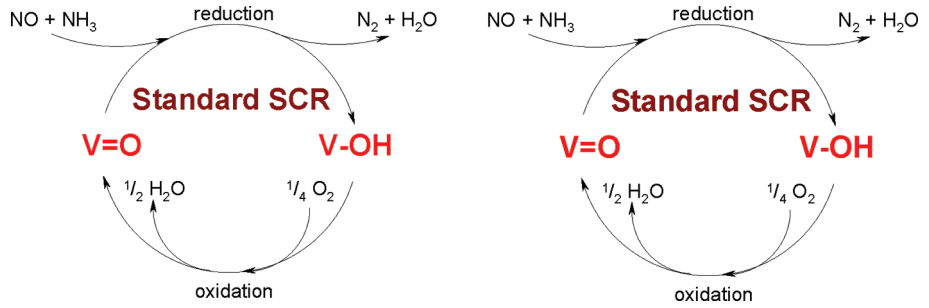

[a] V=O and V−OH are oxidized and reduced vanadium sites, respectively. S=O is a non-reducible oxidic site. Reprinted with permission from ref 281. Copyright 2007 Elsevier B.V.

$$NH_4NO_3 \rightarrow N_2O + 2H_2O \quad \text{ammonium nitrate decomposition} \tag{33}$$

$$NH_4NO_3 + NO \rightarrow N_2 + NO_2 + 2H_2O \quad \text{ammonium nitrate reduction} \tag{34}$$

$$2NO_2 \leftrightarrow N_2O_4 \tag{35}$$

$$N_2O_4 + H_2O \rightarrow HONO + HNO_3 \tag{36}$$

$$HONO + NH_3 \leftrightarrow NH_4NO_2 \tag{37}$$

$$HNO_3 + NH_3 \leftrightarrow NH_4NO_3 \tag{38}$$

$$NH_4NO_2 \rightarrow N_2 + 2H_2O \tag{39}$$

The chemistry described in the above-mentioned reaction sequence underlines the role played by NH_4NO_3 in this process. It involves the dimerization/disproportion of NO_2 and reaction with NH_3 and H_2O to give ammonium nitrite/nitrate, the reduction of ammonium nitrate by NO to ammonium nitrite, and further decomposition to nitrogen. A scheme was ascribed to explain not only the peculiar $DeNO_x$ reactivity at low temperature in the presence of NO_2 and its optimal stoichiometry ($NO/NO_2 = 1/1$), but also the selectivity for all the major N-containing products (N_2, NH_4NO_3, HNO_3, N_2O).

Tronconi et al.[281] investigated by transient reactive experiments NO/NH_3 reaction over a commercial $V_2O_5/WO_3/TiO_2$ catalyst for diesel exhaust after-treatment below 523 K. These experiments pointed out the key catalytic role of the vanadium redox properties that was explained assigning the greater $DeNO_x$ efficiency to the "fast" SCR ($NO/NH_3/NO_2$) and a lower efficiency to the "standard" SCR ($NO/NH_3/O_2$) reaction. They proposed a unifying redox approach in which vanadium sites are reduced by the reaction between NO and NH_3. Afterward they are reoxidized either by oxygen (standard SCR) or by nitrates (fast SCR), with the latter formed via NO_2 disproportion over other nonreducible oxide catalyst components (eqs 40−43, Scheme 1).

Standard SCR:

$$NO + NH_3^* + V^{5+}{=}O \rightarrow N_2 + H_2O + V^{4+}{-}OH \tag{40}$$

$$V^{4+}{-}OH + (1/4)O_2 \rightarrow V^{5+}{=}O + (1/2)H_2O \tag{41}$$

Fast SCR:

$$NO + NH_3^* + V^{5+}{=}O \rightarrow N_2 + H_2O + V^{4+}{-}OH \tag{42}$$

$$V^{4+}{-}OH + NO_3^- + H^+ \rightarrow V^{5+}{=}O + NO_2 + H_2O \tag{43}$$

Vanadium-loaded carbon-based monoliths for on-board NO reduction with ammonia have also been reported.[282] Acid treatment of the carbon support has a strong influence on the reduction of NO.[283] Thus treatment with HNO_3 seems to be more effective than treatment with H_2SO_4 or H_2O_2. Actually the effect of the acidic treatments is closely related to the density of oxygen surface groups created by the oxidation processes.[282] HNO_3 treatment produces the highest number of active surface complexes as carboxyls and lactones, which further enhances the vanadium dispersion and catalytic efficiency. Other metal oxide/active carbon/ceramic monolithic catalysts containing Mn−Fe−Ce and Mn−V−Ce also exhibited both very high efficiency and better tolerance to SO_2 as compared with other supported oxides but also with monometallic and bimetallic Mn or Mn−Ce monolithic catalysts.[284] The adsorption capacity of monolithic catalysts was greatly enhanced due to the attached active carbon.

The role of the vanadium sites in NO and O_2 adsorption processes over supported vanadium was investigated on VO_x/CeO_2-ZrO_2 by means of EPR and IR spectroscopy.[285] Thus, with vanadia deposited on $Ce_{0.10}Zr_{0.90}O_2$ and $Ce_{0.69}Zr_{0.31}O_2$ supports by wet impregnation, better dispersion and higher intrinsic activity of the active sites on CeO_2-ZrO_2 oxides significantly improved the overall activity. Reaction of VO_x/CeO_2-ZrO_2 catalysts with NO led not only to changes in the oxidation state of surface vanadium ions but also to changes in their speciation, resulting in a higher population of more agglomerated reduced oxovanadium species. Subsequent O_2 adsorption on the catalyst surface with preadsorbed NO led to the partial reoxidation of surface vanadium sites and to the formation of O_2^- radicals, accompanied by the formation of surface nitrates. The concentration of cerium is very important in this process. It was found that vanadium is stabilized at the surface mainly in polymeric form for 69 mol % CeO_2, preserving active sites from migration into the matrix, whereas in the case of 10 mol % CeO_2, a relatively large amount of ionic vanadium species is stabilized within the bulk becoming inaccessible to the

reactants from the gas phase (eq. 44).

$$xV_2O_5 + 2(1-x)MeO_2 = 2V_xMe_{1-x}O_2 + \frac{3x}{2}O_2$$

$$\text{where} \quad Me = Ce, Zr \tag{44}$$

Other examples of catalysts include honeycomb structures with an active component, such as Cr, Mn, Fe, Ni, Cu, Ag, Au, Pd, Y, Ce, Nd, W, In, or Ir carried on a carrier composed of TiO_2, a binary oxide such as SiO_2-TiO_2, WO_3-TiO_2, or SiO_2-TiO_2, or a ternary oxide, such as $WO_3-SiO_2-TiO_2$ or $MoO_3-SiO_2-TiO_2$.[286]

4.3.3. Development of Alternative after-Treatment Systems. Another category of NO_x reduction catalysts contains a zeolite exchanged with transition metals and oxidation of the nitrogen monoxide is performed in such a way that the exhaust gas contains 30−70 vol % nitrogen dioxide before contact with the reduction catalyst.[287] Thus zeolites exchanged with specific transition metals have been reported. Preferred transition metals were chromium, iron, nickel, copper, cerium, praseodymium, terbium, or mixtures thereof.

Studies reported by Cavataio et al. [288] showed that base metal/zeolite SCR formulations (Cu- and Fe-ZSM-5) were more thermally stable than a vanadia-based formulation at temperatures typical of diesel applications. Thus, at a hydrothermal aging temperature of 943 K, there was not much change in NO_x reduction performance with NH_3 on Cu/zeolite and Fe/zeolite catalysts. Lower oxygen and higher water concentrations during aging had minimal effect. However, as it was reported before,[13] that longer hydrothermal aging time at a lower temperature (823 K) was more detrimental to NO_x performance, particularly for Cu/zeolite. Like for the case of the SCR with hydrocarbons, Cu/zeolite was active for ammonia oxidation above 573 K with high selectivity for N_2. Fe/zeolite displayed similar behavior but was in general less active, leading to higher NO_x conversion at higher temperatures when the molar ratio of NH_3/NO_x was held at 1. The impact of sulfur was more significant on the Cu-based catalyst than the Fe-based, and mainly noted below 573 K. Both SCR catalysts could be regenerated after exposure to 923 K under lean conditions with mainly SO_2 desorbing.

As mentioned above the impact of sulfur changes with the thermal aging status. Interestingly, the most thermally durable Cu/zeolite SCR exhibits much lower NO_x efficiency after being exposed to the same amount sulfur compared with the less durable one (Figure 29). This result suggested that each base metal/zeolite SCR catalyst has its own characteristic response to sulfur poisoning and thermal durability did not necessarily mean durability to sulfur poisoning. So the sulfur tolerance should be considered equally in addition to the thermal durability in SCR performance for engine applications. The Fe/zeolite SCRs released much lower amounts of SO_2 at higher temperature during the $DeSO_x$ compared with the Cu zeolite SCRs. Thus the control of sulfur poisoning and strategy for $DeSO_x$ is different depending on the formulation.[289]

As for SO_2, the SO_3 aging causes much more significant deactivation for the Cu/zeolite catalysts.[236] SO_2 was the main sulfur compound released during the $DeSO_x$ for the samples aged with SO_2 and SO_3. The amounts of SO_2 released from the SO_3 aged catalysts during the $deSO_x$ were 5−15 times higher than those from the SO_2 aged samples. The NH_3 also interacted with the sulfur compounds formed on the SO_3 aged Cu/zeolite SCR catalysts before the $DeSO_x$.

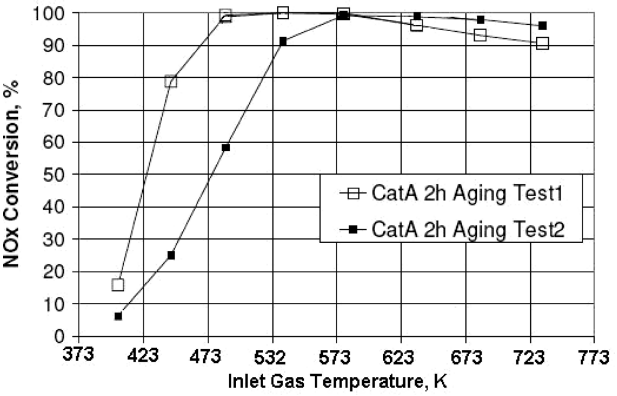

Figure 29. Steady-state NO_x conversions before and after sulfur poisoning for Cu/zeolite SCR catalysts aged at 943 K for 2 h (Test 1 has thermal aging only and Test 2 has thermal aging plus sulfur poisoning (112 ppm)). Reprinted with permission SAE paper 2007-01-1575. Copyright 2007 SAE International.

Base metal/zeolites stored more ammonia at low temperature and less at high temperature.[288] Cu stored more ammonia than Fe catalysts and far more than non-wash-coated cordierite. Exposing the SCR catalyst to less than the saturated value of ammonia at a given temperature resulted in a loss of NO_x performance, except for the Fe catalyst below ~493 K. Fe/zeolite SCR catalyst has less low-temperature NO_x efficiency to lose.[289] In order to compensate for the differences between Fe− and Cu−zeolite based catalysts, the group of Ford[290] suggested the use of a combined Fe−zeolite + Cu−zeolite SCR catalyst system. Indeed, it provides a good compromise between low temperature and high temperature NO_x conversion performance of the two catalysts. The system consisting of 33% Fe−zeolite + 67% Cu−zeolite gave the best overall performance at steady-state conditions. The Cu-only system gave better transient response than the combined system below 573 K. To check the effect of the support in low-temperature SCR of $NO + NO_2$ mixture with NH_3, porous SiO_2 and activated carbon were compared with the traditional TiO_2.[291] It was thus found that the presence of SO_2 and NH_3 was essential for the removal of NO over TiO_2. SO_2 played a crucial role in the oxidation of NO to NO_2 over TiO_2, but with the coexistence of NO and NO_2 in the reaction system, the presence of SO_2 was not essential for the SCR of NO over TiO_2. These results allowed clarification that while reaction 45 occurs over TiO_2, reaction 46 takes place on the three supports

$$NO + NO_2 + 2NH_3 \rightarrow 2N_2 + 3H_2O \tag{45}$$

$$2NO_2 + 2NH_3 \rightarrow N_2 + NH_4NO_3 + H_2O \tag{46}$$

An increase in the nitrogen dioxide content in the exhaust gas greatly improves the efficiency of the reduction catalysts and also decreases aging of the catalysts. In addition, nitrogen dioxide also increases the efficiency of the catalysts, in particular at low temperatures. It is suspected that this positive effect of nitrogen dioxide is based on the fact that the divalent copper ions in the catalyst are reduced to monovalent copper ions due to selective catalytic reduction, which means that their catalytic activity is lowered. As a result of the oxidative components present in the exhaust gas such as oxygen and nitrogen dioxide, the copper ions are reoxidized to divalent copper ions and thus recover their original efficiency. Nitrogen dioxide acts in a

particularly advantageous manner here due to its relatively high oxidizing capacity. This reaction principle applies to all SCR-active transition metal ions, which permit this type of valency change. Except iron, copper and cerium were reported particularly suitable.[287]

Zeolites suitable for this scope are currently ZSM-5, A, beta, X, Y, ferrierite, Linde type L, and faujasite. These zeolites may also be used as a mixture.[287] Exchanged ZSM-5 zeolite with iron or copper showed a particularly high catalytic activity and selectivity for nitrogen production. The formation of side products of the SCR reaction such N_2O was only detected in low amount on Fe−ZSM-5.

A variety of ion exchange processes may be used to prepare such catalysts (solid exchange, exchange in aqueous solution, exchange in polar or nonpolar organic solution). However, the preparation of Fe−ZSM-5 has proven to be especially difficult. Conventional exchange processes in aqueous solution have all proven to be useless because iron(III) compounds can barely penetrate into the pores of a zeolite due to a large hydration shell, and this makes exchange in acid solution very difficult. Exchange in ammoniacal solutions is also unsuitable because iron hydroxide is then formed and precipitates out.[287] Exchange using aqueous solutions of iron(II) salts generally leads in the first place to the oxidation of iron(II) to iron(III), which can be circumvented however by appropriate pretreatment of the solvent with inert gases, such as nitrogen or argon. Apart from iron(II) sulfate and iron(II) chloride, however, only sparingly soluble iron salts are available. With low solubility, the ionic exchange is generally slow. $FeCl_3$ sublimation into H-ZSM-5 represents another alternative to prepare such catalysts.[292] High-temperature $FeCl_3$ sublimation led to active but unstable isolated and hydroxylated iron species ($-Fe(OH)_2$) attached to the ion-exchange positions of ZSM-5.

Copper and iron catalysts based on the ZSM-5 and Cuban natural mordenite zeolites prepared by a conventional ion-exchange method were compared in the selective catalytic reduction of NO using ammonia in presence of H_2O and SO_2 with a commercial catalyst based on $V_2O_5-WO_3-TiO_2$, used as reference.[293,294] Despite the toxicity of vanadium and N_2O formation, $V_2O_5-WO_3-TiO_2$ showed a better NO_x conversion efficiency, while Cu and Fe/MORD do not form N_2O and have better performance than Cu/ZSM-5 or Fe/ZSM-5. The role of the support is indeed very important. Thus, copper-based catalysts supported on mesoporous materials prepared by the impregnation method[295] and tested under similar conditions displayed improved catalytic behavior compared with Cu−ZSM-5 catalyst. Vermiculites intercalated with alumina pillars and modified with transition metals (Cu, Fe) represent another class of microporous catalysts used for the selective reduction of NO with ammonia. Prior to the pillaring process, a raw vermiculite was treated with a solution of nitric acid and then citric or oxalic acid in order to reduce the overall charge of layers.[296] Mesoporous silica SBA-15 modified with copper, iron, Pt, Mn, TiO_x, and VO_x oxides were also studied in SCR of NO by ammonia.[297−300] Clays modified with polymers and promoted with copper oxides were also investigated. The acidic pretreatment and modification with polymer before impregnation with copper were found to improve the efficiency of the clays. However, the performances of these catalysts are modest and addition of copper was consistent with the formation of N_2O.[301] Other investigated systems are carbonaceous materials with N-containing surface groups.[302,303] As N-precursors, gaseous ammonia at high temperature and an aqueous solution of urea, followed by curing in air or nitrogen at 623 K, were proposed. The amount of stable nitrogen introduced into active carbons depends on the nature of the precursors and was less than 4.5 wt %. N-containing species were constituted from mainly pyridinic and pyrrole/pyridone compounds in a close association with oxygen-containing acidic surface species whose type and number depended on the oxidative pretreatment of active carbon, as well as on the curing process. Noteworthy the N-promoted active carbons showed high stability in the temperature range of importance for SCR. Further deposition of metal oxides may improve the performances of these catalysts. Thus, catalysts with large MnO_x distribution (smaller clusters or individual cations) led to lower amounts of N_2O in the products, while bigger aggregates give high amounts of the undesired byproduct.[304]

4.4. SCR of NO_x with Compounds Releasing Ammonia

Several years ago, the European Automobile Manufacturers Association (ACEA for Association des Constructeurs Europeens d'Automobiles, Brussels, Belgium) decided to recommend urea as the precursor for the reducing agent ammonia. In contrast to ammonia, urea is nontoxic and does not require elaborate safety precautions for handling and storage.[305,306] Despite the infrastructure concerns relating to the use of urea in a mobile application as well as the potentially dangerous risks of ammonia break-through or slip, ammonia SCR systems are becoming one of the favored choices for mobile applications to meet the more stringent NO_x emissions. This is, among other reasons, because of the high NO_x conversion percentages possible with ammonia coupled with the ability to optimize the combustion process for maximum power output with minimum fuel consumption.[254]

A more sophisticated approach for mobile applications is to use a compound releasing ammonia.[307,308] While patents discuss reducing reagents in a general sense, they are clearly limited mostly to urea/ammonia reductants. According to this system, a catalytic converter having a typical composition for the reduction of NO_x with ammonia, as an example $V_2O_5-WO_3/TiO_2$ honeycomb catalyst, has a reducing agent storage capacity per unit length that increases in the direction of gas flow. The catalyst is charged with the reducing agent such that transient emissions can be converted by the reducing agent stored in the catalytic converter. Although such a catalyst has shown good performance in many reports and is commercially available, it was found that sustained high-temperature operation can cause catalyst deactivation.[309] Heavy duty diesel engines, which are almost exclusively turbocharged, can produce exhaust gases at greater than 773 K under conditions of high load or high speed, and such temperatures are sufficient to cause catalyst deactivation. Therefore, cooling upstream of the SCR catalyst is important. It may include water injection upstream of the SCR catalyst, or air injection. However, a loss of efficiency of the catalyst was observed using water injection and air injection by modifying the turbocharger leading to higher space velocity over the catalyst, which tends to reduce NO_x conversion.

It is thus preferable to store ammonia on board from a compound that can be hydrolyzed to give ammonia. For this purpose, the hydrolyzable compound is added to the exhaust gas after partial oxidation of the nitrogen monoxide and before contact with the reduction catalyst and then the exhaust gas is passed over a hydrolysis catalyst. However, although the use of a solution of urea (32.5 wt %) dissolved in

water or diesel exhaust fluid is widely used as a source of ammonia, it has a number of issues at low temperature, including freezing below 261 K, solid deposit formation in the exhaust, and difficulties in dosing at exhaust temperatures below 473 K. Additionally, creating a uniform ammonia concentration can be problematic, complicating exhaust packaging and usually requiring a discrete mixer.

Besides ammonia/urea as suitable reductant other reductant fluids including ammonium carbamate may also be considered.[309] Very recently Fulks et al.[310] reviewed a number of other materials as alternative sources of ammonia in order to improve some of the above issues. They found a number of materials showing important properties, including volumetric efficiency (moles of ammonia per liter), mass efficiency (moles of ammonia per gram), and ammonia release. Except ammonium carbamate, metal ammine chlorides (e.g., strontium ammine chloride) were found to offer the most desirable range of properties for use as ammonia source materials.

The control of the *in situ* ammonia formation from urea is however an efficient tool to optimize the reduction in NO_x emissions.[311,312] Several attempts have been reported in this scope. Van Helden et al.[313] using water instead of urea−water solution estimated the concentration of the reducing agent from the water vapor concentration. Wurzenberger and Wanker[314] and Chen and Williams[315] modeled the thermal decomposition as a homogeneous gas phase reaction, and Schaber et al.[316] reported that molten urea evaporates to gaseous urea above 958 K but mainly decomposes directly to NH_3 and HNCO above 973 K. The practical conversion of the aqueous urea solution to ammonia consists of two steps. In the first, the water of the aqueous urea solution sprayed into the flue gas stream evaporates, and urea is thermally decomposed into ammonia and isocyanic acid according to eq 47.

$$H_2N{-}CO{-}NH_2(s) \rightarrow HNCO(g) + NH_3(g) \qquad (47)$$

Isocyanic acid is then hydrolyzed, releasing a second molecule of ammonia and carbon dioxide according to eq 48:

$$HNCO(g) + H_2O(g) \rightarrow NH_3(g) + CO_2(g) \qquad (48)$$

Isocyanic acid also undergoes a series of condensation reactions leading to a variety of solids ranging from cyanuric acid and biuret over ammelide and ammeline and melamine to polymeric forms of melamine resulting in a decrease of decomposition efficiency or a decrease in NO_x reducing performance at the downstream location.[317,318] These latter high molecular weight compounds accumulate on the walls of the exhaust pipe and inside the monolith channels. They are only slowly decomposed under typical reaction conditions. Hence, the catalysts have to be adapted in order to maximize hydrolysis and to minimize condensation/oligomerization of isocyanic acid.

Several models were proposed in the literature to simulate the catalysts' DeNO$_x$ SCR performances. Tronconi et al.[319] reported a complete model of SCR monolith reactors involving NO_x reduction and SO_2 oxidation reactions. An analytical SCR model based on a Tempkin isotherm was developed by Kim et al.[320] to simulate NO_x reduction performance, NH_3 adsorptive properties, the amount of NH_3 slip, and formation of N_2O on metals supported on zeolites. The model was based on experimental data including standard SCR reaction, fast SCR reaction, NH_3 oxidation, N_2O formation, and NO oxidation to NO_2. The predicted data based on the calibrated kinetic parameters showed very good agreement with the test results over the simulated temperature ranges selected to cover a broad range of diesel engine operating conditions. Noteworthy, the model was further validated by vehicle data using an assumption of urea efficiency (80−90%), which considered urea conversion to NH_3, urea mixing, and radial distribution urea efficiency.

Based on SCR performance time and temperature limits, the same group developed simple mathematical equations that related the threshold temperature to the threshold duration time for vehicle application.[321] The transfer functions characterize the NH_3 storage capacity and the BET surface area results as functions of both aging time and aging temperature. From these functions, a NO_x conversion transfer function was also developed that predicted the NO_x conversion vs the measured NO_x conversion within 10% margin of error. Based on it, the removal of nitrogen oxides can be carried out at high efficiency with less variation range for denitration ratio and with extremely less ammonia discharge, which would otherwise cause secondary public pollution.

4.4.1. Hydrolysis of Urea and Related Compounds. Hydrolysis of urea and isocyanic acid can be activated over TiO_2.[318] TiO_2 is an efficient catalyst for the hydrolysis of HNCO to NH_3 and CO_2 over a broad temperature range, that is, above 423 K. In the absence of water, the dissociative adsorption of isocyanic acid produces OH groups or water and Ti−NCO groups. At a longer time of exposure, the formation of cyanuric acid occurs indicating that some of the isocyanic acid molecules do not dissociate and are able to be added to NCO^- groups. In the presence of water, the hydrolysis dominates the surface chemistry so that only the more basic product (ammonia) and the reactant (water) can be directly observed. However, in the presence of additional NO, NH_3, and NO_2 in the reactant gas stream, the reaction rate decreases, when the catalyst runs in chemical regime. While ammonia had little impact on the surface concentrations measured during hydrolysis, the presence of NO and NO_2 led to the accumulation of NCO^- on TiO_2. With NO_2, the surface is quickly covered with nitrates, suggesting that nitrates block catalytically active sites for hydrolysis and delay the conversion of isocyanic acid.

The deposition of a metal like copper on TiO_2, or other supports able to hydrolyze urea like Al_2O_3 and SiO_2, showed that catalysts are active for the selective reduction of NO_x with NH_3 but are inactive for its reduction using solutions of urea.[322] Poisoning of the surface by H_2O_{ads} was suggested, but it is not responsible for all of this decrease in efficiency, and it was postulated that the urea is not hydrolyzing to form NH_3 over these supported catalysts but rather is oxidizing to form N_2 or forming passivated layers of polymeric melamine complexes on the surface.

The influence of urea on the evaporation of urea−water solution has been extensively studied by Birkhold et al.[312] who reported that the decrease in vapor pressure due to increasing concentration of urea in the droplet results in a continuous increase of the droplet temperature and a slower evaporation compared with pure water. Description of the evaporation process on the basis of different physical models allowed the prediction of urea concentration and the temperature of the urea aqueous solution droplets as well as urea particles, which is important for the understanding of their impingement on catalyst and wall. Also, the measuring of the conversion into gaseous reducing agents, NH_3 and HNCO, serves as boundary condition for dimensioning the catalytic converter in which the reduction of the NO_x by ammonia will be conducted. It results

that in real exhaust configurations the urea−water solution does not evaporate and decompose completely. The catalyst must have a sufficient capability for the hydrolysis reaction, especially at temperatures below 1118 K when no significant hydrolysis in the gas phase occurs. Catalysts or surfaces of the exhaust gas system are important parts for spray mixing and reducing agent preparation.

Application of Fe−zeolites for ammonia- and urea-SCR of NO_x in diesel engine is limited by catalyst deactivation with hydrocarbons.[323,324] However, at high temperatures and in the presence of O_2, the carbonaceous deposits will be oxidized to CO_2, and the efficiency can be partially restored after removing of propene. While it is difficult to burn off the carbonaceous deposits at 473 K in the presence of O_2 with the strong oxidant NO_2, the activity did not decrease at this temperature since the carbonaceous deposit is hardly formed on the surface of zeolites under these conditions. As a result, the reaction of NH_3-SCR is still fast in the feed of NO_2. With the increase of temperature, the rate of carbonaceous deposit increased showing that the rate of carbonaceous deposit is higher than the rate of oxidation and decomposition with NO_2 at high temperatures.

The effects of hydrothermal aging of Cu/zeolite urea-selective catalytic reduction catalysts on their reactivity and material properties were assessed by performance tests and multiple characterization techniques. Differences in behavior were found upon application of three aging protocols that consisted of varying temperature during hydrothermal aging with or without exposure to aqueous urea solution.[325] The combination of urea and high-temperature exposure increased the deactivation of Cu/zeolite SCR catalysts beyond that observed by hydrothermal aging alone, with an immediate high-temperature exposure following wetting of the catalyst core with aqueous urea causing the most significant deterioration in performance.

4.4.2. Lean-Burn Oxidation Catalysts. Reducing engine emissions resulting from cold start is a major impediment in meeting emissions standards. For late-model gasoline engines, nearly 60−70% of the total hydrocarbon emissions occur during the cold start. In diesel engines, while the total hydrocarbon concentrations resulting from conventional combustion modes are low, advanced combustion strategies, such as premixed compression ignition, are being used simultaneously to reduce soot and NO_x that tend to produce significant amounts of total hydrocarbon and CO.

A diesel oxidation catalyst that can oxidize all the total hydrocarbon and CO is being proposed to meet the emissions standards in these scenarios. Otherwise, the hydrocarbons would be stored by the subsequent zeolite catalyst. This would be associated with the risk of coking and deactivating the zeolite catalyst. Suitable oxidation catalysts can be used in such a process containing platinum dispersed on metal oxide supports having high specific surface area, preferably γ-alumina. Further stabilization with ~5 wt % SiO_2 makes the system even more beneficial.[287] Additionally, Pt or Pd catalysts deposited upon a ceramic or metal through-flow honeycomb support might be also very suitable. While such an oxidation catalyst is efficient in reducing HC and CO emissions after it is fully warmed, other strategies are being researched to address the cold start engine emissions.[326]

These catalysts have however an important drawback related to a partial volatilization of noble metals during oxidation. It was recently pointed out that there is a high potential for the SCR catalyst to be poisoned by trace levels of Pt from an upstream diesel oxidation catalyst.[327,328] For example, Pt is very efficient for oxidizing NH_3 even at very low concentrations. This is a potential issue for SCR systems because if the front portion of the SCR catalyst is poisoned with Pt, the NH_3 is consumed and the remainder of the SCR catalyst volume cannot function since there is no NH_3 present.

Free noble metal catalysts have also been reported for NO oxidation and NO_x reduction.[329] Among these catalysts, Co_3O_4-based catalysts are the most active ones for both NO oxidation and NO_x reduction reactions in the fast selective catalytic reduction process even at high space velocity and low temperature. Also, the effect of SO_2 concentration on NO_x reduction was found to be almost negligible after WO_3 addition, which resists SO_2 oxidation. Other suitable SCR catalysts include Cu-based catalysts[13] and $LaCo_{1-x}M_xO_3$ (M = Ru, Fe) perovskites.[330]

Typically the reductant is pulse metered into the exhaust gas stream in a manner similar to that used for operating conventional fuel injectors.[331−333] The state of the art has recognized that changes in load from the turbine, furnace, etc., affects the ammonia SCR systems. The variations in load can be determined by sensing the temperature of the exhaust gas.[334] When the exhaust gases are at certain temperatures, a variation in the load is assumed to occur and different or predicted molar NH_3/NO_x ratios are used to account for the adsorptive properties of the catalyst.

The soot-type particulates may also be removed from a particulate trap by "combustion" at relatively low temperature in the presence of NO_2. The incorporation of such a particulate trap avoids accumulation and subsequent back-pressure problems, while simultaneously reducing a proportion of the NO_x.

Hydrocarbon storage modeling for diesel oxidation catalysts offers an elegant solution to optimize this process. Sampara et al.[326] proposed a simple hydrocarbon storage model that describes the adsorption−desorption processes in zeolites incorporated in a diesel oxidation catalyst. The equilibrium data and the remaining rate constant capturing the adsorption time scale were obtained by fitting a Langmuir isotherm. The model considers a typical diesel oxidation catalyst that contains both a storage component (zeolite) and noble metals (for oxidation) using a full scale 1D reactor model, which includes the storage kinetics developed with the oxidation kinetics.[335] Simulations of a simplified warm-up process indicate that the zeolite storage component reduces the overall cold start HC emissions by at least a factor of 2 if the warm-up rate achieves 45−65 K min^{-1}, a range commonly observed during start-up.

4.5. Recent Development of Silver-Based Catalysts for the Selective Reduction of NO_x: Impact of Hydrogen on Mechanistic Features and Nature of Active Sites

4.5.1. Silver-Based Catalysts for SCR with Hydrocarbons. Clearly the use of noble metals is inadequate in the presence of an excess of oxygen because they are nonselective. As was above-mentioned, SCR is very efficient for NO_x reduction as long as the exhaust temperature is within the active temperature range of the catalyst (e.g., >573 K). Unfortunately diesel exhaust temperatures are considerably lower than that required for obtaining good catalyst efficiency (i.e., below "light-off"). This is especially true for light duty applications, which operate at light load for the most part, resulting in very low exhaust temperatures (423−523 K). Even diesel trucks operate under conditions that result in exhaust temperatures below the optimum temperatures for SCR catalysts. Unfortunately, one of the best, most stable SCR catalysts, which is of the

Scheme 2. Reaction Mechanism of NO_2 Reduction with Propene on Ag/H Zeolites [a]

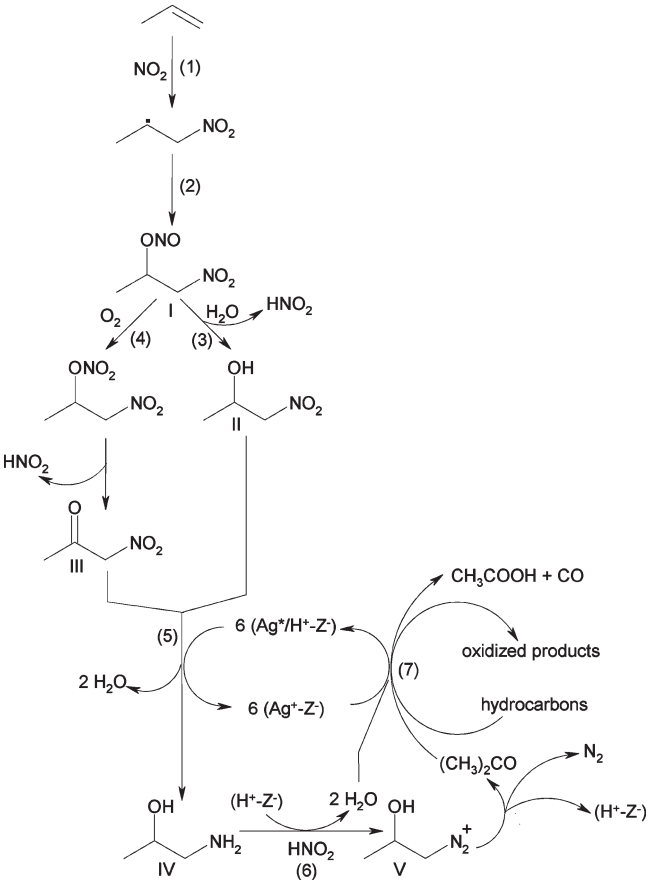

[a] Reprinted with permission from ref 337. Copyright Wiley-VCH Verlag GmbH & Co. KGaA.

zeolite type (e.g., Fe-Beta Zeolite), also has the highest optimum operating temperature. As a result, its effectiveness is greatly diminished at temperatures of interest.[336]

More than 10 years ago silver/proton-exchanged zeolites were reported to represent a very active redox system that outperforms the known catalysts for reduction of NO_2 and is devoid of their disadvantages.[337] In the presence of an excess of oxygen, silver is the only transition metal ion that does not segregate from the zeolite.[338,339] Hence, the stability of the catalyst depends entirely upon the steam stability of the H zeolite. The zeolite framework, its Bronsted acidity, and the specific redox behavior of silver in association with the zeolite were reported as the three key catalyst functions that cooperate to form nitrogen from NO_2 via intermediate nitro, amino, and diazonium compounds. Using a synthetic gas mixture that mimics the exhaust composition of a lean-burn engine with NO_2 as the NO_x component (400 ppm NO_2, 350 ppm propene, 350 ppm CO, 10 vol % CO_2, 10 vol % O_2, and 12 vol % H_2O, balance helium), Martens and co-workers[337] showed that silver ferrierite and mordenite were highly active, particularly Ag/H-FER, with 60% of the NO_x converted into N_2 between 523 and 723 K.

This remarkable catalytic stability was assigned to the low tendency of silver cation in zeolites to undergo hydrolysis and the thermal stability of silver oxide particles. In addition, irrespective of the position or degree of sintering of the metallic silver clusters formed by reduction, the zeolite can be restored to its original form by oxidation (eq 49).

$$n(Ag^+\text{-}Z^-) \xrightarrow[n/2\ H_2O\quad n/4\ O_2]{nH^0} n\,(Ag^0)/\,n\,(H^+\text{-}Z^-) \qquad (49)$$

Scheme 2 describes the reaction mechanism proposed by these authors.[335]

Furthermore She et al. reported a stabilizing effect on the structure and activity of Ag/Al_2O_3 for the selective catalytic reduction of NO_x with CH_4 imparted by the presence of SO_2 in the exhaust gas mixture.[340] The reaction was carried out above 873 K to keep the surface partially free of sulfates. In SO_2-free gases, fast deactivation results in sintering of silver from well-dispersed clusters to nanoparticles and to micrometer-size particles. The structural stabilization by SO_2 was accompanied by stable catalyst efficiency for reduction of NO to N_2 that acts together with the suppression of the direct oxidation of methane.

There are arguments indicating that the selective catalytic reduction of NO_x by CH_4 on silver is structure-sensitive.[341] Pretreatment of Ag−H-ZSM-5 zeolite strongly influences the catalytic performances. Upon thermal treatment in an inert gas stream, thermally induced changes in silver morphology led to the formation of metallic Ag clusters and particles having initially higher activity but lower selectivity for the CH_4-SCR of NO_x. Reaction induces the formation of ill-defined silver oxides, which impacts the adsorptive properties and the diffusivity of oxygen over silver catalysts. Such surface reconstructions lead to a decrease in activity but an enhancement of the selectivity of Ag−H-ZSM-5 catalyst.

In the HC-SCR, the $DeNO_x$ activity of Ag/Al_2O_3 increases with increasing carbon number of alkane reductants.[342,343] Under these conditions, a correlative increase in the rate of alkane oxidation to oxygenates as a possible intermediate is also observed.[344] It was found that oxidation of NO or decane by oxygen is greatly affected by the presence of decane or NO.[345] Monodentate nitrates are formed preferentially and are more reactive compared with the bidentate species. Oxidation of decane mostly yields surface acetates, and the presence of NO_x favors the formation of formates (acrylates). The reaction steps enhanced by the addition of hydrogen to the SCR-NO_x reaction are predominantly the transformation of −CN species into −NCO and hydrocarbon to formates (acrylates). Although NO−NO_2 oxidation is also enhanced by hydrogen, this effect does not contribute to the increased rate of the SCR-NO_x reaction. A small part of very reactive Ag^+ (estimated to be <5%) was reduced to metallic charged $Ag^{n\delta+}$ clusters ($n \leq 8$) during both the decane- and H_2/decane-SCR-NO_x reactions. The number of $Ag^{n\delta+}$ clusters formed depends mainly on the level of NO conversion to nitrogen, regardless of whether the conversion level was attained by the addition of hydrogen or by an increased concentration of decane or oxygen in the feed.

There are also studies proposing a bifunctional reaction mechanism in the HC-SCR on Ag/Al_2O_3 catalysts. It was thus reported that *n*-octane is broken up into smaller hydrocarbon molecules that are then subsequently oxidized to form various aldehydes, while ethanol is also rapidly converted to acetaldehyde.[346] At the same time, NO is oxidized effectively to NO_2 in the presence of reductants. Then more reactive hydrocarbon species (i.e., smaller alkenes, oxygenated hydrocarbons) react with NO_2 over the Ag and Al_2O_3 sites, leading to

N_2. This approach offered an opportunity to improve the overall NO_x reduction performance of Ag/Al_2O_3. Thus, the concept of a staged catalyst system has been examined using Ag/Al_2O_3 for the formation of reaction intermediates and a secondary catalyst (e.g., Al_2O_3 or BaY) for the subsequent N_2 production reaction.[346]

The role of the various oxygenated hydrocarbons in the efficiency of Ag/Al_2O_3 for HC-SCR has been indeed proven after using different types of reductant (Et_2O, ETBE, EtOH, 1-propanol, 2-propanol, *t*-butanol, 1-propanal, ethyl acetate, acetone, C_3H_8).[347] Among these reductants, Et_2O was most effective for achieving high $DeNO_x$ efficiency for HC-SCR and H_2-HC-SCR. However, the degree of the efficiency enhancement was higher for C_3H_8 than for oxygenates. This is consistent with the previous proposal that H_2 enhances $DeNO_x$ efficiency by promoting the oxidative activation of alkane into partially oxidized hydrocarbon intermediates.[344]

4.5.2. NO_x Reduction Using a Reformate Atmosphere. As previously discussed, direct decomposition or reduction of NO_x using residual hydrocarbons present in the exhaust is the most ideal; these reactions do not show sufficient activities in running conditions, especially at low temperature. The use of hydrogen in combination with hydrocarbons has been reported to boost the $DeNO_x$ catalytic activity at temperatures as low as 423 K especially when the active component is silver and overcomes the drawbacks associated with the current technologies for diesel exhaust NO_x removal.[212,213,348−351] Burch et al. assigned the role of hydrogen to its chemical capability to destroy nitrate species that are strongly adsorbed on silver sites, generating nitrite species that can be easily decomposed and reduced to N_2.[352] Thus, hydrogen becomes very effective in regenerating LNTs of stored NO_x. Arve et al.[353] attributed a suplementary role of hydrogen to improved oxidation of the hydrocarbons resulting in the faster formation of amines, which react with activated NO.

The "hydrogen" effect seems to be limited to Ag-based catalysts with γ-Al_2O_3 and MFI zeolite[354,355] as the most effective supports. There is a general agreement that the catalytic activity is promoted by the reductive activation of O_2 with H_2 and the generation of moderately agglomerated Ag_n^+ clusters on the catalyst surface.[356,357] However, there are also investigations that claim that Ag_n^+clusters are not essential for the enhancement of the SCR efficiency and that hydrogen itself participates directly in the reaction mechanism.[356]

Burch reported marked differences in the NO_x conversion for a given catalyst when using different reductants.[357] Diesel fuels contain, in addition to straight hydrocarbons, various cyclic and aromatic compounds. Aromatics and cyclic compounds were reported to exhibit a detrimental effect on NO_x conversion during the SCR reaction because they cannot be oxidized below 673 K.[353,358]

Although H_2-assisted SCR offers significant promises for lean NO_x treatment, the concentration of H_2 in the diesel exhaust is too low for effective cleanup. There is a possibility that fuel optimized engines combined with a urea-SCR system could reduce fuel consumption by 7%, resulting in less CO_2 emission in a global perspective.[359] Therefore, a practical source of H_2 needs to be available on-board a vehicle. New tehnological solutions were proposed in this scope.[360] The silver-based materials also demonstrate good efficiency for the reduction of NO_x with ethanol. The addition of aluminum to Ag-SBA-15 decreases the oxidation of ethanol at high temperatures and simultaneously enhances the reduction of NO_x to N_2.[361] Ag/Al_2O_3, Ag_3PO_4/Al_2O_3, Ag_2SO_4/Al_2O_3, and $AgCl/Al_2O_3$ catalysts showed also high activities for the selective catalytic reduction of NO_x by ethanol.[362] Among these, $AgCl/Al_2O_3$ gave the highest catalytic turnover frequency. The catalytic test and characterization results confirm that Ag^+ is the active silver species for NO_x reduction. A very good correlation has been demonstrated between the high dispersion of Ag^+ and the formation of active intermediates (enolic and −NCO species). The use of the precipitable silver technique was found thus to facilitate the preparation of monolithic Ag/Al_2O_3 catalysts for practical usage.

The reverse microemulsion technique can also provide effective Ag/Al_2O_3 catalysts, in which the dispersion and homogeneity of silver is highly ensured. These catalysts can operate in the presence of ethanol as reductants in lean conditions like the diesel engine or those of gasoline direct injection.[363] A promoting effect for the SCR of NO_x by ethanol can be obtained after palladium addition to Ag/Al_2O_3[364] between 573 and 623 K obeying the Euro III standard for NO_x emission control in diesel engines. The performance of Ag/Al_2O_3 was also evaluated on real diesel engines with an integrated after-treatment system composed of a mixture of Cu/TiO_2 and Pt/TiO_2 using ethanol as reductant dosed via a loop control.[365] The NO_x conversion efficiency went up with an increase of the ethanol dosage, but it caused a significant increase of CO and HC emissions simultaneously. Additionally, Ag/Al_2O_3 effectively reduces the soluble organic fraction in particulate matter but has no effect on dry soot. Dimethyl ether has been used with the same scope. Lean reduction of NO_x with DME occurs with high selectivity to N_2 over Al_2O_3 between 573 and 823 K with lower selectivity over Ag/Al_2O_3 due to the catalysts' sensitivity to gas-phase radical reactions and the efficiency for NO_x reduction with methanol.[366]

The addition of low levels of sulfur (1 ppm SO_2) to the H_2-promoted SCR reactant stream had different effects depending on the temperature at which the reaction took place.[357] This is actually related to the catalysts' efficiency for the oxidation of SO_2 to SO_3 and the subsequent stabilization of silver sulfate. While at low temperature, no significant deactivation takes place, at intermediate temperatures (573−673 K), sulfates are readily formed on the catalyst surface and deactivation is severe. Above 773 K, no deactivation is discernible due to the low thermal stability of silver sulfate. However, even for intermediate temperatures, the deactivated catalyst could be almost fully regenerated by hydrogen-containing regeneration mixes.

Primarily, the function of H_2 seems to be connected with a specific promotion of NO oxidation.[174] This was suggested from the finding that the admixture of H_2 favors the formation of nitrato species during interaction of the sample with NO/O_2, whereas it hinders the formation of these species in the case of NO_2 adsorption. H_2 interferes with the kind of species formed on the Ag surface, and during NO_2 adsorption, the admixture of hydrogen causes the reduction of Ag^+ ions at the surface and additionally the reduction of adsorbed NO_x species. Both effects prevent abundant formation of stable nitrato species and favor the formation of largely unstable nitro and nitrito species.

Ag/Al_2O_3 catalysts also exhibit a very high water and oxygen tolerance.[367] They did not deactivate during simultaneous H_2O and O_2 exposure for 24 h even at 1173 K, which is likely due to the formation of a stable aluminate.

An increase of the Ag/Al_2O_3 catalyst stability was recently reported upon changing the preparation procedure.[368] Silver colloids prepared by reducing $AgNO_3$ in aqueous solution with sodium citrate were embedded in alumina following a sol−gel

procedure. By this methodology, the particle size of silver was preserved not only during $DeNO_x$ reactions but also during exposure to ozone or plasma. The thermal aging led to an enhancement of the conversion of NO parallel to slight alteration of the selectivity with the appearance of low amounts of N_2O despite an increase of Ag^+ species. This suggests that an optimal surface Ag^0/Ag^+ ratio is needed, independently of the size of silver particles. This optimal ratio is induced by the operating conditions during the synthesis route.

The effect of temperature and transient addition of H_2 to the NO_x−SCR reaction showed that the addition and removal of hydrogen had a marked effect on the nitrogen balance at temperatures ranging from 518 to 673 K.[369] At low temperatures (518 K), the addition of hydrogen resulted in the storage of NO_x, whereas the reverse was true at 673 K where NO_x was stored upon removal of hydrogen from the feed. The transient NO_x storage effect could be harnessed to allow continuous high NO_x conversion with intermittent hydrogen addition.

4.5.3. Silver-Based Catalysts for SCR with Ammonia. Richter et al. discovered an unusual activity enhancement of Ag/Al_2O_3 for NH_3-SCR.[370,371] After their discovery, this application was extended to urea since urea hydrolysis on acidic materials such as alumina yields NH_3 and CO_2. Ag/Al_2O_3 was also found to be an effective catalyst for H_2-assisted urea-SCR. Furthermore the addition of 0.5% H_2 in the selective catalytic reduction of NO by urea caused a drastic improvement of NO reduction efficiency of Ag/Al_2O_3.[372] The high NO conversion under high GHSV conditions in a wide temperature range and high SO_2 tolerance made this catalytic system attractive for industrial application. Due to its high efficiency for H_2-assisted HC-SCR reaction at high temperature (773 K), there is a possibility of using urea-free $DeNO_x$ catalysis at high temperature. These properties make it suitable for diesel $DeNO_x$ catalysis, which should be operated under transient conditions in a wide temperature window.

4.6. Synergistic Effects in SCR of NO_x

Synergism is frequently considered as a useful means to affect the catalysis. In the selective catalytic reduction of NO_x[373] using methane and propane and mechanical binary mixtures of commercial Fe−Cr-oxide, Ni−Cr-oxide and Cu−Zn−Al-oxide catalysts that do not contain noble metals, it is possible to achieve such an effect. In the case of the Ni−Cr-oxide and Cu−Zn−Al-oxide, hydrogen formed over the former catalyst in alkane oxidation migrates through the gas phase to the latter catalyst where NO_x is activated with the formation of nitrate structures, which interact with hydrogen giving the products of the overall reaction, N_2 and H_2O. In the presence of the catalyst mixture, the interaction of alkanes and O_2 over Ni−Cr-oxide gives stable products of partial oxidation or oxidative dehydrogenation, which are transported due to interphase diffusion to the Zn−Al-oxide surface.

Single and bimetallic silver-modified Ag−M-ZSM-5 (M = Zr, Cu) and Ag/Al_2O_3 catalysts were synthesized for the same scope using different methods of preparation.[374] It was thus reported that the main drawback for the Ag/Al_2O_3 catalyst can be compensated by combining it with Ag−H-ZSM-5 in a dual bed system. When placed downstream of the Ag/Al_2O_3 catalyst, the silver-modified ZSM-5 catalyst enhances the efficiency of Ag/Al_2O_3 in the low temperature region and also completely oxidizes CO and unburned hydrocarbons. However, several attempts also report that a combination of commercial platinum oxidation catalyst (Johnson Matthey) and Ag/Al_2O_3 leads to unsuccessful results, for instance, when a Pt oxidation catalyst is directly placed after the Ag/Al_2O_3 catalyst with a subsequent decrease of NO_x conversion by about 50%.[375] Subsequent improvements by combining Pt(Pd) with manganese oxide were also reported.[376] MnO_x supported on cordierite monolith wash-coated with γ-Al_2O_3 and MnO_x supported on granulated γ-Al_2O_3 and subsequently modified by doping with 0.1−1.0 wt % Pt or Pd showed a very good efficiency in methane oxidation. However, the extent of the synergetic effect strongly depends on the nature of the platinum precursor.[377]

An improved NO_x removal efficiency was also reported with a combination of model Pt−Rh/Ba/Al and Cu-ZSM-5 catalysts using periodic fluctuations between lean (100 s) and rich (10 s) atmospheres.[378] The mixed catalyst showed a NO_x removal efficiency almost double at 523 and 573 K compared with a system where Pt−Rh/Ba/Al catalyst is located upstream and Cu-ZSM-5 downstream in the gas flow. The effective role of Cu-ZSM-5 is to store NH_3 formed on Pt−RhBa catalyst in rich conditions, to catalyze the NH_3-SCR, and also to provide enough CO, which reacts with NO_x to form NCO species as an intermediate on Pt−Rh/Ba/Al catalyst. These NCO are further hydrolyzed to NH_3 under lean conditions, which acts as a reductant for NO_x.

The catalytic performances of mixtures of NSR Pt−Rh/Ba/Al_2O_3 catalyst with Ag/Al_2O_3, Co/Al_2O_3, or Cu/ZSM-5 were also evaluated for NO_x removal under lean−rich atmosphere.[379] In addition to Cu/ZSM-5 NO_x, the removal efficiency was also increased by adding Co/Al_2O_3 or to Pt−Rh/Ba/Al_2O_3 while adding Ag/Al_2O_3 had no significant influence. Experiments performed by using two catalytic beds (upstream Pt−Rh/Ba/Al_2O_3 and downstream Co/Al_2O_3 or Cu/ZSM-5) suggested that both SCR catalysts are able to reduce NO_x with the NH_3 produced during the rich step on Pt−Rh/Ba/Al_2O_3. The highest efficiency was obtained by using both CO and H_2 as reductant during rich pulses.

A synergistic effect has also been reported on a series of nanocomposite BaO−Fe-ZSM-5 materials that have been investigated to determine the feasibility of combining NO_x trapping and SCR-NH_3 reactions to develop a system that might be applicable to reduce NO_x emissions from diesel-powered vehicles.[380] This system provides: (a) BaO to trap NO_x, (b) hydrolysis sites to convert urea quantitatively into $NH_3 + CO_2$, (c) acid sites to trap any excess NH_3 and prevent NH_3 slip, and (d) redox active sites to catalyze the NO/NH_3 reaction. The presence of Ba with Fe within a ZSM-5 framework enhances the NO_x adsorption and decreases the NH_3 adsorption capacity. Mixing Fe_2O_3 with InH-zeolites (ZSM-5 and mordenite) for the selective catalytic reduction of NO_x with methane and butane revealed that in addition to the increase of the catalytic performance, the presence of iron oxides also improved the durability of the catalyst in the presence of water.[381]

Bifunctional materials comprising a metal-exchanged zeolite of different zeolite frameworks (BEA, FAU, FER, MFI, and MOR) with various Si/Al ratios coated by a metal oxide layer have been prepared and shown to be efficient for the selective catalytic reduction of NO using propylene as a reductant.[382] The use of a nanoparticle sol as metal oxide source provides a method for preventing the insertion of the oxide inside the zeolite pores. These particles adhere to the external zeolite surface and do not form separate oxide particles as in a physical mixture. The temperature benefits obtained by the coating technique largely exceed those observed for coexchanged Ce, Cu zeolites, or

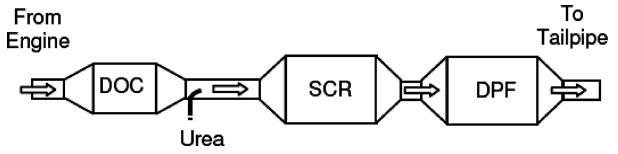

Figure 30. Example of a typical diesel after-treatment system including DOC, SCR, and DPF. Reprinted with permission from SAE paper 2009-01-0897, Copyright 2009 SAE International.

physical mixtures of the functional phases, and the particular topology offers an efficiency enhancement in the presence of water.[383] The affinity toward water and extended coverage of the coating protect the zeolite against degradation by restricting the diffusion of water molecules into the zeolite pores.[384]

4.7. Concomitant Soot and DeNO$_x$ Removal

Presently most of the world's automakers are concentrating on developing and using diesel particulate filters to trap soot from the exhaust gas.[385] While trapping has been solved, the filter regeneration (soot combustion) is a subject of concern, and actual solutions are not fully optimized. The commercialized DPF regeneration technologies are either additive-based, catalyzed filter-based, or continuous regenerating filter-based.[386] There are many known filter structures that can be used to remove particulates from diesel exhaust, including honeycomb wall-flow filters, wound or packed fiber filters, open-cell foams, sintered metal filters, etc. However, ceramic wall-flow filters have received the most attention. These filters are capable of removing over 90% of the particulate material from diesel exhaust and thus can meet this emissions reduction goal.[386] The filter is a physical structure for removing particles from exhaust and the accumulating particles will increase the back pressure from the filter on the engine. Thus particles that accumulate have to be continuously or periodically burned out to maintain an acceptable back pressure level. Unfortunately, the removal of carbon soot particles under lean exhaust conditions requires temperatures (773−823 K) higher than typical diesel exhaust temperatures.

Much progress has been made on improving performance of the DPFs.[387,388] The SCR system complexity can be reduced further by the implementation of SCR-coated DPFs (SCRFs). In this system, a high-porosity (>50%) filter substrate is coated with an SCR formulation, ideally in the pores of the filter walls, so that the DPF and SCR functions can be combined into a single catalyst (Figure 30). The presence of a catalyst to provide soot combustion and thereby regeneration of the filter at temperatures accessible within the diesel engine's exhaust under realistic duty cycles could be another solution. In this way, a CSF or CDPF can be an effective way to provide for >90% particulate reduction along with passive burn-out of the accumulating soot and thereby filter regeneration.

As mentioned above, the SCR washcoat is ideally coated inside the pores of a DPF rather than on the substrate surface, allowing room for adequate SCR washcoat and open DPF channels for gas flow and soot storage. For this scope, Cu/zeolite washcoats were successfully coated on highly porous cordierite and SiC filters. Using this concept, it was reported that the addition of NO_2 in the inlet gas to the SCRF was beneficial up to 50% and then became detrimental to NO_x performance.[388] Soot loading on the SCRF in the engine dynamometer reduced NO_x conversion by as much as 10% between 423 and 698 K, most likely due to coking of the SCRF.

When presented with NH_3, catalyzed diesel particulate filter will primarily convert all NH_3 to (i) N_2O at lower temperatures (below approximately 623−773 K) or (ii) NO_x at higher temperatures (above approximately 623−773 K). Some NO_x and N_2O formation occur over NH_3 slip catalysts but substantially less than that for a catalyzed diesel particulate filter.[390] To allow the cleanup catalyst to function under rich conditions, the catalyst may include an oxygen-storage component, such as ceria.[391] The soot particles trapped by the particle filter can be burned when the engine is supplied with a fuel containing additives capable of lowering the temperature. The composition of the particle filter includes an iron oxide (from ferrocene, iron acetylacetonate, naphtenate, or fatty ester compound) or a mixed iron and cerium oxide.[392,393]

In stationary applications, a number of arrangements routinely use filters upstream of an SCR catalyst with an ammonia reductant injected between filter and SCR catalyst. However, all the temperatures for SCR are high, and the filters, discussed generally, are of the dust particulate type such as electrostatic precipitators.[336] Hug et al.[261] proposed a system in which NH_3 is injected above catalyst beds containing an SCR followed by an oxidation catalyst. The soot filter is catalytically coated to regenerate or burn off the soot at 723 K. It is described as a fibrous bundle, which filters fine soot particles from the exhaust stream that have a carcinogenic effect and is provided in a casing adjacent to an upstream SCR reactor and oxidation catalyst. This system has been applied to a ferry and other large diesel engine applications operating for the most part at steady speeds and higher temperatures than the vehicular applications. In another arrangement of the catalyst, a particulate filter is placed between a NO_x absorber that is periodically regenerated and an oxidation catalyst consisting of supported noble metals (platinum or palladium or a mixture of these).[393,394]

Recently the use of CSF with more complex functions was proposed.[336] Accordingly, an after-treatment system configured with a CSF combining an active oxidation species (Pt), an oxygen storage component (CeO_2), and a binder (ZrO_2) (Pt/ZrO_2−CeO_2) above a zeolite SCR catalyst was suggested to produce substantially better NO_x conversion performance than the zeolite alone, especially for higher normalized stoichiometric ratio levels of reductant and at lower exhaust temperatures. Particularly, the CSF and Fe-Beta-zeolite configuration make the SCR more viable for light duty diesel applications. According to this technology, better utilization of *in situ* NH_3 from the hydrolysis of injected urea aqueous solution than the SCR catalyst alone configuration is reported with very low NH_3 slip under all conditions. This configuration appears as a viable after-treatment system for simultaneous high level (e.g., >80%) reduction of NO_x for diesel engines. Other noble metal-promoted catalysts for this scope contain a combination of Rh and K/La_2O_3.[395] Pt and Rh addition favors the preferential formation of lanthanum oxycarbonate during the calcination step. K/La_2O_3 adsorbs NO_x through the formation of La and K nitrate species when the solid is treated in NO + O_2 between 343 and 763 K. Nitrates become unstable at 633 K particularly in the presence of Rh.

4.7.1. Noble-Metal Free Oxidation Catalysts. Other types of CSF can be used as well although the preferred type is still the one having a relatively high platinum loading since it gives good soot burning (i.e., filter regeneration) characteristics along with other synergy advantages between the CSF and the SCR catalyst. Thus, either V/Ti or zeolite SCR catalysts can be used, but a

zeolite catalyst, such as Beta, is preferred because of its excellent hydrothermal stability.[336] In this configuration, the SCR catalyst exhibited higher NO_x conversion than the SCR catalyst alone at all temperatures, plus it extended the effective NO_x conversion range of the SCR catalyst down to temperatures at least as low as 473 K, which is well below the effective temperature range of the Fe-exchanged Beta-zeolite with 4 wt % ZrO_2 binder catalyst alone.

Finding out the best catalyst deposition on the trap, the best trap design to allow an intimate contact between the reactants, and the catalyst itself are still challenging topics. In this line, the development of a suitable catalyst capable of promoting both soot oxidation and NO_x reduction at comparatively low temperatures (possibly within the range typical of diesel exhaust, 423−653 K) are extremely important.[396−398]

Nanostructured perovskite-type lanthanum ferrites $La_{1-x}A_xFe_{1-y}B_yO_3$ (where A = Na, K, or Rb and B = Cu), prepared by the combustion synthesis method and tested on an engine bench, proved to be effective in the simultaneous removal of soot and NO_x in the temperature range 623−723 K.[399] The best compromise between soot and nitrogen oxide abatement was shown by the La−K−Cu−FeO_3 catalyst, which displayed the highest catalytic efficiency toward carbon combustion and the highest NO conversion. The La−K−Cu−FeO_3-catalyzed filter facilitates the conversion of NO, especially during the regeneration phase, which can turn into savings in any of the NO-reduction techniques (LNT or SCR) possibly adopted downstream of the particulate filter.

Bimetallic potassium−copper and potassium−cobalt catalysts supported on alumina and monometallic zeolites (Co/beta and Cu/beta) for the reduction of NO_x with soot were also investigated in the treatment of the diesel engine exhaust, recommending the bimetallic ones at temperatures between 523 and 673 K. This led to a noticeable increase of the rate of NO_x reduction with soot evolving N_2 and CO_2 as main reaction products.[400] At higher temperature, the catalysts mainly favor the direct soot combustion with oxygen.

Most of the diesel soot oxidation catalysts are developed by tedious routes with subsequent activity testing and characterization. Although these methods have led to the discovery of several promising catalysts, a large unexplored universe of materials remains that may pose superior catalytic activities. As it was mentioned above, alkali metal ions have been reported already to improve the catalyst efficiency and mobility, which may result in an intimate contact between soot and catalyst. On the other hand, increased mobility may also lead to catalyst degradation.[401]

A well-known problem for alkali dopants is the leaching of the alkali ions in the presence of water vapor. To solve this problem, high-throughput techniques have been implemented to search for soot oxidation catalysts free of noble metals and alkaline metals. Olong et al.[402] used in this scope libraries consisting of up to 206 catalysts that were screened for relative heats of reaction by emissivity-corrected infrared thermography. By this approach new catalyst formulations capable of combusting soot at relatively low temperatures were discovered. The hits identified via the high-throughput experiments were successfully synthesized and tested conventionally. The highest efficiency was found for the $Pb_{10}La_5Co_{85}O_x$ catalyst. High-throughput experiments also found that the most significant reaction conditions affecting both the initial NO_x storage and reduction and initial N_2O production are the catalyst temperature and the composition of the reducing agents.[403]

4.8. NO_x Storage Reduction (NSR) Systems: Competition between SCR and NO_x Storage

4.8.1. General Concepts Developed in NSR Systems. In the course of a longer lean phase, the NO_x are stored on the catalyst surface in the form of nitrites and nitrates. Several NO_x adsorbing components (Ba, K, Na, Ca, Li, Mg, etc.) can be used simultaneously in the NSR washcoat with particular temperature dependence of the effective NO_x storage capacity related to the basicity of the used components.[404] Thermal durability is the essential requirement for all after-treatment catalysts used on vehicles for emission control, with no exception for NSRs. Based on several investigations,[404−406] the major thermal aging mechanisms for NO_x storage have been identified. On one hand, thermal aging reduces precious metal dispersion, and on the other, it causes a solid−solid chemical reaction of the NO_x storage component with other oxides in the catalyst. Temperature and the oxygen partial pressure are the major factors influencing precious metal sintering.[407] Above 1073 K, an irreversible destruction of the NO_x storage features takes place while the three-way efficiency of the catalyst remains intact or may even improve. High oxygen content promotes the formation of mobile platinum oxides that accelerate Pt sintering and the loss of catalytic efficiency.

Several studies specifically for diesel vehicles have been carried out.[407−412] Although the fundamentals of NSR are common for both gasoline and diesel applications, there are major differences due to the character of engine operation and control strategies. Since diesel exhaust gas temperatures are lower than those of gasoline by 473−573 K, normal operating conditions cause substantially less thermal damage. In addition, there is a widespread consensus that diesel particular filters are required in addition to lean NO_x trap to meet the stringent 2007 NO_x and particulate matter emission regulations. The diesel particular filters require regular soot regenerations at high temperatures that will cause thermal deactivation of the lean NO_x trap, if particulate filters and the lean NO_x trap are coupled. The filter regeneration requires excess oxygen to burn the accumulated soot. These lean conditions are different from the stoichiometric conditions to which lean NO_x traps are mostly exposed under high temperatures on gasoline vehicles.[407]

A typical NSR formulation includes a catalytic oxidation component, such as platinum, a NO_x-storage component such as barium, and a reduction catalyst (e.g., rhodium). The system preferably comprises a catalyzed absorbent. By "catalyzed", it is meant that the absorbent is intimately associated with the catalytic material effective for the reaction of CO with NO_x.[413] This material may be coprecipitated, coimpregnated, or codeposited with NO_x absorbent. It may also be present as one or more sandwiched layers or serial zones or as fine (e.g., 10−500 μm) particles on or in a layer of absorbent or among particles of absorbent. Whether catalyzed or not, the absorbent may be provided in one unit or a succession of separate units. It is typically on a honeycomb substrate, such as a single honeycomb or multiple honeycombs.

The nature of the absorbent can be (a) compounds, like oxides of alkali metals, alkaline earth metals, rare earth metals, and transition metals capable of forming nitrates or nitrites of adequate stability in absorbing conditions and of evolving nitrogen oxides or nitrogen in regenerating conditions, or (b) adsorptive materials such as zeolites, carbons, and high surface-area oxides, or mixtures of any two or more thereof.[414] Among various absorbent composites, oxides have been proposed for

this purpose are of alkaline earth metal and copper and manganese or cobalt oxides such as $MnO_2-BaCuO_2$ or $MnO_2-SrCuO_2$ possibly with Ce or Y oxide addition. The oxidation component associated with the absorbent or following it can be any that is active and stable. As mentioned above, these catalysts typically comprise one or more noble metals especially Pt, Rh, Pd, and combinations thereof on a high-surface-area washcoat on a honeycomb structure. In lean exhaust, the platinum catalyst speeds oxidizing reactions that lead to NO_x adsorption. In a reducing environment, the catalysts activate reactions by which hydrocarbon reductants are converted to more active species, activate the water−gas shift reaction that produces more active hydrogen from less active CO, and activate reactions by which adsorbed NO_x is reduced and desorbed.[415]

Generally, the nature of the absorbent material should be chosen in order to match the exhaust gas temperatures encountered in exhaust systems for either heavy- or light-duty diesel engines. More strongly basic oxides, for example, BaO are preferred absorbent materials for heavy-duty applications. Particularly preferred is barium absorbent including a catalytically effective amount of platinum. Weaker basic oxides, for example, CuO or AgO are preferred in light-duty applications. A mixture of copper oxide and palladium has been found to be especially effective.[414]

Recent investigations[416,417] suggested that NO_x storage is accomplished via two parallel routes: (i) the disproportionation route, "nitrate route", and (ii) the "nitrite route", where NO is oxidized in the presence of oxygen to form nitrite species followed by oxidation to nitrates. However, the literature reports several versions of these mechanisms with different levels of complexity.[405,418−423] These refer to the NO_x storage/reduction mechanism based on a single type of barium site, the shrinking core mechanism or the global models assuming that NO_x diffusion inside the barium clusters is the rate-controlling step in the NO_x storage process.[12] In these models, no distinction is made between reactivity of surface and bulk barium sites toward NO_x storage[424] although in the literature there is some evidence on multiple types of barium sites that differ in reactivity.[425] Barium close to Pt sites is generally considered to be more reactive than barium sites located further away.[426]

Barium can be present in the catalyst as BaO, $Ba(OH)_2$, or $BaCO_3$, depending on the reaction conditions. NO_x storage occurs preferentially at BaO, then at $Ba(OH)_2$ followed by $BaCO_3$ sites.[427] The nature of the reductants is also very important for this process being connected with the catalyst regeneration.[178,428] While CO facilitates only $Ba(NO_3)_2$ decomposition, H_2 enables both the decomposition and the reduction.

Using a $Pt/Ba/\gamma\text{-}Al_2O_3$ catalyst Scholz et al.[424] showed that alternating flows of $NO-O_2-He$ and H_2-He between 1063 and 1183 K, approximately 93% of the barium is involved in NO_x storage as the pretreated catalyst is exposed to 9 h lean conditions and that the subsequent rich phase shows incomplete regeneration of stored NO_x, even after 15 h rich exposure with H_2. Cyclic steady state was reached after 3 lean/rich cycles, at which only 60% of the total barium is involved in the NO_x storage. The NO oxidation efficiency of the catalyst decreases till steady cycling is achieved. The NO/H_2 reaction is favored over H_2 consumption by O_2. When applying lean/rich cycling on the order of seconds, these authors indicated that the catalyst history and the lean/rich timing affect the number of cycles requiring a closed nitrogen balance. Another catalyst with promising storage−reduction performance is $Pt/Ba/CeO_2$.[429] Barium can be also replaced by potassium.[430]

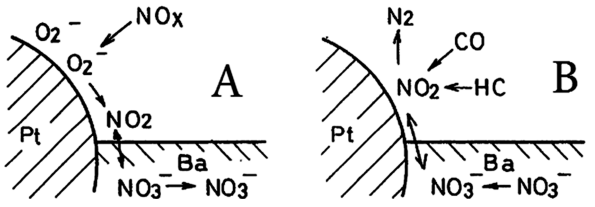

Figure 31. (A, B) Diagrams explaining the NO_x absorption and discharge functions. Reprinted with permission from ref 448. Copyright 2010 Springer.

Details of the mechanism of the NO_x absorption and discharge functions of the NO_x absorber catalyst are still under the debate.[12] It is considered that the NO_x absorption and discharge functions of the NO_x absorber catalyst are carried out based on the mechanism shown in Figure 31. This mechanism is described taking a NO_x absorber catalyst having platinum and barium carried on the carrier. The presence of other precious metals, alkali metals, alkali earth metals, or rare earth metals is supposed to not change this mechanism.[431]

When the exhaust gas flowing into the NO_x absorber catalyst becomes very lean, the concentration of oxygen in the inflow exhaust gas greatly increases. As shown in Figure 31A, the oxygen, O_2, is adsorbed at the surface of platinum Pt in the form of oxygen ions, O_2^-. Nitrogen oxide, NO_x, in the inlet exhaust gas reacts with O_2^- on Pt to form nitrogen dioxide. Part of this formed nitrogen dioxide, NO_2, is oxidized on platinum, Pt, absorbed by the NO_x absorber catalyst, bonded to barium oxide, BaO, and dispersed into the NO_x absorber catalyst in the form of nitric acid ions, NO_3^-. Thus, nitrogen oxide, NO_x, is absorbed by the NO_x absorber catalyst.[36] This mechanism occurs as long as the concentration of oxygen in the inlet exhaust gas is high.

A lean NO_x trap can produce ammonia during denitration. Accordingly, it has been proposed to combine NSR and ammonia-SCR catalysts into one system.[432−434] Ammonia produced by the NSR during regeneration is captured by the SCR catalyst for subsequent use in reducing NO_x, thereby improving conversion efficiency over a stand-alone NSR with no increase in fuel penalty or precious metal usage and reducing the ammonia slip.[435,436] NH_3-SCR catalysts have the benefit of containing no precious metal, a significant cost saving relative to NSR in addition to a wider range of operating temperatures where NO_x conversion can be achieved.[437] Further enhancements were noted by positioning the NSR and SCR formulations in alternating zones and ultimately a same brick double-layer NSR/SCR configuration. Figure 32 shows the results from flow reactor studies comparing the coupled NSR/SCR system with a traditional NSR.[407]

A detailed analysis of the catalytic behavior in the storage/reduction of NO_x of single $Pt-Ba/Al_2O_3$ NSR and Fe-ZSM-5 SCR systems and of combined NSR/SCR configurations under clean conditions (i.e., in the absence of CO_2 and H_2O in the feed stream) was recently provided by Bonzi et al.[438] When the zeolite SCR catalyst was mixed with the NSR sample (physical mixture) during the rich phase, the SCR catalyst traps ammonia, which being intermediate in N_2 formation led to a decrease in the evolution of nitrogen at the reactor outlet. Ammonia stored on the SCR catalyst then reacts with NO_x during the subsequent lean phase, leading to a significant N_2 evolution: this increases the

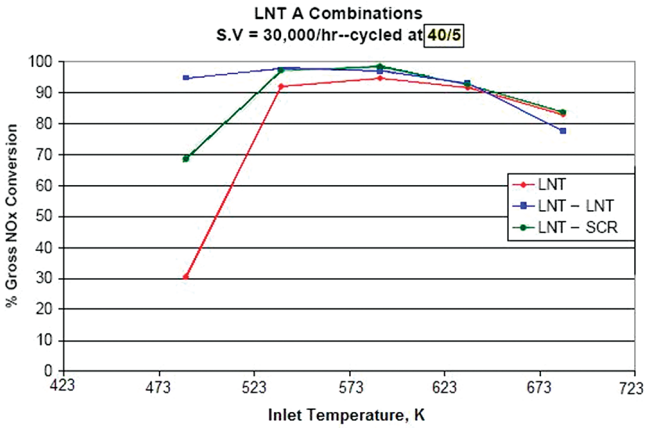

Figure 32. Lean NO_x trap-SCR (LNT) (combined NSR/SCR system) performance compared with a conventional LNT with equivalent precious metal. Reprinted with permission from SAE paper 2004-01-0156, Copyright 2004 SAE International.

NO_x removal efficiency and the N_2 selectivity compared with a single Pt−Ba/Al_2O_3 catalyst.

Regeneration involves the removal of most of the oxygen from the exhaust, which generally implies extra injection of reducing agents into the exhaust. The reactions between reductant and oxygen can take place in the NSR, but it is generally preferred for the reactions to occur in a catalyst upstream of the NSR, whereby the heat of reaction does not cause large temperature increases within the NSR at every regeneration step. Combustion or reforming reactions are promoted. The reformer uses both oxidation (Pt or Pd) and steam reforming (Rh) catalysts to produce syngas from diesel fuel at exhaust gas temperatures. However, temperatures from ∼773 to ∼973 K are required for effective reformate production, which are substantially higher than typical diesel exhaust temperatures. To be operative at exhaust gas temperature, a relatively large amount of catalyst must be used.[439] Therefore the reformer is heated by injecting fuel at a rate that leaves the exhaust lean, whereby the injected fuel combusts to generate heat. After warm up, the fuel injection rate is increased to provide a rich exhaust. Less precious metal catalyst is required when reforming at steam reforming temperatures compared with reforming diesel fuel at exhaust temperature regardless of whether reforming is through partial oxidation and steam reforming or exclusively through partial oxidation reactions. In principal, if reformate production proceeds through partial oxidation reforming as in reaction 50:[415,440]

$$CH_{1.85} + O_2 \rightarrow CO_2 + 0.925H_2 \quad (50)$$

0.925 mol of reformate could be obtained from each mole of carbon atoms in the fuel. $CH_{1.85}$ is used to represent diesel fuel having a typical carbon-to-hydrogen ratio. If reformate production proceeds through reaction 51:

$$CH_{1.85} + H_2O \rightarrow CO + 1.925H_2 \quad (51)$$

2.925 mol of reformate could in principle be obtained from each mole of carbon atoms in the fuel. In practice, yields are lower than theoretical ones due to the limited efficiency of conversion of fuel, the limited selectivity for reforming reactions over complete combustion reactions, the necessity of producing heat to drive steam reforming, and the loss of energy required to heat the exhaust. The operation of an inline reformer can be modeled in terms of the following three reactions:[391]

$$0.684CH_{1.85} + O_2 \rightarrow 0.984CO_2 + 0.632H_2O \quad (52)$$

$$0.316CH_{1.85} + 0.316H_2O \rightarrow 0.316CO + 0.608H_2 \quad (53)$$

$$0.316CO + 0.316H_2O \rightarrow 0.316CO_2 + 0.316H_2 \quad (54)$$

Equation 52 is an exothermic complete combustion by which oxygen is consumed. Equation 53 is an endothermic steam reforming, while reaction 54 is the water−gas shift reaction, which is comparatively thermal neutral and is not of great importance because both CO and H_2 are effective for regeneration. In theory, the temperature of the reformer can be controlled through the fuel injection rate. For example, if the reformer is heating, the fuel injection rate can be increased to increase the extent of reaction 53 (endothermic steam reforming), while the extent of reaction 52 (exothermic complete combustion), which is limited by the exhaust oxygen concentration, remains essentially constant. In practice, this approach often cannot be used.[391] The size and catalyst loading of the reformer are limited for economic reasons. The efficiency of the fuel reformer is generally insufficient to accommodate high fuel injection rates. As a result, the reformer tends to heat as reformate is being produced particularly when exhaust oxygen composition is in the range 8−15 vol %.

Combining two NSR units can ensure a first control signal to denitrate the NO_x trap supplying rich exhaust to the fuel reformer whereby the fuel reformer produces a reformate-containing rich exhaust−reductant mixture that denitrates and a second NSR to desulfate the NO_x trap component, where supplying rich exhaust to the fuel reformer produces a reformate-containing rich exhaust−reductant that desulfates the NSR. Careful control of the purge event is required to prevent NO_x reduction to NH_3 rather than the desired N_2.[407] The first and second NSRs are selected to have different formulations providing different minimum effective desulfation and different maximum safe desulfation temperatures. A novel approach for purging was presented recently with the advantage of the decrease in NO_x storage capacity with increasing temperature.[441] After storing NO_x on the storage material, propylene (C_3H_6) was oxidized on the trap under net lean conditions. The resulting exotherm caused some of the stored NO_x to be released. Since the release occurred under lean conditions, the released NO_x is not reduced to N_2 by the NSR but is emitted primarily as NO. Since the release of NO_x from the NSR is promoted in this approach by lean hydrocarbon oxidation, it is important to estimate the temperatures of the platinum sites and NO_x storage sites during oxidation reactions. This information is very useful for modeling the operation of coupled NSR/SCR systems described above. In this scope, Theis and Gulari[442] proposed a very elegant methodology to estimate these temperatures during propylene (C_3H_6) oxidation under net lean conditions.

Several nitrogen compounds can be produced during the regeneration phase in periodically operated NO_x storage and reduction catalyst. Besides the main product N_2, also NO, N_2O, and NH_3 can be formed depending on the duration of the regenerative step, temperature, and gas composition.[443] Dynamic behavior of NSR samples implies investigation of the catalysts during periodic lean/rich operation at different temperatures.

Scheme 3. Reactions Involved in the NO_x Storage Reduction Catalytic Reactions

$$NO + 1/2O_2 \rightarrow NO_2$$
$$2NO_2 + BaCO_3 + 1/2O_2 \rightarrow Ba(NO_3)_2 + CO_2$$
$$2NO_2 + BaCO_3 + 3/2O_2 \rightarrow Ba(NO_3)_2 + CO_2$$
$$Ce_2O_3 + 1/2O_2 \rightarrow Ce_2O_4$$
$$H_2 + Ce_2O_4 \rightarrow H_2O + Ce_2O_3$$
$$H_2 + 1/2O_2 \rightarrow H_2O$$
$$5/2H_2 + NO \rightarrow NH_3 + H_2O$$
$$Ba(NO_3)_2 + 8H_2 \rightarrow 2NH_3 + 5H_2O + BaO$$
$$Ba(NO_3)_2 + 3H_2 \rightarrow 2NO + 3H_2O + BaO$$
$$2NH_3 + 3/2O_2 \rightarrow N_2 + 3H_2O$$
$$2NH_3 + 3Ce_2O_4 \rightarrow N_2 + 3Ce_2O_4 + 3H_2O$$
$$4NH_3 + 6NO \rightarrow 5N_2 + 6H_2O$$
$$10/3NH_3 + Ba(NO_3)_2 \rightarrow 16/3N_2 + 5H_2O + BaO$$
$$BaO + CO_2 \rightarrow BaCO_3$$

Using commercial $PtRh/Ba/CeO_2/\gamma\text{-}Al_2O_3$ monolithic catalyst with H_2, CO, and C_3H_6 as reducing agents and the implementation of a spatially distributed NSR models by Koci et al.[443] confirmed that NH_3 is formed via the NO/H_2 reaction and reacts subsequently with oxygen and NO_x producing N_2. These authors reported a good agreement with experiments assuming that the ammonia formation during the NO_x reduction by CO and HCs at higher temperatures proceeds via the water−gas shift and steam-reforming reactions producing hydrogen. The oxygen storage effects influence the dynamics of the stored NO_x reduction. Scheme 3 presents the reactions involved in the NSR cycle on this catalyst. The first step, that is, the oxidation of NO to NO_2 occurs on Pt while the reduction step takes place on Rh.

At laboratory scale, many other catalytic systems have been investigated. Recently double-layered NO_x trap catalysts,[444−446] in which the external layer has the function of SO_x trap and a composition close including $MgAl_2O_4$ or $MgAl_2O_4.CeO_2$, have been reported as advanced sulfur-resistant NO_x traps. It was also reported that the addition of 1 wt % of transition metals with redox properties such as Pt, Pd, V, and Ru to the hydrotalcite increases its efficiency due to the combination of the redox properties of these metals and the acid−base properties of the hydrotalcite.[447,448] Mg/Al hydrotalcites with copper or cobalt in the structure have been described as active catalysts for the SO_x, NO, and N_2O removal by Palomares et al.,[449] while hydrotalcite derived materials as NO_x storage/reduction catalysts were proposed by Fornasari et al.[450] and Centi et al.[451] Noteworthy the best results were obtained with a noble metal free catalyst, namely, with one derived from a hydrotalcite with a molar ratio Co/Mg/Al = 15/60/25 and containing 1 wt % V. This material showed a higher efficiency, at low temperatures and in the presence of H_2O and SO_2, than a $Pt-Ba/Al_2O_3$ reference catalyst. The material behavior was assigned to the adequate combination of the vanadium redox properties and the hydrotalcite basic properties, together with the sulfur tolerance of this material.

NSRs also accumulate SO_x as a combustion product of sulfur ordinarily present in fuel. SO_x adsorbs more strongly than NO_x and necessitates a more stringent, though less frequent, regeneration. Desulfation requires elevated temperatures as well as a reducing atmosphere.[452,453] Extra heat production is typically provided through the same types of reactions as used to remove excess oxygen from the exhaust.[391] On the other hand, high temperature exposure sinters precious metals inducing a loss of NO_x conversion to N_2.

Simulation of the sulfur deactivation of the NO_x storage performance of BaO/Al_2O_3 and $Pt/BaO/Al_2O_3$ catalysts led to a model suggesting that the storage of NO_x occurs on two storage sites, one for complete NO_x uptake and one for a slower NO_x sorption.[454−456] The adsorption of SO_x competes on both sites and on one additional one, which represents bulk storage. The present model was built of six submodels: (i) NO_x storage under sulfur-free conditions; (ii) SO_2 storage on NO_x storage sites; (iii) SO_2 oxidation by oxygen ions O_2^- to SO_3 on Pt; (iv) SO_3 storage on bulk sites; (v) SO_2 interaction with platinum in the presence of H_2; (vi) oxidation of accumulated sulfur compounds on platinum by NO_2. The reaction sequence involves the following elementary steps:

$$SO_2(g) + Pt \leftrightarrow Pt{-}SO_2 \quad (55)$$
$$Pt{-}O + Pt{-}SO_2 \leftrightarrow Pt{-}SO_3 + Pt \quad (56)$$
$$Pt{-}SO_3 \leftrightarrow Pt + SO_3(g) \quad (57)$$
$$H_2(g) + 2Pt \leftrightarrow 2Pt{-}H \quad (58)$$
$$Pt{-}SO_2 + 2Pt \leftrightarrow Pt{-}S + 2Pt{-}O \quad (59)$$
$$2Pt{-}H + Pt{-}S \leftrightarrow H_2S(g) + 3Pt \quad (60)$$
$$2Pt{-}H + Pt{-}O \leftrightarrow 3Pt + H_2O(g) \quad (61)$$
$$Pt{-}S + 2Pt{-}NO_2 \leftrightarrow 2Pt{-}SO_2 + 2Pt{-}NO \quad (62)$$

It results that SO_x in exhaust gas can adsorb on the catalyst according to a mechanism similar to the NO_x. Part of the formed SO_3 on the surface of platinum (Pt) is bonded to barium oxide BaO in the NO_x absorber catalyst, then dispersed into the NO_x absorber catalyst in the form of sulfate ions and forms $BaSO_4$.[36] The high stability of barium sulfate gradually lowers the NO_x storage capacity.

As a matter of fact, deterioration of the NO_x absorbing capability of the solid can roughly be divided into two types, (i) irreversible thermal aging and (ii) reversible (by treatment) chemical poisoning such as sulfur. Therefore the design of the exhaust gas post-treatment device should also consider the presence of SO_x and its content.[457] However, in the exhaust gas purifier for an internal combustion engine, the above two different types of deterioration are handled in the same manner and the permissible amount of absorbed NO_x is set based on the NO_x absorbing capacity after judgment on deterioration.[458] Therefore, the deterioration degree of the NO_x absorber catalyst can be detected from the above time elapsed.

Figure 33 schematically shows the concentrations of unburned hydrocarbon HC, carbon monoxide CO, and oxygen O_2 as typical elements contained in exhaust gas discharged from the combustion chamber. As shown in Figure 33, the concentrations of hydrocarbon HC and carbon monoxide CO increase as the air-to-fuel ratio of the mixture supplied into the combustion chamber

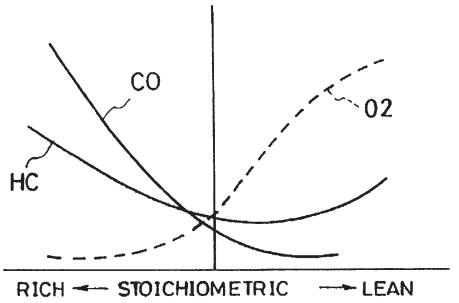

Figure 33. The concentrations of unburned HC, CO, and O_2 contained in the diesel exhaust gas. From ref 458, U.S. Patent 6,345,498, 2002, to Mitsubishi Denki Kabushiki Kaisha Jpn.

becomes richer and the concentration of oxygen O_2 increases as the air-to-fuel ratio of the mixture becomes leaner.[458] These hydrocarbons HC and carbon monoxide CO react with oxygen ions O_2^- on the surface of platinum to be oxidized. Under these conditions, NO_x is discharged from the NO_x absorber catalyst in a short period of time. Nitrogen dioxide NO_2 reacts with the unburned hydrocarbon HC and carbon monoxide CO to be reduced as shown in Figure 31B. When nitrogen dioxide NO_2 thus disappears from the surface of platinum, nitrogen dioxide NO_2 is discharged from the NO_x absorber catalyst continuously.

Before the NO_x absorbing capability of the NO_x absorber catalyst is saturated, nitrogen oxide NO_x must be discharged from the NO_x absorber catalyst. To this end, it is necessary to estimate how much the NO_x absorber catalyst absorbs nitrogen oxide NO_x.[458] In order to extend the life of the absorber catalyst and of the particulate filter a post-fuel-injection operation to activate the catalyst converter has been proposed.[459] This allows the regeneration of a sustainable temperature or of the filter protectable temperature.

However, the long-term aging of the NO_x-storage catalyst is largely due to factors that cannot be recreated on synthetic gas bench, for instance, the exotherms created by the complex mixture of hydrocarbons present in diesel fuel, and the highly transient operating conditions on a real engine.[460]

4.8.2. Free Noble Metals Traps. Fe-based zeolites were suggested to offer the best compromise for combined NSR/SCR applications, due primarily to better thermal durability of Fe vs Cu zeolites under high-temperature lean rich cycling. However, today novel Cu-zeolite formulations developed by the catalyst manufacturers equal or exceed the Fe-zeolites in their thermal durability while showing significant advantages related to low-temperature NO_x conversion and mitigation of H_2S emissions during lean NO_x trap desulfation.[433] Using such formulations, the NSR/SCR system achieved NO_x conversion equivalent to that of a NSR containing 2 times fewer noble metals.

Good results were also reported for SO_x traps derived from Cu/Al hydrotalcite.[461] The analysis of the SO_2 uptake curves as a function of the Cu/Al ratio and reaction temperature indicates that the reaction mechanism of SO_2 uptake depends on irreversible chemisorption of SO_2 and subsequent oxidation by copper and a nearly irreversible bulk diffusion of the sulfate species. The rate of these processes depends on (i) the Cu/Al ratio and nature of the surface copper species, (ii) the surface area of the catalyst, (iii) the reaction conditions, and (iv) the degree of sulfation. The SO_x trap having a Cu/Al ratio of 1:2 might represent a significant breakthrough exhibiting better performances with respect to a reference "state-of-the-art" SO_x trap containing 2 wt % Pt.

$[Ca_{24}Al_{28}O_{64}]^{4+}\cdot 4O^-/K$ has been reported as another noble-metal-free NO_x storage/reduction catalyst with a very good efficiency in NO removal, including NO conversion, N_2 selectivity, and sulfur tolerance. These features were evidenced by using hydrogen and C_3H_6 as reducing agents in a fixed-bed flow reactor[462] and then confirmed from a comparative study with Pt/$BaAl_2O_4-Al_2O_3$, $BaFeO_3$, and $BaZrO_3$ catalysts,[463,464] suggesting that in this case NO was first adsorbed on K_2O and O^- sites and then converted to NO_3^- or NO_2^- as NO_x storage intermediates.

$(n)MnO_x-(1-n)CeO_2$ binary oxides have also been studied for the sorptive NO removal and subsequent reduction of NO_x sorbed to N_2 at low temperatures ($\leq$423 K).[465] The solid solution with a fluorite-type structure was found to be effective for oxidative NO adsorption, which yielded nitrate (NO_3^-) or nitrite (NO_2^-) species on the surface depending on temperature, O_2 concentration in the gas feed, and composition of the binary oxide (n). The reactivity of the adsorbed NO_x toward H_2 was examined for MnO_x-CeO_2 impregnated with Pd, which is known as a nonselective catalyst toward the NO/H_2 reaction in the presence of an excess of oxygen. These studies provided evidence that the role of Pd is to generate reactive hydrogen atoms, which spillover onto the MnO_x-CeO_2 surface and reduce nitrite/nitrate adsorbing thereon. Despite the lower reducibility of nitrate and the competitive H_2/O_2 combustion, Pd/MnO_x-CeO_2 attained 65% NO conversion at 423 K.

Takahashi et al.[466] reported that the reduction efficiency decreases in the order $H_2 > CO > C_3H_6$ below 673 K, thus not all of the NO_x storage sites could be fully regenerated even using an excess of CO or C_3H_6, while all the NO_x storage sites could be fully regenerated if an adequate amount of H_2 is supplied. One or more compounds decomposable to CO in the conditions of the system, for example, formic acid and formic esters such as methyl formate, may be also used.[413] H_2 generation more favorably occurs through the water–gas shift reaction rather than through the steam reforming reaction. This difference can reasonably explain why CO is more efficient for the reduction of the stored NO_x than C_3H_6, and hinted as a promising approach to enhance the low-temperature performance of the storage and reduction catalysts through the H_2 generation.

NO_x storage presents as a principal disadvantage the unequal competition for sorbing catalytic sites between NO_x, CO_2, and SO_x. In fact, adsorption selectivity follows the sequence $SO_x > CO_2 > NO_x$.[467] By use of 12-tungstaphosphoric acid hexahydrate ($H_3PW_{12}O_{40}\cdot 6H_2O$, named HPW),[468,469] it was found that storage and desorption of NO and NO_2 proceed via an equimolar ratio without nitrate formation. The mechanism of absorption involves the substitution of lattice water molecules and formation of a $[H^+(NO_2^-, NO^+)]$ complex. During the cooling phase and in the presence of water, near 373 K, reverse substitution occurs. These structures can be dispersed on common Ce–Zr and Ti–Zr based materials, but in this scope it is important to get an isoelectric point around 7 to preserve the HPW structure.[470] Since the NO_x reduction process is performed between cyclic lean/rich mixtures, redox support properties play a main role. This system can act as a multifunctional catalyst being also active for the reduction of NO_x by methane in excess oxygen.[389] The behavior of the catalyst against deactivation depends on the support properties, such as oxygen mobility, oxygen storage capacity, and the possibility of *in situ* hydrogen formation from steam methane reforming or water–gas shift reaction.

The NO_x reduction function of HPW catalysts is provided by the presence of two types of active sites:[467] (a) metallic sites

(M^0) generated by hydrogen or CO reduction of platinum; (b) cationic sites formed on the reduced surface of the support (M^+) and possibly by the interaction between HPW protons and noble metals $(metal-H)^{\delta+}$. CO, CO_2, and H_2 can react to generate $C_xH_yO_z$ on the metal and on the support. These reactive oxygenate compounds can assist the reduction of NO into N_2. After NO_x desorption, NO_2 can be reduced into NO, which can be adsorbed on cationic sites generating N_2 and adsorbed oxygen. The adsorbed oxygen will complete the oxidation of $C_xH_yO_z$ compounds generating CO_2 and H_2O and regenerating the cationic sites for a new cycle. Methodologies for modeling such smart catalytic converters combining NO_x storage, ammonia production and SCR were recently reported.[139]

4.9. DeNO$_x$ Procedures with Reformer Gas Generated on Board

Another approach for a diesel combustion engine is to use catalytic fuel reformer adapted to generate hydrogen-containing reformer gas that can be fed upstream in the exhaust-gas catalytic converter.[471] The effect of feeding hydrogen-containing gas to exhaust gas from a lean-burn internal combustion engine in order to reduce nitrogen oxides was proposed more than one decade ago.[472] It is thus possible to achieve a relatively high reduction of nitrogen oxides using the supplied hydrogen at relatively low temperature at special DeNO$_x$ catalytic converters even when an excess of oxygen is present. To generate the hydrogen-containing gas, it was initially proposed to use a catalytic reformer in which fuel, which is available on board, reacts with the exhaust gas from the internal combustion engine. The initial catalytic composition consisted of a noble metal coupled with copper, chromium, and nickel oxides. Heating the reformer to its operating temperature and maintaining this operating temperature are achieved by the quantitative control of the flow of hot exhaust gas to the reformer. However, hot exhaust gas is not available immediately after the internal combustion engine has been started; consequently, it takes a certain time to heat up the installation.

Alternately, the reducing agent can be fed to the exhaust gas from an air-compressing internal combustion engine, that is, an internal combustion engine that is usually operated with excess air by late injection of fuel.[473] Depending on the injection time, this fuel is used to heat the exhaust-gas after-treatment device by means of catalytic oxidation at an exhaust-gas catalytic converter or as a reaction partner for reducing the level of nitrogen oxides at a DeNO$_x$ catalytic converter. On account of the method by which it is provided, the reducing agent that is made available consists predominantly of hydrocarbons. However, these hydrocarbons are relatively slow to react compared with hydrogen, and consequently, neither the heating of the exhaust-gas after-treatment device nor the catalytic reduction in the levels of nitrogen oxides at low exhaust-gas temperatures is possible.

However, the setting is preferably such that the soot limit for the reforming process is not reached.[471] In this case, the known processes of partial hydrocarbon oxidation take place in the reformer or at the reformer catalytic converter. In addition, steam reforming may in some cases take place on account of the steam content of the exhaust gas supplied. The result of these processes is a reformer gas that as its combustible constituents contains in addition to carbon monoxide and low hydrocarbons, primarily hydrogen. On account of the high reactivity of the reformer gas, it can be oxidized by the oxygen in the exhaust gas even at low exhaust-gas temperatures at the oxidation catalytic converter. The heat of reaction, which is liberated in the process, heats the oxidation catalytic converter to above its light-off temperature, which is crucial for other exhaust-gas components, so that the converter reaches its state in which it is capable of normal operation.

The type of hydrocarbons is of crucial importance. Relatively high NO conversion rates can be achieved with short-chain or unsaturated hydrocarbons. As mentioned, hydrogen is very effective below 473 K, while fuel injection in the exhaust gas is relatively ineffective. The implementation of a reformer to provide low hydrocarbons and hydrogen as reducing agents generally induces a fuel penalty. To overcome this aspect, Law et al.[474,475] proposed to produce hydrogen via the vapor phase reforming of ethylene glycol (EG). They investigated the EG reforming and DeNO$_x$ in two independently controlled but connected reforming and DeNO$_x$ reaction units such that the products from the reforming unit could be fed to the feed stream of the DeNO$_x$ unit. H_2 and CO were generated from the reforming of ethylene glycol over $Na-Pt/Al_2O_3$ catalysts while NO_x reduction was carried out over Pd/Ti−PILC catalysts. EG reforming reactions were conducted at 503 K, and the effective reduction of NO_x was achieved at 458 K. An inconvenience of the method for the DeNO$_x$ catalyst is related to significant deactivation phenomena induced by the presence of water and unreacted ethylene glycol from the reforming unit.

The efficiency of Pt and Pd based catalysts for the reduction of NO under lean burn conditions (5 vol % O_2) and in presence of excess water (10% H_2O) was reported by Ueda et al.[476] more than 10 years ago. All Pd-based catalysts displayed two distinct conversion maxima for the reduction of NO, one centered at 373 K and the second at 573 K. At low temperature, the efficiency results from the reaction between H_2 and NO, while at high temperature it is the result of the reaction between H_2 and NO_2 generated under the reaction conditions. The maximum NO_x conversion varied significantly with the nature of the support. In the series TiO_2, Al_2O_3, MgO, and SiO_2, titania showed the best efficiency and alumina the smallest. Zeolites have also been reported for the reduction of NO_x under lean conditions and in the presence of H_2O and CO_2.[477] Thus, supporting palladium and cerium on mordenite resulted in high NO_x conversion with high nitrogen selectivity that has been interpreted in terms of a synergic co-operation between CO and H_2.

4.10. NO$_x$ Reduction by Hydrogen

Jones et al. were the first who reported in 1971 the effective NO_x reduction by H_2 in slight excess of O_2 using a Pt/Al_2O_3 catalyst.[478] The high NO_x conversions observed between 338 and 473 K are however associated with high yields of nitrous oxide. At maximum DeNO$_x$ efficiency, the molar ratio of N_2/N_2O was close to the unity. Burch et al.[479] proposed a reaction mechanism involving the reduction of the active Pt sites by H_2 followed by adsorption and dissociation of NO. According to this mechanism, N_2O is produced by reaction between chemisorbed N atoms and NO molecules on neighboring Pt sites. In addition to N_2O, ammonia can also be released from this process. NH_3 emissions from gasoline-fueled vehicles have become an important source of pollution affecting urban air chemistry.[480] NH_3 influences the acidity of atmospheric depositions, and it is involved in secondary aerosol formation. The extent of traffic-related hydrogen (H_2) emissions and its impact on atmospheric redox chemistry is not well understood but is of growing importance when it is more considered for DeNO$_x$ processes.

In the last years, some improvements of the H_2-DeNO_x catalysts have been reported on Pt-based catalysts revealing considerable low-temperature activity even under strongly oxidizing conditions[481] Many supports have been investigated in this reaction (La_2O_3, MgO, Y_2O_3, CaO, CeO_2, TiO_2, SiO_2), but most of them led a significant production of N_2O typically on Pt-based catalysts.[136,482−485] On the other hand, mixed oxides such as $MgO-CeO_2$ were found more effective to promote the selective reduction of NO into N_2 by H_2 on Pt under process conditions similar to those encountered in the NH_3-SCR in the low-temperature range of 423−473 K with a feed stream containing 1000 ppm NO, 5% O_2, 5% H_2O, 10% CO_2, 0−0.5% CO, and using 1.5% H_2 in the feed as reducing agent. The use of hydrogen eliminates some disadvantages compared with ammonia such as catalyst deterioration, ammonia slip, ash odor, air-heater fouling, and a high running cost.[486] Granger and co-workers showed that perovskite-supported palladium catalysts are efficient for NO_x abatement in a mixture $H_2/NO/O_2$ at low temperature (<423 K).[487] Other studies stressed the role of the palladium precursor indicating that $Pd(NO_3)_2$ leads to a higher reactivity compared with chlorinated precursors[488] and that tetramine nitrate palladium is even better than those.[489] The presence of a second element like cerium or cobalt was also found to enhance the catalytic efficiency of palladium in this reaction.[477,490] The addition of cobalt stabilizes the activity of the Pd^{2+} species in the presence of methane.

Deactivation of Pd-MOR catalyst becomes significant above 723 K and is essentially related to steam dealumination and agglomeration of active sites. At 673 K, the catalyst showed a deactivation during the first days on stream that was caused by chemisorption of the sulfur.[491]

The effects of reaction temperature on the chemical structure and surface concentration of the active NO_x intermediate species using these catalysts was also investigated on $Pt/MgO-CeO_2$.[492] Two active NO_x intermediate species were identified by SSITKA−DRIFTS, one located in the vicinity of the $Pt-CeO_2$ support interface region (nitrosyl $[NO^+]$ coadsorbed with a nitrate $[NO_3^-]$ species on an adjacent $Ce_4^+-O_2^-$ site pair) and the second located in the vicinity of the Pt−MgO support interface region. The chemical structure of the second kind of active NO_x species was found to depend on the reaction temperature. NO_x intermediates that lead to N_2 formation were found to be practically independent of reaction temperature (393−573 K) and significantly larger than 1 equivalent monolayer of surface Pt. Efstathiou and co-workers[493,494] also reported a series of supported Pt-based catalysts on perovskite ($La_{0.7}Sr_{0.2}Ce_{0.1}FeO_3$, $La_{0.5}Sr_{0.2}Ce_{0.51}MnO_3$) and $MgO-CeO_2$[495,496] with pronounced low-temperature activity as well as substantially enhanced N_2 selectivity up to 80−90%. Detailed examinations performed by this group indicate a different reaction mechanism compared with that elucidated for Pt/Al_2O_3.[479] They postulated chemisorption of NO_x on the support resulting in nitro and nitrato surface species, while H_2 adsorbs dissociatively on Pt. Chemisorbed H atoms then spill over to the support reducing the NO_x surface complexes to release N_2 and H_2O, thus suppressing the formation of N_2O. Except $Pd/LaCoO_3$[497] and platinum other metals like Ru, Ir, Rh, Pd, and Ag[357] revealed no or at least low performance in excess O_2.

The effect of the support was also evidenced by a catalyst consisting of tetragonal ZrO_2 (carrier), amorphous WO_3 (promoter), and Pt (catalytic component).[498] Compared with typical Pt catalysts this one exhibits a pronounced N_2 selectivity explained on the basis of a promoter effect. The promoter increases the electron density on Pt, while NO_x species adsorbed on WO_3/ZrO_2 play no role in H_2-$DeNO_x$. Under realistic conditions, this catalyst is stable toward hydrothermal and SO_x aging but it does not operate at high temperatures (>573 K) because H_2 reacts completely on the catalyst with the excessive O_2. Depending on the temperature of the $DeNO_x$ catalytic converter or the oxygen/fuel ratio set in the reformer, the reformer process can be controlled in such a way that a more or less hydrogen-rich or a more or less hydrocarbon-rich reformer gas is obtained. As a result, optimum reduction in the levels of nitrogen oxides can be achieved over a wider temperature range.

In situ, microreactor-based, energy-dispersive EXAFS (EDE) and mass spectrometry measurements allow the identification of the nature of the active sites in the reaction of NO and N_2O with hydrogen.[499] Investigation of 5 wt % $Rh/\gamma\text{-}Al_2O_3$ catalysts showed that the reduction of NO by H_2 to N_2 occurs on reduced metallic sites, while it stopped at N_2O on oxidized sites. In this way, the selectivity of the reduction of NO by H_2 can be directly correlated with the phase of the rhodium. Rh on alumina is rapidly oxidized by NO, and as NO levels are increased the catalyst selectivity tends toward the production of N_2O rather than the desired N_2. More reducing conditions promote Rh particle formation at progressively lower temperatures that tend toward the limit of the intrinsic stability of the oxidic phase that forms spontaneously at low temperature under NO. This phase is responsible for the significant NO conversion and is also the source of the transient production of N_2O.

Some controversies on the nature of intermediate because of the formation of reaction products in the gas phase observed below the temperature for the thermal decomposition of nitrates/nitrites species led the conclusion that hydrogen may directly react with those ad-NO_x species.[500] The formation of NH_3 has to be lessened due to its well-known intrinsic toxicity. Once a noble metal surface has been cleaned of oxygen successive hydrogenation of adsorbed N (from NO dissociation) by H atoms, as described in Table 3, may occur leading ultimately to NH_3 formation.

Kouakou et al. investigated the formation of ammonia during the purge of a commercial NO_x trap on an engine test-bench in real conditions.[501] The experiments carried out at 553 K showed exothermic processes after the switch in rich conditions related to the oxidation of the reducing agents by oxygen adsorbed species. These reactions provided vacant Pt sites for the dissociation and the reduction of NO_x release from the decomposition of nitrates to ammonia and nitrogen. The time dependency of hydrogen exposure showed that the evolution of NH_3 was delayed compared with the switch in rich conditions and that the purge duration is a key parameter because it determines the local ratio of $[NO_x]/[Red]$ in the NO_x trap. Ammonia was detected after the switch in lean conditions, which has been attributed to its slow desorption.

Interesting reductive properties were also presented by perovskite-type oxides of the form $SrFe^{3+,5+}O_{3\pm0.5}$ containing iron in mixed oxidation states III and V toward lean-$deNO_x$ using CH_4 and H_2. The behavior of these catalysts was assigned to their extensive ability for oxygen reversible adsorption.[502] However, the drawback of such materials is their low specific surface area typical for materials prepared via ceramic methods. Interestingly, materials with the same chemical composition but prepared via wet methods do not expose the same active sites. The activity toward N_2 formation in H_2 lean-$DeNO_x$ reaction is greatly favored by a charge disproportionation of iron species.

La-based perovskites doped with palladium synthesized by a modified citrate route ($LaFe_{0.95-x}Co_xPd_{0.05}O_3$, x = 0.475, 0.4, 0.3) were also investigated during the H_2-SCR of NO_x.[503] The perovskite-containing mixture of crystal phases including orthorhombic and cubic perovskites, cobalt oxide, and strongly bonded palladium oxide displayed better activity in NO_x conversion and N_2 selectivities than the pure orthorhombic perovskite phase with traces of iron oxide and weak bonded palladium oxide. The same behavior was observed with $H_2O + CO_2$ and in the presence of CO in the feed. To explain this behavior, it was proposed that the mixed phases contribute to the stabilization of palladium with small palladium crystallites in its surface showing different crystal planes or forming alloys with La.

5. SCR OF NO_X USING BIODIESEL AND SYNTHETIC GAS-TO-LIQUID (GTL) FUELS

5.1. Biodiesel as a Renewable Fuel

Biodiesel fuel derived from vegetable oil, animal fat, or waste cooking oil consists of the methyl esters of fatty acids. Due to the U.S. Renewable Fuel Standard and European legislation, which requires 36 billion gallons of renewable fuel in 2022,[99] the use of biodiesel becomes more common every year. With the anticipated widespread use of biodiesel, it is important to fully understand biodiesel's impact on new and existing engine and emission control technologies.[504]

The chemical composition of biodiesel differs from diesel because of the presence of the ester group. For the soy biodiesel, more than 80% of the molecules contain one or more double bonds. On the other hand, diesel is composed of paraffins, naphthenes, and aromatics.

Experiments reported by Williams et al.[504] using Fe-zeolite as SCR catalyst, ultralow sulfur diesel, diesel fuel blend with different contents of biodiesel, and pure biodiesel showed different catalytic behaviors. The mildly polar ester group in biodiesel, as well as the ability for double bonds to interact with acidic sites, was suggested to lead to stronger chemisorption. In addition, the presence of several oxygenated compounds in the pure biodiesel exhaust was characterized, in particular, methylacrylate and higher molecular weight homologues produced from the thermal decomposition of soy methylesters. A potential explanation for the low-temperature efficiency observed for pure biodiesel was correlated with the results reported previously by Arve et al.[505] who tested a methyl ester and various hydrocarbons as NO_x reductant over a Ag/Al_2O_3 catalyst. They found a reduction of the efficiency below 673 K, higher with biodiesel than with *n*-octane. Thus, the NO_x reduction below 573 K should be caused by reaction with adsorbed biodiesel or biodiesel reaction products rather than by reaction with NH_3.

The Ag/Al_2O_3 catalyst was also investigated in reducing NO_x emissions using exhaust gas from the diesel engine operation on diesel, biodiesel, and low-temperature Fischer−Tropsch synthetic diesel. Compared with diesel fuel, biodiesel combustion produces a higher amount of NO_x with reduced concentrations of HCs, while both HC and NO_x emissions were reduced in the engine exhaust from the combustion of synthetic diesel fuel. The use of Ag/Al_2O_3 catalysts in a passive mode HC-SCR system showed good NO_x reduction under the different molar HC/NO_x ratios, following the order diesel > SD > RME when the respective fuels are used for combustion. The introduction of optimized H_2 concentrations is however necessary to reduce the catalyst deactivation.[506−509]

The Ag/Al_2O_3 catalyst was also reported to reduce NO_x and particulate matter emissions from a diesel engine using both ethanol-selective catalytic reduction of NO_x and a biodiesel−ethanol−diesel fuel blend.[510] In addition to what was presented above compared with diesel fuel, the use of biodiesel increases particulate matter emissions by 14% due to the increase in the soluble organic fraction of particulate matter, but it greatly reduced the Bosch smoke number (or Bacharach smoke number) by 60%−80%. However, under these conditions due to ethanol adding to the system as reductant, the total hydrocarbons and CO emissions increase significantly during the SCR of NO_x process. To eliminate these emissions, two diesel oxidation catalyst assemblies were suggested to be placed after the Ag/Al_2O_3 converter. This combination was reported to effectively reduce both NO_x and particulate matter emissions even without using diesel particle filters.

There are several studies indicating that ethanol selective catalytic reduction of NO_x on Ag/Al_2O_3 is a promising technology in reducing NO_x from diesel engines.[511] Experimental reports showed that using ethanol reductant on low-loading Ag/Al_2O_3 can result in greater than 90% of NO_x reduction. However this is possible only for temperatures below 773 K. Tham et al. proposed a detailed surface mechanism that has been established by performing SPSR simulations (eqs 63−97).[511]

$$NO + Ag(*) \rightarrow NO(*) + Ag(B) \quad (63)$$

$$NO(*) + Ag(B) \rightarrow NO + Ag(*) \quad (64)$$

$$NO_2 + Ag(*) \rightarrow NO_2(*) + Ag(B) \quad (65)$$

$$NO_2(*) + Ag(B) \rightarrow NO_2 + Ag(*) \quad (66)$$

$$H(*) + O(*) + Ag(B) \rightarrow OH(*) + Ag(*) \quad (67)$$

$$H(*) + OH(*) + Ag(B) \rightarrow H_2O(*) + Ag(*) \quad (68)$$

$$2OH(*) \rightarrow H_2O(*) + O(*) \quad (69)$$

$$H_2O(*) + Ag(B) \rightarrow H_2O + Ag(*) \quad (70)$$

$$NO(*) + O(*) + Ag(B) \rightarrow NO_2(*) + Ag(*) \quad (71)$$

$$C_2H_5O(*) + Ag(*) \rightarrow CH_3CHO(*) + H(*) + Ag(B) \quad (72)$$

$$CH_3CHO(*) + O(*) \rightarrow CH_3COO(*) + H(*) \quad (73)$$

$$CH_3COO(*) + Ag(*) \rightarrow CH_2COO(*) + H(*) + Ag(B) \quad (74)$$

$$CH_2COO(*) + NO_2(*) + Ag(B) \rightarrow CHNOOH(*) + CO_2 + Ag(*) \quad (75)$$

$$CHNOOH(*) + Ag(*) \rightarrow NCO(*) + H_2O(*) + Ag(B) \quad (76)$$

$$NCO(*) + NO_2(*) + Ag(B) \rightarrow N_2 + CO_2 + O(*) + Ag(*) \quad (77)$$

dx.doi.org/10.1021/cr100168g |*Chem. Rev.* 2011, 111, 3155–3207

$$2NCO(*) + 2O(*) + 4Ag(B) \rightarrow N_2 + 2CO_2 + 4Ag(*) \quad (78)$$

$$CH_3CHO + Ag(*) \rightarrow CH_3CHO(*) + Ag(B) \quad (79)$$

$$CH_3CHO(*) + Ag(B) \rightarrow CH_3CHO + Ag(*) \quad (80)$$

$$C_2H_5O(*) + Ag(*) \rightarrow CH_3(*) + CH_2O(*) + Ag(B) \quad (81)$$

$$CH_3(*) + Ag(*) \rightarrow CH_2(*) + H(*) + Ag(B) \quad (82)$$

$$CH_2(*) + Ag(*) \rightarrow CH(*) + H(*) + Ag(B) \quad (83)$$

$$CH(*) + Ag(*) \rightarrow C(*) + H(*) + Ag(B) \quad (84)$$

$$C(*) + O(*) + Ag(B) \rightarrow CO(*) + Ag(*) \quad (85)$$

$$CO(*) + O(*) + 2Ag(B) \rightarrow CO_2 + 2Ag(*) \quad (86)$$

$$CO(*) + Ag(B) \rightarrow CO + Ag(*) \quad (87)$$

$$CH_2O(*) + Ag(*) \rightarrow HCO(*) + H(*) + Ag(B) \quad (88)$$

$$HCO(*) + Ag(*) \rightarrow CO(*) + H(*) + Ag(B) \quad (89)$$

$$C_2H_5OH + 2Ag(*) \rightarrow CH_3(*) + CH_2OH(*) + 2Ag(B) \quad (90)$$

$$CH_2OH(*) + Ag(*) \rightarrow CH_2O(*) + H(*) + Ag(B) \quad (91)$$

$$CH_2OH(*) + H(*) + Ag(*) \rightarrow CH_3OH(*) + Ag(B) \quad (92)$$

$$CH_3OH(*) + Ag(*) \rightarrow CH_3O(*) + H(*) + Ag(B) \quad (93)$$

$$CH_3O(*) + Ag(*) \rightarrow CH_2O(*) + H(*) + Ag(B) \quad (94)$$

$$C_2H_5OH + 2Ag(*) \rightarrow C_2H_5O(*) + H(*) + 2Ag(B) \quad (95)$$

$$O_2 + 2Ag(*) \rightarrow 2O(*) + 2Ag(B) \quad (96)$$

$$2O(*) + 2Ag(B) \rightarrow O_2 + 2Ag(*) \quad (97)$$

According to this mechanism, the poor performance of ethanol-SCR above 773 K was explained by the predominant desorption of NO and ethanol at the expense of gas-phase ethanol oxidation. In addition, the quality and impurities resulting from the various production methods of biodiesel can lead to blended fuels with varying levels of known contaminates such as Na and K.[512] The alkyl ester-based biodiesel specification for contaminate levels is outlined in ASTM D6751 and EN14214. Both specifications have the established limit at 5 mg/kg or 5 ppm by weight (sum of Na + K).[513]

Deactivation due to the presence of alkali metal has been reported in platinum-based oxidation catalysts, lean NO_x traps and vanadium-based SCR catalysts.[512,514,515] Incorporation of K within precious metal based lean NO_x absorbers has been shown to help the increase of the NO_x storage capacity. Unfortunately, thermal aging resulted in significant K migration leading to lower hydrocarbon performance from precious metal poisoning and mechanical durability issues from cordierite attack. Cu/zeolite-based SCR formulations and vanadium-based SCR formulations were also severely deactivated by contamination with Na or K. For the Cu/zeolite SCR catalyst, the low-temperature NO_x conversion (standard and fast SCR reaction) and the NH_3 storage capacity steadily decreased as a function of Na/K contamination level. Increasing levels of K exposure resulted in lower NO_x conversion due to lower NH_3 storage capacity. As the zeolite collapsed, various Cu states were likely created that resulted in various NH_3 oxidation efficiency and selectivity to NO_x. All these effects were associated with a decline in BET surface area, in NH_3 storage capacity, and in acid sites, having a subsequent impact on NO_x conversion.

The deactivation of commercial type $V_2O_5-WO_3-TiO_2$ catalysts by aerosols of potassium compounds was also confirmed by exposing the catalyst in a laboratory scale reactor to a layer of KCl particles or fly ash from biomass combustion and by exposing full-length monolithic catalysts to pure KCl or K_2SO_4 aerosols in a bench-scale reactor.[516] Moderate deactivation was observed for catalyst plates exposed to a layer of KCl particles at 623 K for 2397 h, while no deactivation was found for catalyst plates exposed for 2970 h to fly ash (consisting mainly of KCl and K_2SO_4). However, a fast deactivation was reported for catalysts exposed to pure KCl or K_2SO_4 aerosols at 623 K in the bench-scale reactor. The deactivation rates for exposed catalysts were about 1% and 0.4% per day, respectively, because the potassium salt, deposited on the catalyst outer wall, partly decreases the diffusion rate of NO and NH_3 into the catalyst. The capacity for NH_3 chemisorption decreases as a function of exposure time, which reveals that Brønsted acid sites had reacted with potassium compounds blocking the catalytic cycle. It was thus concluded that chemical poisoning of active sites is the dominating deactivation mechanism but physical blocking of the surface area may also contribute to the loss of efficiency in practical applications.[517]

5.2. Synthetic GTL Fuel

Ultraclean, high cetane number fuels derived from a Fischer–Tropsch process are a promising alternative,[518−520] and they are gaining attention from fuel companies and research groups. GTL (gas-to-liquid) is one of these fuels, but actually Fischer–Tropsch processes enable the final liquid fuel to be obtained from renewable sources, as it is the case of the BTL (biomass-to-liquid). Fischer–Tropsch fuels have been reported to reduce the main diesel emissions, both regulated and unregulated.

To reduce the NO_x emissions using such fuel, Rodriguez-Fernandez et al. proposed[520] the use of after-treatment devices consisting of a hydrocabon-selected catalytic reduction system and a reformed exhaust gas recirculation in addition to the main liquid diesel fuel, thus enabling the engine to operate in dual fuelling conditions. One weight percent Pt/Al_2O_3 HC-SCR catalyst was located in the engine exhaust to provide NO_x reduction. The statistical analysis pointed out that, at a 95% confidence level, the fuel used and the reformed exhaust gas recirculation type and ratio are the most significant factors that affect NO_x emissions.

5.3. Emissions Post-treatment for Light Duty Vehicles

According to U.S. legislation, the light duty vehicle category includes all vehicles of less than 3859 kg (passenger cars, light light-duty trucks, and heavy light-duty trucks), while Europe considers as light duty vehicles of less than 3500 kg. More than a decade ago, to reduce emissions of these vehicles, several measures for spark-ignition engines were considered including the following: (i) three-way catalysts with closed-loop control; (ii) changes in engine design and combustion conditions; (iii)

electronically controlled ignition; (iv) special measures for reducing cold-start and idling emissions; (v) exact fuel metering by fuel injection; (vi) exhaust gas recirculation.[521] Most of these measures refer to technological issues.

Almost in the same period the principle of the *nitrogen storage catalyst* was first published by Toyota for lean-burn gasoline engine application.[522] As mentioned in section 4.8, this technology requires a discontinuous lean/rich engine operation mode leading to oxidizing and reducing exhaust gas atmospheres. From that moment, the main challenge for the diesel engine was the development of the rich engine operating mode that enabled by the introduction of flexible diesel commonrail injection systems.[523] Nowadays, the combination of *nitrogen storage reduction* and *selective catalytic reduction* systems appears to be the more feasible solution for light duty vehicles in order to meet future standard regulation. Passenger and light duty diesel vehicles will require up to 90% NO_x conversion over the Federal Test Procedure in the U.S. to meet future Tier 2 Bin 5 standards. This accomplishment is especially challenging for low exhaust temperature applications that mostly operate in the 473−623 K temperature regime.[524,525]

5.3.1. SCR Catalysts Capable to Reach the Required Standards for Light Duty Vehicles. In a recent contribution, Catavaio et al. assumed an enhanced durability of Cu/zeolite-based SCR catalysts.[525] SCR catalysts formulated with Cu/zeolites have shown the potential to deliver the level of performance required by the present standards in the fresh state, but their performance can easily deteriorate. High-temperature SCR deactivation modes are unavoidable due to the requirements necessary to actively regenerate DPF and purge SCRs from sulfur and hydrocarbon contamination. In order to solve this problem, Catavaio et al.[525,526] proposed a technological solution—a careful vehicle temperature control of these events is necessary to prevent unintentional thermal damage but not always possible—and a catalytic one—the improvement of the Cu/zeolite robustness.[236,288] Thus, hydrothermal aging of Cu/zeolite resulted in a remarkable high-temperature hydrothermal stability up to 1223 K while maintaining stable low-temperature NO_x efficiency.

One main durability requirement of SCR formulations involves withstanding the high-temperature process of regenerating particulate filters from accumulated soot. Unrefined engine exhaust temperature control coupled with inexact temperature measurement may also expose SCR catalysts to additional overtemperature conditions. Therefore, metal/zeolite formulations are more appropriate for diesel applications than vanadia-containing formulations.[527] Two important parameters for selecting the proper SCR formulation involve the exhaust temperature profile and the NO_2/NO_x ratio expected during typical driving conditions.

To check the endurance of these catalysts under real conditions, SCR of NO_x with aqueous urea and a CDPF have been considered as one of the emission control systems for light duty diesel vehicles.[528] With this scope, a system containing a copper/zeolite SCR catalyst was aged on the engine dynamometer using an aging cycle that mimics both city and highway driving modes with an increase of the temperature up to 823 K. The laboratory post-mortem characterizations revealed a nonuniform deterioration profile of the SCR catalyst along the flow and brick radial directions due to nonuniform exposure to exotherms, urea, ash, and poisoning components and the engine operation conditions during the aging.

For diesel applications, cold start accounts for a large amount of the total NO_x emissions for light-duty vehicles and is a key focus for reducing NO_x emissions.[529] For cold start NO_x improvement, the SCR catalyst would be best located as the first catalyst in the after-treatment system. However, engine-out hydrocarbons and no diesel oxidation catalyst upstream to generate an exotherm for desulfation can result in degraded SCR catalyst performance. Recent advances in vanadia-based SCR catalyst technology have shown also better low-temperature NO_x performance and improved thermal durability.[278] Focusing on cold start operation, the system optimization except the catalyst durability with the decrease of the precious metal content is another target.[530] In such a respect, the use of new compounds based on alumina and ceria led to an enhancement of desulfation.

5.3.2. Reductants. In order to fulfill the standard regulations another target is the selection of the most efficient reductant. Ammonia released from different compounds is still considered the best solution as reductant.[531] Urea-based selective catalytic reduction has the potential to meet the emission standards for NO_x in the next decade and is under continuous development.[527,532,533] SCR of NO_x using aqueous urea had the advantage from the beginning of requiring no new infrastructure and does not pose any new customer compliance issues. In addition, urea SCR has high and durable NO_x conversion over a wider temperature window, a lower equivalent fuel penalty, and lower system cost.[534−536] Recently a procedure was disclosed to use urea in catalytic production of hydrogen that might have a great impact on the catalyst performance.[537] This method proposes the generation of hydrogen directly on a vehicle, by passing urea over a catalyst, such as a nickel−chromium wire catalyst.

$$(NH_2)_2CO + H_2O \rightarrow 3H_2 + N_2 + CO_2 \qquad (98)$$

The steam reforming of urea is facile. Compared with the common steam reforming of hydrocarbons ($\Delta H^\circ = +206$ kJ/mol) this reaction is only mildly endothermic ($\Delta H^\circ = 64$ kJ/mol). Reaction 98 is an equilibrium that is coupled with the water−gas shift reaction 99

$$CO + H_2O \rightleftarrows H_2 + CO_2 \qquad (99)$$

Even in the absence of excess water, the thermodynamic calculations show that the hydrogen content of the gas produced is 52% with coproducts N_2 (24%), CO (20%), and CO_2 (0.05%). The excess of water is driving the reaction in the direction of forming more hydrogen and carbon dioxide. Another advantage of this catalyst is the fact the excess of ammonia is cracked to hydrogen according to eq 100:

$$2NH_3 \rightarrow 3H_2 + N_2 \qquad (100)$$

5.3.3. Biodiesel Effects on Light Duty Vehicles. The growing interest in diesel powered passenger cars in combination with a desire to reduce dependency on imported petroleum has increased attention on the operation of light-duty diesel vehicles on fuels blended with biodiesel.[538] However, there is only limited information related to the impact of biodiesel fuels on the performance of advanced emission control systems. One of several factors to be considered when operating a vehicle on biodiesel blends is a better understanding of the impact and performance of the fuel on the emission control system. In order to fulfill the standards as in the case of heavy vehicles, the combination of two different emission control systems has been proposed: a NO_x adsorber catalyst coupled with a diesel particle filter and a SCR catalyst coupled with a diesel particle filter. The optimization of such a system should consider the calibration, regeneration, and desulfurization of the NO_x adsorber catalyst and the diesel particle filter regeneration as previously discussed.

Recent data reported that from the emission control standpoint only marginal effects were observed as a result of the

biodiesel operation.[539,540] The NO_x storage catalyst showed lower tailpipe emissions, which were attributed to the lower exhaust temperature profile during the test cycle. The SCR catalyst tailpipe results were fuel neutral and the engine-out emissions formation showed increased NO_x and decreased HC emissions with the biodiesel blend.

6. CONCLUSIONS, PROSPECTS AND FUTURE TRENDS IN POSTCOMBUSTION CATALYSIS

Very recently, the European Parliament imposed new standards to reduce CO_2 emissions (Regulation (EC) No 443/2009 of the European Parliament and of the Council of 23 April 2009 setting emission performance standards for new passenger cars as part of the Community's integrated approach to reduce CO_2 emissions from light-duty vehicles).

This new regulation requires all parties to formulate and then implement national and appropriate regional programs containing measures to mitigate climate change. In this respect, the Commission proposed in January 2007 that, in the context of international negotiations, the European Union should pursue the objective of a 30% reduction of greenhouse gas emissions by developed countries by 2020 (compared with 1990 levels) and that the Union itself should make a firm independent commitment to achieve at least a 20% reduction of greenhouse gas emissions by 2020 (compared with 1990 levels), irrespective of reductions achieved by other developed countries. This objective was endorsed by the European Parliament and the Council.

This Regulation also builds on a well-established process of measuring and monitoring the CO_2 emissions of vehicles registered in the Community in accordance with Decision No 1753/2000/EC of the European Parliament and of the Council of 22 June 2000 establishing a scheme to monitor the average specific emissions of CO_2 from new passenger cars. The setting of CO_2 emissions reduction requirements is intended to provide Community-wide predictability and planning security for vehicle manufacturers across their new car fleet in the Community. In consequence, the light-duty engine technology is focused on downsizing to deliver lower CO_2 emissions, enabled by advances in boost and exhaust gas recirculation.[540]

For catalysis, this would have several consequences: (i) The first concerns DeNO_x systems enabling much lower fuel consumption levels. To answer this challenge the NO_x control would be more probably centered on further improvement of the selective catalytic reduction performances. (ii) The second will concern identification of the catalysts able to consume the released CO_2.

It is obvious that only an integrate approach will fulfill future requirements in terms of emission control of atmospheric pollutants, in particular NO_x, with major drawbacks associated with low NO_x concentration in the exhaust gas and an excess of oxygen, which generally favor the competitive oxidation of the reducing agent at the expense of the reductive reactions to form harmless nitrogen. In such operating conditions, the intermediate production of N_2O is usually enhanced for low level of NO_x conditions and must be avoided because of its high global warming power. The emissions of N_2O are not actually regulated in Europe but might be considered in the future. This implies development of intrinsically active and selective catalytic systems to lower outlet NO emission and also to reduce the steric hindrance of end-of-pipe systems, the main objective being a significant reduction of noble metal loading in the actual technologies. Subsequent developments in the catalyst architecture are probably a prerequisite step to lower diffusion limitations and improve the thermal stability by minimizing thermal sintering reactions to fulfill future requirements in terms of durability. Clearly, the development of novel materials will represent a key point in the future technologies that will be implemented for NO_x abatement.

6.1. Which Technology?

Among the strategies actually implemented, the selective reduction of NO_x by hydrocarbons and urea compete with NO_x storage/reduction systems. Regarding SCR systems, the technology developed for heavy duty vehicles using urea as a precursor for the *in situ* ammonia formation to promote the SCR of NO_x in lean conditions seems to be appropriate with the development of iron-based catalyst on acidic materials but needs downstream of the SCR catalyst the combination with an oxidation catalyst mainly composed of Pt to get an optimal NO_2/NO ratio. Kim et al.[541] provided an alternative practical solution to high cost and poor thermal durability of conventional catalytic lean NO_x systems. They developed strontium-doped perovskite materials ($La_{1-x}Sr_xCoO_3$) capable of efficiently replacing platinum currently used for such technology. They showed excellent performance with higher conversion of NO to NO_2. Nevertheless some questioning points remain for further adaptation to light vehicles due to steric hindrance constraints. In this case, a compact system is needed to minimize detrimental effects of the engine efficiency and fuel consumption. Two different approaches can be envisaged, which consist of improving the catalytic performance of the materials or adding extra reducing agents via reformate produced from fuel reforming. To avoid penalities on the fuel consumption on board alcohol might be envisaged. An option such as this seems to be considered particularly for the implementation of combined technologies. Today, a growing interest is focused on the *in situ* formation of ammonia because it can represent a particular interest in the combined lean NO_x trap + SCR system proposed in which ammonia produced on board on the NO_x trap reduction catalysts can also be used as reactant in coupled SCR systems.[380] Recent work demonstrates that Cu:SAPO-5 and Cu:SAPO-11 synthesized using hydrothermal ion exchange method led not only to a 6-fold increased Cu incorporation but also to an increased stability of copper as bidentate Cu species that might represent a significant breakthrough compared to previous attempts.[542] In this way, the overall concentration of NO_x released in the atmosphere could be considerably lower accounting for the entire storage/regeneration cycle of NO_x trap systems.

6.2. Added Values of Fundamental Approaches To Rationalize Macroscopic Performances of End-of-Pipe Technologies?

As examined, up to now most surface science studies were essentially focused on model catalysts under UHV conditions, which are not representative of polycrystalline ones running typically at atmospheric pressure. As indicated, the support plays a determining role, particularly under lean conditions, depending on the strength of alkane, alkene, or oxygenate adsorption. Nowadays the development of surface science studies had lead to the preparation of supported catalysts on metal oxides under UHV conditions bridging the gap between model surfaces and practical ones. It is now possible to investigate in a more fruitful direction consisting of the examination of NO_x interaction with organic molecules such as ethylene, benzene, and ethanol. It is obvious that the implementation of such studies implies the development of efficient system detection to get more precise information on the possible intermediates and on the nature of

elementary steps. Combination with DFT calculation should lead to a more detailed reaction scheme in order to predict transient performances of catalysts under realistic conditions. Fundamental approaches should have some practical repercussions to control the extent of interaction between the active phase and the support and related synthesis protocols to optimize such interactions.

AUTHOR INFORMATION

Corresponding Author

*P.G.: tel. +32 3 20 43 49 38, fax +32 3 20 43 65 61, e-mail Pascal.granger@univ-lille1.fr. V.I.P.: tel. +4021 4103178, fax +4021 3159249, e-mail vasile.parvulescu@g.unibuc.ro.

BIOGRAPHIES

Pascal Granger (1964) studied at the University of Poitiers and obtained his Ph.D. degree in applied chemistry in 1992. After a postdoctoral position at the Lille University, he obtained a permanent position in 1994 and became full professor in 2003. Now, he is head of the heterogeneous department of the Solid State and Catalysis Laboratory in Lille. He is currently involved in mechanism and kinetics of heterogeneous catalytic reactions, in the development of *in situ* and operando spectroscopic characterization especially for reactions involved in postcombustion catalysis and catalytic DeNO$_x$ and DeN$_2$O abatement processes. He is author and coauthor of 70 publications in refereed international journals and one book.

Vasile I. Parvulescu received his master's degree in Catalysis from the Polytechnic University of Bucharest in 1979 and in 1986 gained his Ph.D. in Chemistry from the same university, where he investigated the selectivity of bi- and multimetal catalysts in hydrogenation of aromatic hydrocarbons. After several years as high-signor researcher at the Institute of Inorganic and Rare Metals, in 1992 he joined the University of Bucharest, where he become full professor in 1999. His current interest concerns the study of heterogeneous catalysts for green and fine chemistry and environmental protection. He authored more than 200 papers, 25 patents, and 4 books.

ABBREVIATIONS

AES	Auger electron spectroscopy
CSF	catalyzed Soot Filter
CDPF	catalyzed diesel particulate filter
CSTR	continuous stirred-tank reactor
DFT	density functional theory
DOC	diesel oxidation catalyst
DPF	diesel particulate filter
ESC	European steady-state cycle
ESR	electronic spin resonance
ETC	European transient cycle
EXAFS	extended X-ray absorption fine structure
FTIR spectroscopy	
Fourier transform infrared spectroscopy	
FTP	federal test procedure
HRTEM	high-resolution transmission electron microscopy
IRAS	infrared reflection absorption spectroscopy
LEIS	low-energy ion scattering
LNTs	lean NO_x traps
MVEG	mobile vehicle emissions group
NSCR	nonselective catalyst reduction
NSR	NO_x storage reduction catalyst
OSC	oxygen storage properties
SCR	selective catalytic reduction
SCRF	SCR-coated diesel particulate filter
SMSI	strong metal support interaction
SNCR	selective noncatalytic reduction
SOF	soluble organic fraction
SPSR	surface perfectly stirred reactor
SRC	storage reduction catalyst
SSITKA	steady-state isotopic transient kinetic analysis
TON	turnover number
TPD	temperature-programmed desorption
TWC	three-way catalyst
UBI-QEP	
index-quadratic exponential potential	
UHV	ultrahigh vacuum
UPS	ultraviolet-ray photoelectron spectroscopy
XPS	X-ray photoelectron spectroscopy

REFERENCES

(1) http://www.dieselnet.com/standards/us/ld.php.
(2) http://www.dieselnet.com/standards/us/ld_t2.php.
(3) http://www.dieselnet.com/standards/us/nonroad.php.
(4) Trichard, J. M. *Stud. Surf. Sci. Catal.* **2007**, *171*, 211.
(5) Centi, G.; Perathoner, S. *Stud. Surf. Sci. Catal.* **2007**, *171*, 1.
(6) Garin, F. *Catal. Today* **2004**, *89*, 255.
(7) Garcia, M. A.; Pitchon, V.; Kienneman, A. *Environ. Int.* **2005**, *31*, 445.
(8) Hums, E. *Catal. Today* **1998**, *42*, 25.
(9) Koltsakis, G. C.; Stamatelos, A. M. *Prog. Energy Combust. Sci.* **1997**, *23*, 1.

(10) Kaspar, J.; Fornasiero, P.; Hickey, N. *Catal. Today* **2003**, *77*, 419.
(11) Fritz, A.; Pitchon, V. *Appl. Catal., B* **1997**, *13*, 1.
(12) Roy, S.; Baiker, A. *Chem. Rev.* **2009**, *109*, 4054.
(13) Parvulescu, V. I.; Grange, P.; Delmon, B. *Catal. Today* **1998**, *46*, 233.
(14) Burch, R.; Breen, J. P.; Meunier, F. C. *Appl. Catal., B* **2002**, *39*, 283.
(15) Djéga-Mariadassou, G.; Berger, M.; Gorce, O.; Park, J. W.; Pernot, H.; Potvin, C.; Thomas, C.; Da Costa, P. *Stud. Surf. Sci. Catal.* **2007**, *171*, 145.
(16) Shelef, M. *Chem. Rev.* **1995**, *95*, 209.
(17) Taylor, K. C. *Catal. Rev. Sci. Eng.* **1993**, *35*, 457.
(18) Shelef, M.; Graham, G. W. *Catal. Rev. Sci. Eng.* **1994**, *36*, 433.
(19) Ichihara, S.; Onoda, H.; Garr, G. T.; Psaras, D.; Engler, B. H.; Lox, E. S.; Osgathe, K.; Ohata, T.; Tsuchitani, K. *SAE Tech. Pap. Ser.* **1994**No. 940928.
(20) Kim, S.; D'Aniello, M. J. J. *Appl. Catal.* **1989**, *56*, 45.
(21) Nunan, J. G.; Willianson, W. B.; Robota, H. J.; Henk, M. G. *SAE Tech. Pap. Ser.* **1995**No. 950258.
(22) Ismagilov, Z. R.; Shkrabina, R. A.; Koryabkina, N. A.; Arendarskii, D. A.; Shikina, N. V. In *Catalysis and Automotive Pollution Control*; Kruse, N., Frennet, A., Eds.; Elsevier: Amsterdam, 1998; Vol. IV.
(23) Di Monte, R.; Fornasiero, P.; Kaspar, J.; Graziani, M.; Gatica, J. M.; Bernal, S.; Gomez Herrero, A. *Chem. Commun.* **2000**, 2167.
(24) Kaspar, J.; Fornasiero, P.; Graziani, M. *Catal. Today* **1999**, *50*, 285.
(25) Cuif, J. P.; Blanchard, G.; O., T.; Seigneurin, A.; Marczi, M.; Quéméré, E. *SAE Tech. Pap. Ser.* **1997**No. 970463.
(26) Rossignol, S.; Gérard, F.; Duprez, D. *J. Mater. Chem.* **1999**, *9*, 1615.
(27) Kacimi, S.; Barbier, J. J.; Taha, R.; Duprez, D. *Catal. Lett.* **1993**, *22*, 343.
(28) Rohart, E.; Larcher, O.; Hédouin, C.; Allain, M.; Macaudière, P.; Deutsch, S. *SAE Tech. Pap. Ser.* **2004**No. 04-01-1274.
(29) Cant, N. W.; Angove, D. E.; Chambers, D. C. *Appl. Catal., B* **1998**, *17*, 63.
(30) Wan, C.-Z.; Dettling, J. C. U.S. Patent 4,714,694, 1987, to Engelhard Co., U.S.A.
(31) Ohata, T.; Terui, S.; Shiraishi, E. U.S. Patent 4,708,946, 1987, to Nippon Shokubai Co., Ltd, Jpn.
(32) van den Tillaart, J. A. A.; Leyrer, J.; Eckhoff, S.; Lox, E. S. *Appl. Catal., B* **1996**, *10*, 53.
(33) Perrichon, V.; Laachir, A.; Bergeret, G.; Fréty, R.; Tournayan, L.; Touret, O. *J. Chem. Soc., Faraday Trans.* **1994**, *90*, 773.
(34) Matsumoto, S.; Miyoshi, N.; Masayasu, S. U.S. Patent 4,808,564, 1989, to Toyota Kabushiki Kaisha, Jpn.
(35) Fujitani, Y.; Muraki, H.; Kondoh, S.; Tomita, M.; Nakamura, T.; Yokota, K.; Sobukawa, H. U.S. Patent 4,367,162, 1983, to Kabushiki Kaisha Toyota Chuo Kenshyusho, Jpn.
(36) Bozon, A.; Koberstein, E.; Pletka, H. D.; Volker, H.; Lakatos, E. U.S. Patent 4,294,726, 1981, to Deutsche, Gold-und Silber-scheideanstalt Vormals Roessler, DE.
(37) Finabiki, M. AU Patent 615721, 1991, to Engelhard Corporation, U.S.A.
(38) Kupe, J. EP Patent 1219351 A1, 2002, to Delphi Technologies, Inc., U.S.A.
(39) Stephens, R. E. U.S. Patent 3,899,444, 1975, to Ethyl Corporation, U.S.A.
(40) Wan, C.-Z. U.S. Patent 5,057,483, 1991, to Engelhard Corporation, U.S.A.
(41) Santos, H.; Costa, M. *Int. J. Heat Mass Transfer* **2008**, *51*, 1409.
(42) Li, H.; Zhang, L.; Dai, H.; He, H. *Inorg. Chem.* **2009**, *48*, 4421.
(43) Burch, R.; Millington, P. J. *Catal. Today* **1995**, *26*, 185.
(44) Gobin, O. C.; Schüth, F. *J. Comb. Chem.* **2008**, *10*, 835.
(45) Garcia-Cortes, J. M.; Perez-Ramirez, J.; Illan-Gomez, M. J.; Kapteijn, F.; Moulijn, J. A.; Salinas-Martinez, C. *React. Kinet. Catal. Lett.* **2000**, *70*, 199.
(46) Carniti, P.; Gervasini, A.; Modica, V. H.; Ravasio, N. *Appl. Catal., B* **2000**, *28*, 175.
(47) Chi, Y.; Chuang, S. S. C. *Catal. Today* **2000**, *62*, 303.
(48) Pietrogiacomi, D.; Sannino, D.; Tuti, S.; Ciambelli, P.; Indovina, V.; Occhiuzzi, M.; Pepe, F. *Appl. Catal., B* **1999**, *21*, 141.
(49) Xie, G.; Liu, Z.; Zhu, Z.; Liu, Q.; Ge, J.; Huang, Z. *J. Catal.* **2004**, *224*, 36.
(50) Xie, G.; Liu, Z.; Zhu, Z.; Liu, Q.; Ge, J.; Huang, Z. *J. Catal.* **2004**, *224*, 42.
(51) Trovarelli, A.; de Leitenburg, C.; Boaro, M.; Dolcetti, G. *Catal. Today* **1999**, *50*, 353.
(52) Lobree, L. J.; Hwang, I. C.; Reimer, J. A.; Bell, A. T. *Catal. Lett.* **1999**, *63*, 233.
(53) Decyk, P.; Kim, D. K.; Woo, S. I. *J. Catal.* **2001**, *203*, 369.
(54) Guzman Vargas, A.; Delahay, G.; Coq, B.; Lima, E.; Bosch, P.; Jumas, J. C. *Catal. Today* **2005**, *110*, 294.
(55) Vradman, L.; Herskowitz, M.; Capek, L.; Wichterlova, B.; Brosius, R.; Martens, J. A. *Ind. Eng. Chem. Res.* **2005**, *44*, 4523.
(56) Capek, L.; Vradman, L.; Sazama, P.; Herskowitz, M.; Wichterlova, B.; Zukerman, R.; Brosius, R.; Martens, J. A. *Appl. Catal., B* **2007**, *70*, 53.
(57) Imai, H.; Ogawa, T.; Sugimoto, K.; Kataoka, M.; Tanaka, Y.; Ono, T. *Appl. Catal., B* **2005**, *55*, 259.
(58) Chen, X. Y.; Shen, S. C.; Chen, H. H.; Kawi, S. *J. Catal.* **2004**, *221*, 137.
(59) Boix, A. V.; Aspromonte, S. G.; Miro, E. E. *Appl. Catal., A* **2008**, *341*, 26.
(60) Gutierrez, L. B.; Miro, E. E.; Ulla, M. A. *Appl. Catal., A* **2007**, *321*, 7.
(61) Gutierrez, L.; Lombardo, E. A. *Appl. Catal., A* **2009**, *360*, 107.
(62) Pârvulescu, V. I.; Centeno, M. A.; Grange, P.; Delmon, B. *J. Catal.* **2000**, *191*, 445.
(63) Dubois, L. H.; Hasma, P. K.; Somorjai, G. A. *J. Catal.* **1980**, *65*, 318.
(64) Serri, J. A.; Cardillo, M. J.; Becker, G. E. *J. Chem. Phys.* **1982**, *76*, 2175.
(65) Gorte, R. J.; Schmidt, L. D.; Gland, J. L. *Surf. Sci.* **1981**, *109*, 367.
(66) Park, Y. O.; Masel, R. I.; Stolt, K. *Surf. Sci.* **1983**, *131*, 385.
(67) Banholzer, W. F.; Park, Y. O.; Mak, K. M.; Masel, R. I. *Surf. Sci.* **1983**, *128*, 176.
(68) Gohdrone, J. M.; Park, Y. O.; Masel, R. I. *J. Catal.* **1985**, *95*, 244.
(69) Oh, S. H.; Fischer, G. B.; Carpenter, J. E.; Goodman, D. W. *J. Catal.* **1986**, *100*, 360.
(70) Peden, C. H. F.; Goodman, D. W.; Blair, D. S.; Berlowitz, P. J.; Fisher, G. B.; Oh, S. H. *J. Phys. Chem.* **1988**, *92*, 1563.
(71) Root, T. W.; Schmidt, L. D.; Fischer, G. B. *Surf. Sci.* **1983**, *134*, 30.
(72) Yates, J. T. J.; Thiel, P. A.; Weinberg, W. H. *Surf. Sci.* **1979**, *82*, 45.
(73) Granger, P.; Lecomte, J. J.; Leclercq, L.; Leclercq, G. *Appl. Catal., A* **2001**, *218*, 257.
(74) Berlowitz, P. J.; Peden, C. H. F.; Goodman, D. W. *J. Phys. Chem.* **1988**, *92*, 5213.
(75) Fujitani, T.; Nakamura, I.; Kobayashi, Y.; Takahashi, A.; Haneda, M.; Hamada, H. *J. Phys. Chem. B* **2005**, *109*, 17603.
(76) Belton, D. N.; DiMaggio, C. L.; Ng, K. Y. S. *J. Catal.* **1993**, *144*, 273.
(77) Aryafar, M.; Zaera, F. *J. Catal.* **1998**, *175*, 316.
(78) Piccolo, L.; Henry, C. R. *Surf. Sci.* **2000**, *452*, 198.
(79) Hopstaken, M. J. P.; van Gennip, W. J. H.; Niemansverdriet, J. W. *Surf. Sci.* **1999**, *433*−*435*, 69.
(80) Overbury, S. H.; Mullins, D. R.; Kundakovic, L. *Surf. Sci.* **2001**, *470*, 243.
(81) Whitman, L. J.; Ho, W. *Surf. Sci.* **1988**, *204*, 725.
(82) Lambert, R. M.; Comrie, C. M. *Surf. Sci.* **1974**, *46*, 61.
(83) Peden, C. H. F.; Belton, D. N.; Schmieg, S. J. *J. Catal.* **1995**, *155*, 204.
(84) Belton, D. N.; DiMaggio, C. L.; Schmieg, S. J.; Ng, K. Y. S. *J. Catal.* **1995**, *157*, 559.

(85) Ng, K. Y. S.; Belton, D. N.; Schmieg, S. J.; Fisher, G. B. *J. Catal.* **1994**, *146*, 394.
(86) Granger, P.; Dathy, C.; Lecomte, J. J.; Leclercq, L.; Mabilon, G.; Prigent, M.; Leclercq, G. *J. Catal.* **1998**, *173*, 304.
(87) Granger, P.; Lecomte, J. J.; Dathy, C.; Leclercq, L.; Leclercq, G. *J. Catal.* **1998**, *175*, 194.
(88) Hecker, W. C.; Bell, A. T. *J. Catal.* **1984**, *85*, 389.
(89) Solymosi, F.; Kiss, J. *Surf. Sci.* **1981**, *108*, 641.
(90) Hecker, W. C.; Bell, A. T. *J. Catal.* **1983**, *84*, 200.
(91) Oh, S. H. *J. Catal.* **1990**, *124*, 477.
(92) Cho, B. K. *J. Catal.* **1991**, *131*, 74.
(93) Dathye, A. K.; Kalakkad, D. S.; Yao, M. H.; Smith, D. J. *J. Catal.* **1995**, *155*, 148.
(94) Martinez-Arias, A.; Soria, J.; Conesa, J. C. *J. Catal.* **1997**, *168*, 364.
(95) Shyu, J. Z.; Otto, K. *J. Catal.* **1989**, *115*, 16.
(96) Bernal, S.; Calvino, J. J.; Cauqui, M. A.; Pérez Omil, J. A.; Pintado, J. M.; Rodriguez-Izquierdo, J. M. *Appl. Catal., B* **1998**, *16*, 127.
(97) Krause, K. R.; Schabes-Retchkiman, P.; Schmidt, L. D. *J. Catal.* **1992**, *134*, 204.
(98) Bernal, S.; Botana, F. J.; Calvino, J. J.; Cifredo, G. A.; Pérez Omil, J. A.; Pintado, J. M. *Catal. Today* **1995**, *28*, 219.
(99) Energy Independence and Security Act of 2007 (Public Law 110−140), December 2007.
(100) Golunski, S. E.; Hatcher, H. A.; Rajaram, R. R.; Truex, T. J. *Appl. Catal., B* **1995**, *5*, 367.
(101) Yao, H. C.; Yao, Y. F. Y. *J. Catal.* **1984**, *86*, 254.
(102) Fernández-García, M.; Martínez-Aria, A.; Salamanca, L. N.; Coronado, J. M.; Anderson, J. A.; Conesa, J. C.; Soria, J. *J. Catal.* **1999**, *187*, 474.
(103) Krause, J. M.; Schmidt, L. D. *J. Catal.* **1994**, *148*, 22.
(104) Zafiris, G. S.; Gorte, R. J. *J. Catal.* **1993**, *143*, 86.
(105) Nibbelke, R. H.; Nievergeld, A. L.; Hoebink, J. H. B. J.; Marin, G. B. *Appl. Catal., B* **1998**, *19*, 245.
(106) Nibbelke, R. H.; Campman, M. A. J.; Hoebink, J. H. B. J.; Marin, G. B. *J. Catal.* **1997**, *171*, 358.
(107) Granger, P.; Delannoy, L.; Lecomte, J. J.; Dathy, C.; Leclercq, L.; Leclercq, G. *J. Catal.* **2002**, *207*, 202.
(108) Lööf, P.; Kasemo, B.; Andersson, S.; Frestad, A. *J. Catal.* **1991**, *130*, 181.
(109) Taylor, K. C. In *Catalysis- Science and Technology*; Anderson, J. R., Boudart, M., Eds.; Springer-Verlag: Berlin, 1984; Vol. 5.
(110) Powell, B. R.; Chen, Y. L. *Appl. Catal.* **1989**, *53*, 233.
(111) Beck, D. D.; DiMaggio, C. L.; Fisher, G. B. *Surf. Sci.* **1993**, *297*, 303.
(112) Hu, Z.; Allen, F. M.; Wan, C. Z.; Heck, R. M.; Steger, J. J.; Lakis, R. E.; Lyman, C. E. *J. Catal.* **1998**, *174*, 13.
(113) Persson, K.; Jansson, K.; Järås, S. G. *J. Catal.* **2007**, *245*, 401.
(114) Beck, D. D.; Capehart, T. W.; Wong, C.; Belton, D. N. *J. Catal.* **1993**, *144*, 311.
(115) Wong, W.; McCabe, R. W. *J. Catal.* **1989**, *119*, 47.
(116) Lox, E. S. J.; Engler, B. H. In *Environmental Catalysis*; Ertl, G., Knozinger, H., Weitkamp, J., Eds.; Wiley/VCH: Weinheim, Germany, 1999.
(117) Oh, S. E.; Carpenter, J. E. *J. Catal.* **1986**, *98*, 178.
(118) Barbier, J.; Marécot, P.; Del Angel, G.; Bosch, P.; Boitiaux, J. P.; Didillon, B.; Dominguez, J. M.; Schifter, I.; Espinosa, G. *Appl. Catal., A* **1994**, *116*, 179.
(119) Pirault, L.; El Azami El Idrissi, D.; Marécot, P.; Dominguez, J. M.; Mabilon, G.; Prigent, M.; Barbier, J. *Stud. Surf. Sci. Catal.* **1995**, *96*, 193.
(120) Marécot, P.; Pirault, L.; Mabilon, G.; Prigent, M.; Barbier, J. *Appl. Catal., B* **1994**, *5*, 57.
(121) He, R.; Kasuka, H.; Mavrikakis, M.; Dumesic, J. A. *J. Catal.* **2003**, *217*, 209.
(122) Abild-Pedersen, F.; Anderson, M. P. *Surf. Sci.* **2007**, *601*, 1747.
(123) Anderson, J. A. *J. Catal.* **1993**, *142*, 153.
(124) Granger, P.; Delannoy, L.; Leclercq, L.; Leclercq, G. *J. Catal.* **1998**, *177*, 141.
(125) Rogemond, E.; Essayem, N.; Fréty, R.; Perrichon, V.; Primet, M.; Chevrier, M.; Gauthier, C.; Mathis, F. *J. Catal.* **1999**, *186*, 414.
(126) Jansen, W. P. A.; Harsen, J. M. A.; Gon, A. W. D. v. d.; Hoebink, J. H. B. J.; Shouten, J. C.; Brongersma, H. H. *J. Catal.* **2001**, *204*, 420.
(127) Renouprez, A. J.; Trillat, J. F.; Morawek, B.; Massardier, J.; Bergeret, G. *J. Catal.* **1998**, *179*, 390.
(128) Schmal, M.; Baldanza, M. A.; Vannice, M. A. *J. Catal.* **1999**, *185*, 138.
(129) Renouprez, A. J.; Trillat, J. F.; Bergeret, G.; Delichère, P.; Rousset, J. L.; Massardier, J.; Loffreda, D.; Simon, D.; Delbecq, F.; Sautet, P. *J. Catal.* **2001**, *198*, 243.
(130) Shustorovich, E.; Sellers, H. *Surf. Sci. Rep.* **1998**, *31*, 1.
(131) Shustorovich, E.; Bell, A. T. *Surf. Sci.* **1991**, *253*, 386.
(132) Shustorovich, E.; Bell, A. T. *Surf. Sci.* **1993**, *289*, 127.
(133) Dhainaut, F.; Pietrzik, S.; Granger, P. *Catal. Today* **2007**, *119*, 94.
(134) Dhainaut, F.; Pietrzik, S.; Granger, P. *Appl. Catal., B* **2007**, *70*, 100.
(135) Dhainaut, F.; Pietrzik, S.; Granger, P. *J. Catal.* **2008**, *258*, 296.
(136) Frank, B.; Emig, G.; Renken, A. *Appl. Catal., B* **1998**, *19*, 45.
(137) Hecker, W.; Bell, A. T. *J. Catal.* **1985**, *92*, 247.
(138) Backman, H.; Arve, K.; Klingstedt, F.; Murzin, D. Y. *Appl. Catal., A* **2006**, *304*, 86.
(139) Zukerman, R.; Vradman, L.; Herskowitz, M.; Liverts, E.; Liverts, M.; Massner, A.; Weibel, M.; Brilhac, J. F.; Blakeman, P. G.; Peace, L. J. *Chem. Eng. J.* **2009**, *155*, 419.
(140) Tian, K.; Tu, X. Y.; Dai, S. S. *Surf. Sci.* **2007**, *601*, 3186.
(141) Pérez Jigato, M.; Somasundram, K.; Termath, V.; Handy, N. C.; King, D. A. *Surf. Sci.* **1997**, *380*, 83.
(142) Delbecq, F.; Moraweck, B.; Vérité, L. *Surf. Sci.* **1998**, *396*, 156.
(143) Rainer, D. R.; Vesecky, S. M.; Koranne, M.; Oh, W. S.; Goodman, D. W. *J. Catal.* **1997**, *167*, 234.
(144) Eichler, A.; Hafner, J. *J. Catal.* **2001**, *204*, 118.
(145) Machida, M.; Watanabe, T. *Appl. Catal., B* **2004**, *52*, 281.
(146) Burch, R.; Coleman, M. D. *J. Catal.* **2002**, *208*, 435.
(147) Gonçalves, F.; Figueiredo, J. L. *Appl. Catal., B* **2006**, *62*, 181.
(148) Bonzel, H. P.; Bradshow, A. M.; Ertl, G. *Physics and Chemistry of Alkali Metal Adsorption*; Elsevier: Amsterdam, 1989.
(149) Nakamura, N.; Fujitani, T.; Hamada, H. *Surf. Sci.* **2002**, *514*, 409.
(150) Nakamura, N.; Hamada, H.; Fujitani, T. *Surf. Sci.* **2003**, *544*, 45.
(151) Orita, H.; Nakamura, N.; Fujitani, T.; Hamada, H. *Surf. Sci.* **2004**, *571*, 102.
(152) Topsøe, H. *J. Catal.* **2003**, *216*, 155.
(153) Topsøe, N. Y. *Science* **1994**, *265*, 1217.
(154) Topsøe, N. Y. *Catal. Today* **2006**, *113*, 58.
(155) Dumesic, J. A.; Topsøe, N. Y.; Topsøe, H.; Chen, Y.; Slabiak, J. *J. Catal.* **1996**, *163*, 409.
(156) Xu, L.; McCabe, R. W.; Hammerle, R. H. *Appl. Catal., B* **2002**, *39*, 51.
(157) Dulaurent, O.; Chandes, K.; Bouly, C.; Bianchi, D. *J. Catal.* **2000**, *192*, 262.
(158) Chafik, T.; Dulaurent, O.; Gass, J. L.; Bianchi, D. *J. Catal.* **1998**, *179*, 503.
(159) Bourane, A.; Dulaurent, O.; Salasc, S.; Sarda, C.; Bouly, C.; Bianchi, D. *J. Catal.* **2001**, *204*, 77.
(160) Kondarides, D. I.; Chafik, T.; Verykios, X. E. *J. Catal.* **2000**, *193*, 303.
(161) Kondarides, D. I.; Chafik, T.; Verykios, X. E. *J. Catal.* **2000**, *191*, 147.
(162) Chafik, T.; Kondarides, D. I.; Verykios, X. E. *J. Catal.* **2000**, *190*, 446.
(163) Arai, H.; Tominaga, H. *J. Catal.* **1976**, *43*, 131.
(164) Chafik, T.; Efstathiou, A. M.; Verykios, X. E. *J. Phys. Chem. B* **1997**, *101*, 7968.

(165) Almusaiteer, K. A.; Chuang, S. S. C. *J. Catal.* **1998**, *180*, 161.
(166) Unland, M. *J. Phys. Chem.* **1973**, *77*, 1952.
(167) Dujardin, C.; Mamede, A. S.; Payen, E.; Sombret, B.; Huvenne, J. P.; Granger, P. *Top. Catal.* **2004**, *30−31*, 347.
(168) Almusaiteer, K. A.; Chuang, S. C. C.; Tan, C. D. *J. Catal.* **2000**, *189*, 247.
(169) Krishnamurthy, R.; Chuang, S. S. C.; Balakos, M. W. *J. Catal.* **1995**, *157*, 512.
(170) Bourane, A.; Bianchi, D. *J. Catal.* **2004**, *222*, 499.
(171) Thibault-Starzyk, F.; Seguin, E.; Thomas, S.; Daturi, M.; Arnolds, H.; King, D. A. *Science* **2009**, *324*, 1048.
(172) Alexeev, O. S.; Krishnamoorthy, S.; Ziebart, M. S.; Yaluris, G.; Roberie, T. G.; Amiridis, M. D. *Catal. Today* **2007**, *127*, 176.
(173) Lesage, T.; Saussey, J.; Malo, S.; Hervieu, M.; Hedouin, C.; Blanchard, G.; Daturi, M. *Appl. Catal., B* **2007**, *72*, 166.
(174) Bentrup, U.; Richter, M.; Fricke, R. *Appl. Catal., B* **2005**, *55*, 213.
(175) Zuzaniuk, V.; Meunier, F. C.; Ross, J. R. H. *J. Catal.* **2001**, *202*, 340.
(176) Nova, I.; Castoldi, L.; Lietti, L.; Tronconi, E.; Forzatti, P.; Prinetto, F.; Ghiotti, G. *J. Catal.* **2004**, *222*, 377.
(177) Bion, N.; Saussey, J.; Haneda, M.; Daturi, M. *J. Catal.* **2003**, *217*, 47.
(178) Liu, Z.; Anderson, J. A. *J. Catal.* **2004**, *224*, 18.
(179) Hayes, R. E.; Kolaczkowski, S. T.; Thomas, W. *J. Comput. Chem. Eng.* **1992**, *16*, 645.
(180) Leung, D.; Hayes, R. E.; Kolaczkowski, S. T. *Can. J. Chem. Eng.* **1996**, *74*, 94.
(181) Groppi, G.; Tronconi, E.; Forzatti, P. *Catal. Rev. Sci. Eng.* **1999**, *41*, 227.
(182) Kolaczkowski, S. T. *Catal. Today* **1999**, *47*, 209.
(183) Wanker, R.; Raupenstrauch, H.; Standinger, G. *Chem. Eng. Sci.* **2000**, *55*, 4709.
(184) Tischer, S.; Deutschmann, O. *Catal. Today* **2005**, *105*, 407.
(185) Tomasic, V. *Catal. Today* **2007**, *119*, 106.
(186) Oh, S. E.; Cavendish, J. C. *Ind. Eng. Chem. Prod. Res. Dev.* **1982**, *21*, 29.
(187) Subramanian, B.; Varma, A. *Ind. Eng. Chem. Prod. Res. Dev.* **1985**, *24*, 512.
(188) Chen, D. S. K.; Bissett, E. J.; Oh, S. H.; Ostrom, V. *SAE Tech. Pap. Series* **1988**No. 880282.
(189) Voltz, S. E.; Morgan, C. R.; Liederman, D.; Jacob, S. M. *Ind. Eng. Chem. Prod. Res. Dev.* **1973**, *12*, 294.
(190) Dubien, C.; Schweich, D. *Stud. Surf. Sci. Catal.* **1998**, *116*, 399.
(191) Mannila, P.; Salmi, T.; Haario, H.; Luoma, M.; Härkönen, M.; Sohlo, J. *Appl. Catal., B* **1996**, *7*, 179.
(192) Granger, P.; Lecomte, J. J.; Leclercq, L.; Leclercq, G. *Appl. Catal., A* **2001**, *208*, 369.
(193) Zhdanov, V. P. *J. Catal.* **1996**, *162*, 147.
(194) Cho, B. K. *J. Catal.* **1996**, *162*, 149.
(195) Cho, B. K. *J. Catal.* **1994**, *148*, 697.
(196) Granger, P.; Malfoy, P.; Leclercq, G. *J. Catal.* **2004**, *223*, 142.
(197) Granger, P.; Malfoy, P.; Esteves, P.; Leclercq, L.; Leclercq, G. *J. Catal.* **1999**, *187*, 321.
(198) Mac Cabe, R. W.; Wong, C. *J. Catal.* **1990**, *121*, 422.
(199) Adlhoch, W.; Kohler, R.; Linz, H. G. *Z. Phys. Chem. (NF)* **1980**, *120*, 111.
(200) Banse, B. A.; Wickham, D. T.; Koel, B. E. *J. Catal.* **1989**, *119*, 238.
(201) Cho, B. K.; Shanks, B. T.; Baylet, J. E. *J. Catal.* **1989**, *115*, 486.
(202) Granger, P.; Dhainaut, F.; Pietrzik, S.; Malfoy, P.; Mamede, A. S.; Leclercq, L.; Leclercq, G. *Top. Catal.* **2006**, *39*, 65.
(203) Burch, R.; Fornasiero, P.; Southward, B. W. L. *J. Catal.* **1999**, *182*, 234.
(204) Burch, R.; Watling, T. C. *J. Catal.* **1997**, *169*, 45.
(205) Burch, R.; Sullivan, J. A. *J. Catal.* **1999**, *182*, 489.
(206) Mhadeshwar, A. B.; Winkler, B. H.; Eiteneer, B.; Dancu, D. *Appl. Catal., B* **2009**, *89*, 229.
(207) Kameoka, S.; Chafik, T.; Ukisu, Y.; Miyadera, T. *Catal. Lett.* **1998**, *51*, 11.
(208) Gao, H.; He, H. *Spectrochim. Acta, Part A* **2005**, *61*, 1233.
(209) Backman, H.; Jensen, J.; Klingstedt, F.; Salmi, T.; Murzin, D. Y. *Appl. Catal., A* **2005**, *294*, 49.
(210) Breen, J. P.; Burch, R.; Hardacre, C.; Hill, C. J. *J. Phys. Chem. B* **2005**, *109*, 4805.
(211) Breen, J. P.; Burch, R.; Hardacre, C.; Hill, C. J.; Rioche, C. *J. Catal.* **2007**, *246*, 1.
(212) Satokawa, S.; Shibata, J.; Shimizu, K.; Satsuma, A.; Hattori, T. *Appl. Catal., B* **2003**, *42*, 179.
(213) Shibata, J.; Shimizu, K.; Satokawa, S.; Satsuma, A.; Hattori, T. *Phys. Chem. Chem. Phys.* **2003**, *5*, 2154.
(214) Richter, M.; Bentrup, U.; Eckelt, R.; Schneider, M.; Pohl, M. M.; Fricke, R. *Appl. Catal., B* **2004**, *51*, 261.
(215) Tronconi, E.; Nova, I.; Ciardelli, C.; Chatterjee, D.; Bandl-Konrad, G.; Burkhardt, T. *Catal. Today* **2005**, *105*, 529.
(216) Ciardelli, C.; Nova, I.; Tronconi, E.; Chatterjee, D.; Bandl-Konrad, B.; Weibel, M.; Krutzsch, B. *Appl. Catal., B* **2007**, *70*, 80.
(217) Ciardelli, C.; Nova, I.; Tronconi, E.; Konrad, B.; Chatterjee, D.; K., E.; Weibel, M. *Chem. Eng. Sci.* **2004**, *59*, 5301.
(218) Guethenke, A.; Chaterjee, D.; Weibel, M.; Krutzch, B.; Koci, P.; Marek, M.; Nova, I.; Tronconi, E. *Adv. Chem. Eng.* **2008**, *33*, 103.
(219) deVries, J. E.; Yao, H. C.; Baird, R. J.; Gandhi, H. S. *J. Catal.* **1983**, *84*, 8.
(220) Plummer, H. K. J.; Shinozaki, S.; Adams, K. M.; Gandhi, H. S. *J. Mol. Catal.* **1983**, *20*, 251.
(221) Halasz, I.; Brenner, A.; Shelef, M. *Appl. Catal.* **1992**, *82*, 51.
(222) Ioan, B.; Miyazaki, A.; Aika, K. *Appl. Catal., B* **2005**, *59*, 71.
(223) Castillo, S.; Morán-Pineda, M.; Molina, V.; Gómez, R.; López, T. *Appl. Catal., B* **1998**, *15*, 203.
(224) Seker, E.; Gulari, E. *J. Catal.* **1998**, *179*, 339.
(225) Castillo, S.; Morán-Pineda, M.; Gómez, R.; López, T. *J. Catal.* **1997**, *172*, 263.
(226) Nishihata, Y.; Mizuki, J.; Akao, T.; Tanka, H.; Uenishi, M.; Kimura, M.; Okamoto, T.; Hamada, N. *Nature* **2002**, *418*, 164.
(227) Tan, I.; Tanaka, H.; Uenishi, M.; Kajita, N.; Taniguchi, M.; Y., N.; Mizuki, J. *SAE Tech. Pap. Ser.* **2003**No. 2003-01-0812.
(228) Tanaka, H.; Tan, I.; Uenishi, M.; Taniguchi, M.; Kimura, M.; Nishihata, Y.; Mizuki, J. *J. Alloys Compd.* **2006**, *408−412*, 1071.
(229) Uenishi, M.; Tanaka, H.; Taniguchi, M.; Tan, I.; Sakamoto, Y.; Matsunaga, S.; Yokota, K.; Kobayashi, T. *Appl. Catal., A* **2005**, *296*, 114.
(230) Uenishi, M.; Taniguchi, M.; Tanaka, H.; Kimura, M.; Nishihata, Y.; Mizuki, J.; Kobayashi, T. *Appl. Catal., B* **2004**, *57*, 265.
(231) Nishihata, Y.; Mizuki, J.; Tanaka, H.; Uenishi, M.; Kimura, M. *J. Phys. Chem. Solids* **2005**, *66*, 274.
(232) Tanaka, H.; Mizuno, N.; Misono, M. *Appl. Catal., A* **2003**, *244*, 371.
(233) Tanaka, H.; Tan, I.; Sato, N.; Narita, K.; Kimura, M.; Uenishi, M.; Kajita, N.; Taniguchi, M. *SAE Tech. Pap. Ser.* **2003**No. 2003-01-0813.
(234) Dacquin, J. P.; Cabié, M.; Henry, C. R.; Lancelot, C.; Dujardin, C.; Raouf, S. R.; Granger, P. *J. Catal.* **2010**, *270*, 299.
(235) Tennison, P.; Lambert, C.; Levin, M. *SAE Tech. Pap. Ser.* 2004No. 2004-01-1291.
(236) Cheng, Y.; Montreuil, C.; Cavataio, G.; Lambert, C. *SAE Tech. Pap. Ser.* **2009**No. 2009-01-0898.
(237) Papadakis, K.; Odenbrand, C. U. I.; Creaser, D. *SAE Tech. Pap. Ser.* **2003**No. 2003-01-1884.
(238) Papadakis, K.; Odenbrand, C. U. I.; Creaser, D. *Top. Catal.* **2004**, *30−31*, 215.
(239) Papadakis, K.; Odenbrand, C. U. I.; Sjoblom b, J.; Creaser, D. *Appl. Catal., B* **2007**, *70*, 215.
(240) Patchett, J. A.; Verbeek, R. P.; Grimston, K. R.; Rice, G. W.; Calabrese, J. L.; van Genderen, M. U.S. Patent 20020152745, 2002, to Engelhard Co., NL.
(241) Tourtellotte, J. F. U.S. Patent 3,656,915, 1972, to Chemical Construction Corportion, U.S.A.

(242) Yoshimoto, M.; Nakatsuji, T.; Yoshida, K. U.S. Patent 5,180,567, 1993, to Sakay Chemical Industry Co, Ltd, Jpn.
(243) Shirai, D.; Hiramoto, H.; Kanaya, I.; Ueno, H. U.S. Patent 2007/0175204, 2007, to Tokyo Roki Co, Ltd and Nissan Diesel Motor Co.,Ltd., Jpn.
(244) Ruman, M. A.; Donahue, R. J.; Liegeois, D. D. U.S. Patent 6,622,481, 2003, to Brunswick Co., U.S.A
(245) Nakano, M. U.S. Patent 7,421,838, 2008, to Nissan Motor Co., Ltd, Jpn.
(246) Hirano, T.; Sato, Y.; Nomoto, K. U.S. Patent 2008/0307777, 2008.
(247) Takahashi, H.; Umezawa, K.; Tsutsui, Y. U.S. Patent 7,367,182, 2008, to Mitsubishi Fuso Truck and Bus Corporation, Jpn.
(248) Brück, R.; Scheeder, A. U.S. Patent 7,597,859, 2009, to Emitec Gesellschaft fuer Emissionstechnolgie GmbH, DE
(249) Demura, T. U.S. Patent 2010/0024399, 2010, to Toyota Jidosha Kabushiki Kaisha, Jpn.
(250) Sung, S.; Rabinowitz, H. N.; Smaling, R. M. U.S. Patent 6,087,298, 2000, to Engelhard Corporation, U.S.A.
(251) Takahashi, Y. U.S. Patent 6,260,353, 2002, to Mitsubishi Jidosha Kogyo Kabushiki Kaisha, Jpn.
(252) Tamura, Y.; Nakayama, O.; Koga, K. U.S. Patent 6,532,733, 2003, to Mitsubishi Jidosha Kogyo Kabushiki Kaisha, Jpn.
(253) Hirata, H.; Kakinohana, M.; Ibe, M. U.S. Patent 20090019844, 2009, to Toyota Jidosha Kabushiki Kaisha, Jpn.
(254) Patchett, J. A.; Verbeek, R. P.; Grimston, K. R.; Rice, G. W.; Calabrese, J. L.; Van Genderen, M. U.S. Patent 6,581,374, 2003, to Engelhard Corporation, U.S.A and Tno, Automotive, NL.
(255) Gladden, J. R. U.S. Patent 4,188,364, 1980, to Caterpillar Tractor Co. U.S.A.
(256) Gladden, J. R. U.S. Patent 4,403,473, 1983, to Caterpillar Tractor Co. U.S.A.
(257) Kobayashi, M.; Kinoshita, F.; Hagi, M.; Inoue, A.; Uno, T. U.S. Patent 5,116,579, 1992, to Nippon Shokubai Kagaku Kogyo Co., Ltd., Jpn.
(258) Walker, J.; Speronello, B. K. *SAE Tech. Pap. Ser.* **1992**No. 921673.
(259) Girard, J.; Snow, R.; Cavataio, G.; Lambert, C. *SAE Tech. Pap. Ser.* **2007**No. 2007-01-1581.
(260) Lepperhoff, S.; Huthwohl, S.; Pischinger, F. *SAE Tech. Pap. Ser.* **1992**No. 925022.
(261) Hug, H. T.; Mayer, A.; Hartenstein, A. *SAE Tech. Pap. Ser.* **1993**No. 930363.
(262) Luders, H.; Backes, R.; Huthwohl, G.; Ketcher, D. A.; Horrocks, R. W.; Hurley, R. G.; Hammerle, R. H. *SAE Tech. Pap. Ser.* **1995**No. 952493.
(263) Koebel, M.; Elsener, M.; Marti, T. *Combust. Sci. Technol.* **1996**, *121*, 85.
(264) Horvath, B.; Geyer, J.; Krauss, H. L. *Z. Anorg. Allg. Chem.* **1976**, *426*, 141.
(265) Imanari, M.; Watanabe, Y.; Matsuda, S.; Nakajima, F. *In Proceedings 7th International Congress on Catalysis, Tokyo, 1980*; Seiyama, T., Tanabe, K., Eds.; Elsevier: Amsterdam, 1981, p 604.
(266) Miyamoto, A.; Yamazaki, Y.; Inomata, M.; Murakami, Y. *J. Phys. Chem.* **1981**, *85*, 2366.
(267) Chien, J. W. *J. Am. Chem. Soc.* **1971**, *93*, 4675.
(268) Bond, G. C.; Brockmann, K. *Faraday Discuss. Chem. Soc.* **1981**, *72*, 235.
(269) Roozeboom, F.; Fransen, T.; Mars, P.; Gellings, P. *Z. Anorg. Allg. Chem.* **1979**, *449*, 25.
(270) van Hengstum, A. J.; van Ommen, J. G.; Bosch, H.; Gellings, P. *Appl. Catal.* **1983**, *5*, 207.
(271) van Ommen, J. G.; Hoving, K.; Bosch, H.; van Hengstum, A. J.; Gellings, P. J. *Z. Phys. Chem. (NF)* **1983**, *134*, 99.
(272) Kyenski, J.; Baiker, A.; Glinski, M.; Dollenmeier, P.; Wokaun, A. *J. Catal.* **1986**, *101*, 1.
(273) Vogt, E. T. C.; Boot, A.; Van Dillen, A. J.; Geus, J. W.; Janssen, F. J. J. G.; Van Den Kerkhof, F. M. G. *J. Catal.* **1988**, *114*, 313.
(274) Zhang, X.; Li, X.; Wu, J.; Yang, R.; Zhang, Z. *Catal. Lett.* **2009**, *130*, 235.
(275) Parvulescu, V. I.; Parvulescu, V.; Boghosian, S.; Jung, S. M.; Grange, P. *J. Catal.* **2003**, *217*, 172.
(276) Stark, W. J.; Wegner, K.; Pratsinis, S. E.; Baiker, A. *J. Catal.* **2001**, *197*, 182.
(277) Stark, W. J.; Baiker, A.; Pratsinis, S. E. *Part. Part. Syst. Charact.* **2002**, *19*, 306.
(278) Girard, J. W.; Montreuil, C.; Kim, J.; Cavataio, G.; Lambert, C. *SAE Tech. Pap.* **2008**No. 2008-01-1029.
(279) Phil, H. H.; Reddy, M. P.; Kumar, P. A.; Ju, L. K.; Hyo, J. S. *Appl. Catal., B* **2008**, *78*, 301.
(280) Topsøe, N.-Y.; Anstromb, M.; Dumesic, J. A. *Catal. Lett.* **2001**, *76*, 11.
(281) Tronconi, E.; Nova, I.; Ciardelli, C.; Chatterjee, D.; Weibel, M. *J. Catal.* **2007**, *245*, 1.
(282) Boyano, A.; Iritia, M. C.; Malpartida, I.; Larrubia, M. A.; Alemany, L. J.; Moliner, R.; Lazaro, M. J. *Catal. Today* **2008**, *137*, 222.
(283) Teng, H.; Tu, Y.-T.; Lai, Y.-C.; Lin, C.-C. *Carbon* **2001**, *39*, 575.
(284) Tang, X.; Hao, J.; Yi, H.; Li, J. *Catal. Today* **2007**, *126*, 406.
(285) Adamski, A.; Gil, B.; Sojka, Z. *Catal. Today* **2008**, *137*, 292.
(286) Shirono, K.; Koyanagi, T. U.S. Patent 20090214397, 2009, to JGC Catalysts and Chemicals Ltd., Jpn.
(287) Schafer-Sindlinger, A.; Pfeifer, M.; Spurk, P.; Demel, Y.; Kreuzer, T.; Lox, E. S. U.S. Patent 20050196333, 2005, to Umicore AG & Co., KG, De.
(288) Cavataio, G.; Girard, J.; Patterson, J. E.; Montreuil, C.; Cheng, Y.; Lambert, C. K. *SAE Tech. Pap.* **2007**No. 2007-01-1575.
(289) Cheng, Y.; Montreuil, C.; Cavataio, G.; Lambert, C. *SAE Tech. Pap. Ser.* **2008**No. 2008-01-1023.
(290) Girard, J.; Cavataio, G.; Snow, R.; Lambert, C. *SAE Tech. Pap. Ser.* **2008**No. 2008-01-1185.
(291) Azhar Uddin, M.; Shimizu, K.; Ishibe, K.; Sasaoka, E. *J. Mol. Catal. A: Chem.* **2009**, *309*, 178.
(292) Krishna, K.; Makkee, M. *Catal. Today* **2006**, *114*, 23.
(293) Moura de Oliveira, M. L.; Monteiro Silva, C.; Moreno-Tost, R.; Lopes Farias, T.; Jimenez-Lopez, A.; Rodriguez-Castellon, E. *Appl. Catal., B* **2009**, *88*, 420.
(294) Moura de Oliveira, M. L.; Monteiro Silva, C.; Moreno-Tost, R.; Lopes Farias, T.; Jimenez-Lopez, A.; Rodriguez-Castellon, E. *Appl. Catal., A* **2009**, *366*, 13.
(295) Moreno-Tost, R.; Oliveira, M. L.; Eliche-Quesada, D.; Jiménez-Jiménez, J.; Jiménez-López, A.; Rodríguez-Castellón, E. *Chemosphere* **2008**, *72*, 608.
(296) Chmielarz, L.; Kustrowski, P.; Michalik, M.; Dudek, B.; Piwowarska, Z.; Dziembaj, R. *Catal. Today* **2008**, *137*, 242.
(297) Segura, Y.; Chmielarz, L.; Kustrowski, P.; Cool, P.; Dziembaj, R.; Vansant, E. F. *Appl. Catal., B* **2005**, *61*, 69.
(298) Chmielarz, L.; Kustrowski, P.; Dziembaj, R.; Cool, P.; Vansant, E. F. *Appl. Catal., B* **2006**, *62*, 369.
(299) Segura, Y.; Chmielarz, L.; Kustrowski, P.; Cool, P.; Dziembaj, R.; Vansant, E. F. *J. Phys. Chem. B* **2006**, *110*, 948.
(300) Huang, J.; Tong, Z.; Huang, Y.; Zhang, J. *Appl. Catal., B* **2008**, *78*, 309.
(301) Motak, M. *Catal. Today* **2008**, *137*, 247.
(302) Szymanski, G.; Grzybek, T.; Papp, H. *Catal. Today* **2004**, *90*, 51.
(303) Grzybek, T.; Klinik, J.; Samojeden, B.; Suprun, V.; Papp, H. *Catal. Today* **2008**, *137*, 228.
(304) Grzybek, T.; Klinik, J.; Motak, M.; Papp, H. *Catal. Today* **2008**, *137*, 235–4491.
(305) Kleemann, M.; Elsener, M.; Koebel, M.; Wokaun, A. *Ind. Eng. Chem. Res.* **2000**, *39*, 4120.
(306) Position Papers, J., 2003, http://www.acea.be.
(307) Schmelz, H. U.S. Patent 5,833,932, 1998, to Siemens Aktiengesellschaft.
(308) Neufert, R.; Mathes, W.; Schobert-Schaefer, D.; Hofmann, L. U.S. Patent 5,785,937, 1998, to Siemens Aktiengesellschaft, De.
(309) Andreasson, A.; Chandler, G. R.; Goersmann, C. F.; Warren, J. P.; Huethwohl, G. U.S. Patent 7,498,010, 2009, to Johnson Matthey

Public Ltd Co, GB, Daimler AG, De, HJS Fahrzeugtechnik GmbH & Co KG, De.
(310) Fulks, G.; Fisher, G. B.; Rahmoeller, K.; Wu, M.-C.; , E.; Tan, J. *SAE Tech. Pap.* **2009**No. 2009-01-0907.
(311) Havenith, C.; Verbeek, R. P. *SAE Tech. Pap. Ser.* **1997**No. 970185.
(312) Birkhold, F.; Meingast, U.; Wassermann, P.; Deutschmann, O. *Appl. Catal., B* **2007**, *70*, 119.
(313) van Helden, R.; Verbeek, R.; Willems, F. *SAE Tech. Pap. Ser.* **2004**No. 2004.
(314) Wurzenberger, J. C.; Wanker, R. *SAE Tech. Pap. Ser.* **2005**No. 2005-01-0948.
(315) Chen, M.; Williams, S. *SAE Tech. Pap. Ser.* **2005**No. 2005-01-0969.
(316) Schaber, P. M.; Colson, J.; Higgins, S.; Thielen, D.; Anspach, B.; Brauer, J. *Thermochim. Acta* **2004**, *424*, 131.
(317) Fang, H. L.; DaCosta, H. F. M. *Appl. Catal., B* **2003**, *46*, 18.
(318) Hauck, P.; Jentys, A.; Lercher, J. A. *Appl. Catal., B* **2007**, *70*, 91.
(319) Tronconi, E.; Beretta, A.; Elmi, A. S.; Forzatti, P.; Malloggi, S.; Baldacci, A. *Chem. Eng. Sci.* **1994**, *49*, 4277.
(320) Kim, J. Y.; Cavataio, G.; Patterson, J. E.; Laing, P. M.; Lambert, C. K. *SAE Tech. Pap. Ser.* **2007**No. 2007-01-1573.
(321) Cavataio, G.; Kim, J. Y.; Warner, J. R.; Girard, J. W.; Upadhyay, D.; Lambert, C. K. *SAE Tech. Pap. Ser.* **2009**No. 2009-01-1282.
(322) Sullivan, J. A.; Doherty, J. A. *Appl. Catal., B* **2005**, *55*, 185.
(323) He, C.; Wang, Y.; Cheng, Y.; Lambert, C. K.; Yang, R. T. *Appl. Catal., A* **2009**, *368*, 121.
(324) Li, J.; Zhu, R.; Cheng, Y.; Lambert, C. K.; Yang, R. *Environ. Sci. Technol.* **2010**, *44*, 1799.
(325) Cheng, Y.; Hoard, J.; Lambert, C.; Kwak, J. H.; Peden, C. H. F. *Catal. Today* **2008**, *136*, 34.
(326) Sampara, C. S.; Bissett, E. J.; Assanis, D. *Chem. Eng. Sci.* **2008**, *63*, 5179.
(327) Jen, H.-W.; Girard, J. W.; Cavataio, G.; Jagner, M. J. *SAE Tech. Pap. Ser.* **2008**No. 2008-01-2488.
(328) Cavataio, G.; Jen, H.-W.; Girard, J. W.; Dobson, D.; Warner, J. R.; Lambert, C. K. *SAE Tech. Pap. Ser.* **2009**No. 2009-01-0627.
(329) Irfan, M. F.; Goo, J. H.; Kim, S. D. *Appl. Catal., B* **2008**, *78*, 267.
(330) Mota, N.; Alvarez-Galvan, M. C.; Villoria, J. A.; Rosa, F.; Fierro, J. L. G.; Navarro, R. M. *Top. Catal.* **2009**, *52*, 1995.
(331) Brand, R.; Engler, B.; Kleine-Moellhoff, P.; Koberstein, E. U.S. Patent 4,963,332, 1990, to Degussa Aktiengesellschaft, De.
(332) Lane, W. H.; Peterson, R. N.; Smith, A. L.; White, S. T.; Learned, D. J. International Patent WO 006270, 1996, to Caterpillar Inc., U.S.A.
(333) Polcer, J. U.S. Patent 5,047,220, 1991, to Foster Wheeler Energy Co., U.S.A.
(334) Shiraishi, Y.; Ukawa, N. U.S. Patent 4,314,345, 1982, to Mitsubishi Jukogyo Kabushiki Kaish.
(335) Sampara, C. S.; Bissett, E. J.; Chmielewski, M. *Ind. Eng. Chem. Res.* **2008**, *47*, 311.
(336) Kakwani, R. M.; Voss, K. C.; Patchett, J. A.; Grimston, K. R. U. S. Patent 7,143,578, 2006, to Engelhard Corporation, U.S.A.
(337) Martens, A.; Cauvel, A.; Francis, A.; Hermans, C.; Jayat, F.; Remy, M.; Keung, M.; Lievens, J.; Jacobs, P. A. *Angew. Chem., Int. Ed.* **1998**, *37*, 1901.
(338) Jacobs, P. A.; Uytterhoeven, J. B.; Beyer, H. K. *J. Chem. Soc., Faraday Trans.* **1977**, *73*, 1755.
(339) Jacobs, P. A. *Stud. Surf. Sci. Catal.* **1986**, *29*, 357.
(340) She, X.; Flytzani-Stephanopoulos, M.; Wang, C.; Wang, Y.; Peden, C. H. F. *Appl. Catal., B* **2009**, *88*, 98.
(341) Shia, C.; Cheng, M.; Qu, Z.; Bao, X. *J. Mol. Catal. A: Chem.* **2005**, *235*, 35.
(342) Shimizu, K.; Satsuma, A.; Hattori, T. *Appl. Catal., B* **2000**, *25*, 239.
(343) Shimizu, K.; Shibata, J.; Yoshida, H.; Satsuma, A.; Hattori, T. *Appl. Catal., B* **2001**, *30*, 151.
(344) Shimizu, K.; Shibata, J.; Satsuma, A.; Hattori, T. *Phys. Chem. Chem. Phys.* **2001**, *3*, 880.
(345) Sazama, P.; Capek, L.; Drobná, H.; Sobalík, Z.; Dedecek, J.; Arve, K.; Wichterlová, B. *J. Catal.* **2005**, *232*, 302.
(346) Lee, H.; Schmieg, S. J.; Oh, S. H. *Appl. Catal., A* **2008**, *342*, 78.
(347) Shimizu, K.-I.; Tsuzuki, M.; Satsuma, A. *Appl. Catal., B* **2007**, *71*, 80.
(348) Satokawa, S. *Chem. Lett.* **2000**, 294.
(349) Burch, R.; Breen, J. P.; Hill, C. J.; Krutzsch, B.; Konrad, B.; Jobson, E.; Cider, L.; Eranen, K.; Klingstedt, F.; Lindfors, L.-E. *Top. Catal.* **2004**, *30/31*, 19.
(350) Eranen, K.; Klingstedt, F.; Arve, K.; Lindfors, L.-E.; Murzin, D. Y. *J. Catal.* **2004**, *227*, 328.
(351) Klingstedt, F.; Arve, K.; Eranen, K.; Murzin, D. Y. *Acc. Chem. Res.* **2006**, *39*, 273.
(352) Burch, R. *Catal. Rev. Sci. Eng.* **2004**, *46*, 271.
(353) Arve, K.; Backman, H.; Klingstedt, F.; Eranen, K.; Murzin, D. Y. *Appl. Catal., B* **2007**, *70*, 65.
(354) Shibata, J.; Takada, Y.; Shichi, A.; Satokawa, S.; Satsuma, A.; Hattori, T. *J. Catal.* **2004**, *222*, 368.
(355) Shibata, J.; Shimizu, K.-i.; Takada, Y.; Shichi, A.; Yoshida, H.; Satokawa, S.; Satsuma, A.; Hattori, T. *J. Catal.* **2004**, *227*, 367.
(356) Satokawa, S.; Shibata, J.; Shimizu, K.-i.; Satsuma, A.; Hattori, T.; Kojima, T. *Chem. Eng. Sci.* **2007**, *62*, 5335.
(357) Breen, J. P.; Burch, R.; Hardacre, J.; Hill, C. J.; Krutzsch, B.; Bandl-Konrad, B.; Jobson, E.; Cider, L.; Blakeman, P. G.; Peace, L. J.; Twigg, M. V.; Preis, M.; Gottschling, M. *Appl. Catal., B* **2007**, *70*, 36.
(358) Houel, V.; James, D.; Millington, P.; Pollington, S.; Poulston, S.; Rajaram, R.; Torbati, R. *J. Catal.* **2005**, *230*, 150.
(359) Gabrielsson, P. L. T. *Top. Catal.* **2004**, *28*, 177.
(360) Fisher, G. B.; Dimaggio, C. L.; Rahmoeller, K. M.; Sellnau, M. C. U.S. Patent 20100000202, 2010, to Delphi Technologies, Inc., U. S.A.
(361) Boutros, M.; Trichard, J.-M.; Da Costa, P. *Appl. Catal., B* **2009**, *91*, 640.
(362) He, H.; Li, Y.; Zhang, X.; Yu, Y.; Zhang, C. *Appl. Catal., A* **2010**, *375*, 258.
(363) da Silva, R.; Cataluna, R.; Martinez-Arias, A. *Catal. Today* **2009**, *143*, 242.
(364) He, H.; Yu, Y. *Catal. Today* **2005**, *100*, 37.
(365) Dong, H.; Shuai, S.; Li, R.; Wang, J.; Shi, X.; He, H. *Chem. Eng. J.* **2008**, *135*, 195.
(366) Tamm, S.; Ingelsten, H. H.; Skoglundh, M.; Palmqvist, A. E. C. *Top. Catal.* **2009**, *52*, 1813.
(367) Nakatsuji, T.; Yasukawa, R.; Tabata, K.; Ueda, K.; Niwa, M. *Appl. Catal., B* **1998**, *17*, 333.
(368) Pârvulescu, V. I.; Cojocaru, B.; Pârvulescu, V.; Richards, R.; Li, Z.; Cadigan, C.; Granger, P.; Miquel, P.; Hardacre, C. *J. Catal.* **2010**, *272*, 92.
(369) Breen, J. P.; Burch, R.; Hill, C. J. *Catal. Today* **2009**, *145*, 34.
(370) Richter, M.; Fricke, R.; Eckelt, R. *Catal. Lett.* **2004**, *94*, 115.
(371) Kondratenko, E.; Kondratenko, V. A.; Richter, M.; Fricke, R. *J. Catal.* **2006**, *239*, 23.
(372) Shimizu, K.-I.; Satsuma, A. *Appl. Catal., B* **2007**, *77*, 202.
(373) Burdeinaya, T. N.; Matyshak, V. A.; Tretyakov, V. F.; Glebov, L. S.; Zakirova, A. G.; Carvajal Garcia, M. A.; Arias Villanueva, M. E. *Appl. Catal., B* **2007**, *70*, 128.
(374) Konova, P.; Arve, K.; Klingstedt, F.; Nikolov, P.; Naydenov, A.; Kumar, N.; Murzin, D. Y. *Appl. Catal., B* **2007**, *70*, 138.
(375) Eranen, K.; Lindfors, L.-E.; Klingstedt, F.; Murzin, D. Y. *J. Catal.* **2003**, *219*, 25.
(376) Yashnik, S. A.; Kuznetsov, V. V.; Ismagilov, Z. R.; Ushakov, V. V.; Danchenko, N. M.; Denisov, S. P. *Top. Catal.* **2004**, *30/31*, 293.
(377) Yashnik, S. A.; Ismagilov, Z. R.; Porsin, A. V.; Denisov, S. P.; Danchenko, N. M. *Top. Catal.* **2007**, *42*−*43*, 465.
(378) Corbos, E. C.; Haneda, M.; Courtois, X.; Marecot, P.; Duprez, D.; Hamada, H. *Catal. Commun.* **2008**, *10*, 137.
(379) Corbos, E. C.; Haneda, M.; Courtois, X.; Marecot, P.; Duprez, D.; Hamada, H. *Appl. Catal., A* **2009**, *365*, 187.

(380) Sullivan, J. A.; Keane, O. *Appl. Catal., B* **2007**, *70*, 205.
(381) Serra, R.; Vecchietti, V.; Miro, E.; Boix, A. *Catal. Today* **2008**, *133*−*135*, 480.
(382) Neylon, M. K.; Castagnola, M. J.; Castagnola, N. B.; Marshall, C. L. *Catal. Today* **2004**, *96*, 53.
(383) Pârvulescu, V. I.; Grange, P.; Delmon, B. *Appl. Catal., B* **2001**, *33*, 223.
(384) Castagnola, M. J.; Neylon, M. K.; Marshall, C. L. *Catal. Today* **2004**, *96*, 61.
(385) Seo, J.-M.; Chang, H.-S.; Kim, S.-K. *SAE Pap.* **2006**No. 2006-01-0422.
(386) Nickolas, S. G.; White, A. D.; Kotrba, A. J.; Yetkin, A. *SAE Paper* **2006**No. 2006-01-1089.
(387) Lee, J. H.; Paratore, M.; Brown, D. *SAE Paper* **2008**No. 2008-01-0072.
(388) Cavataio, G.; Girard, J. W.; Lambert, C. K. *SAE Tech. Pap.* **2009**No. 2009-01-0897.
(389) Gomez-Garcia, M. A.; Zimmermann, Y.; Pitchon, V.; Kiennemann, A. *Catal. Commun* **2007**, *8*, 400.
(390) Girard, J. W.; Cavataio, G.; Lambert, C. K. *SAE Tech. Pap.* **2007**No. 2007-01-1572.
(391) Mccarthy Jr., J. E.; Bailey, O. H. U.S. Patent 20080282670, 2008.
(392) Harle, V.; Rocher, L. U.S. Patent WO107364, 2008, to Rhodia operations, Fr.
(393) Murachi, M.; Okawara, S.; Kojima, K.; Kondo, T. U.S. Patent 5,746,989, 1998, to Toyota Jidosha Kabushiki Kaisha, Jpn.
(394) Alcorn, W. R. U.S. Patent 4,912,776, 1990, to W. R. Grace & Co.-Conn., U.S.A.
(395) Sanchez, B. S.; Querini, C. A.; Miro, E. E. *Appl. Catal., A* **2009**, *366*, 166.
(396) Fino, D.; Fino, P.; Saracco, G.; Specchia, V. *Appl. Catal., B* **2003**, *43*, 243.
(397) Fino, D.; Russo, N.; Saracco, G.; Specchia, V. *J. Catal.* **2003**, *242*, 38.
(398) Russo, N.; Fino, D.; Saracco, G.; Specchia, V. *J. Catal.* **2005**, *229*, 459.
(399) Mescia, D.; Caroca, J. C.; Russo, N.; Labhsetwar, N.; Fino, D.; Saracco, G.; Specchia, V. *Catal. Today* **2008**, *137*, 300.
(400) Nejar, N.; Illan-Gomez, M. J. *Appl. Catal., B* **2007**, *70*, 261.
(401) Querini, C. A.; Cornaglia, L. M.; Ulla, M. A.; Miro, E. E. *Appl. Catal.* **1999**, *20*, 165.
(402) Olong, N. E.; Stowe, K.; Maier, W. F. *Catal. Today* **2008**, *137*, 110.
(403) Hendershot, R. J.; Vijay, R.; Snively, C. M.; Lauterbach, J. *Appl. Catal., B* **2007**, *70*, 160.
(404) Kobayashi, T.; Yamada, T.; Kayano, K. *SAE* **1997**No. 970745.
(405) Hepburn, J. S.; Thanasiu, E.; Dobson, D. A.; Watkins, W. L. *SAE Pap.* **1996**No. 962051.
(406) Fekete, N.; Kemmler, R.; Voigtländer, D.; Krutzsch, B.; Zimmer, E.; Wenninger, G.; Strehlau, W.; Van den Tillaart, J. A. A.; Leyrer, J.; Lox, E. S.; Müller, W. *SAE Pap.* **1997**No. 970746.
(407) Cheng, Y.; Cavataio, J. V.; Hoard, J. W.; Hammerle, R. H. *SAE* **2004**No. 2004-01-0156.
(408) Parks, J. E.; Wagner, G. J.; Epling, W. E.; Sanders, M. W.; Campbell, L. E. *SAE* **1999**No. 1999-01-3557.
(409) Bouchez, M.; Dementhon, J.-B.; Messaoudi, I.; Guyon, M.; Noirot, R. *SAE* **2001**No. 2001-01-1934.
(410) Künkel, C.; Ingemar Odenbrand, C. U. *SAE* **2001**No. 2001-01-3666.
(411) Fang, H. L.; Huang, S. C.; Yu, R. C.; Wan, C. Z.; Howden, K. *SAE* **2002**No. 2002-01-2889.
(412) Schenk, C.; McDonald, J.; Olson, B. *SAE* **2001**No. 2001-01-1351.
(413) Twigg, M. V.; Wilkins, A. J. J. U.S. Patent 6,857,265, 2005, to Johnson Matthey Pub. Ltd Co.
(414) Twigg, M. V. U.S. Patent 7,404,933, 2008, to Johnson Matthey Public Ltd Co, GB.
(415) Ginter, D. M.; Mccarthy, J. E. U.S. Patent 20080168763, 2008, to Eaton Co., U.S.A.
(416) Castoldi, L.; Nova, I.; Lietti, L.; Forzatti, P. *Catal. Today* **2004**, *96*, 43.
(417) Epling, W.; Parks, J.; Campbell, G.; Yezerets, A.; Currier, N.; Campbell, L. *Catal. Today* **2004**, *96*, 21.
(418) Epling, W.; Campbell, L.; Yezerets, A.; Currier, N.; Parks, J. *Catal. Rev. Sci. Eng.* **2004**, *46*, 163.
(419) Olsson, L.; Fridell, E.; Skoglundh, M.; Andersson, B. *Catal. Today* **2002**, *73*, 263.
(420) Laurent, F.; Pope, C. J.; Mahzoul, H.; Delfosse, L.; Gilot, P. *Chem. Eng. Sci.* **2003**, *58*, 1793.
(421) Theis, J. I.; Gobel, U.; Kogel, M.; Kreuzer, T. P.; Lindner, D.; Lox, E.; Ruwisch, L. *SAE Tech. Pap.* **2002**, No. Special Edition SP-1676, 1.
(422) Olsson, L.; Blint, R. J.; Fridell, E. *Ind. Eng. Chem. Res.* **2005**, *44*, 3021.
(423) Tuttlies, U.; Schmeisser, V.; Eigenberger, G. *Top. Catal.* **2004**, *30/31*, 187.
(424) Scholz, C. M. L.; Gangwal, V. R.; Hoebink, J. H. B. J.; Schouten, J. C. *Appl. Catal., B* **2007**, *70*, 226.
(425) Broqvist, P.; Gronbeck, H.; Fridell, E.; Panas, I. *Catal. Today* **2004**, *96*, 71.
(426) Mahzoul, H.; Brilhac, J. F.; Gilot, P. *Appl. Catal., B* **1999**, *20*, 47.
(427) Lietti, L.; Forzatti, P.; Nova, I.; Tronconi, E. *J. Catal.* **2001**, *204*, 175.
(428) James, D.; Fourre, E.; Ishii, M.; Bowker, M. *Appl. Catal., B* **2003**, *45*, 147.
(429) Buchel, R.; Strobel, R.; Baiker, A.; Pratsinis, S. E. *Top. Catal.* **2009**, *52*, 1709.
(430) Castoldi, L.; Lietti, L.; Matarrese, R.; Forzatti, P. *Top. Catal.* **2009**, *52*, 1713.
(431) Hepburn, J. EP Patent 0778072 A2, 1997, to Ford Motor Company Ltd. (GB), Ford France SA (Fr), Ford-werke aktiengesekkschaft (De).
(432) Stanglmaier, R. H.; Roecker, R. C.; Roberts Jr., C. E.; Stewart, D. W. U.S. Patent 6,732,507, 2004, to Southwest Research Institute, U.S.A.
(433) Xu, L.; McCabe, R.; Ruona, W.; Cavataio, G. *SAE Tech. Pap.* **2009**No. 2009-01-0285.
(434) Weibel, M.; Waldbusser, N.; Wunsch, R.; Chatterjee, D.; Bandl-Konrad, B.; Krutzsch, B. *Top. Catal.* **2009**, *52*, 1702.
(435) Gandhi, H. S.; Cavataio, J. V.; Hammerle, R. H.; Cheng, Y. U. S. Patent US2004/0076565, 2004, to Ford Co, U.S.A.
(436) Snow, R.; Cavataio, G.; Dobson, D.; Montreuil, C.; Hammerle, R. *SAE* **2007**No. 2007-01-1244.
(437) Lambert, C. K.; Hammerle, R. H.; McGill, R. N.; Khair, M. K. *SAE* **2004**No. 2004-01-1292.
(438) Bonzi, R.; Lietti, L.; Castoldi, L.; Forzatti, P. *Catal. Today* **2010**, *151*, 376.
(439) Betta, R. D.; Cizeron, J. U.S. Patent 20040050037, 2004.
(440) Yan, J. U.S. Patent 20080196397, 2008, to Eaton Co., U.S.A.
(441) Theis, J.; Gulari, E. *SAE Tech. Pap.* **2006**No. 2006-01-0210.
(442) Theis, J.; Gulari, E. *Appl. Catal., B* **2007**, *74*, 40.
(443) Koci, P.; Plata, F.; Stepanek, J.; Kubicek, M.; Marek, M. *Catal. Today* **2008**, *137*, 253.
(444) Guttridge, D. L.; Li, J.; Hurley, R. G.; Kudla, R. J.; Watkins, W. L. H. U.S. Patent 2003129124, 2003, to Ford Global Techn. Inc., U.S.A.
(445) Guttridge, D. L.; Li, J.; Chattha, M. S.; Kudla, R. J.; Watkins, W. L. H. EP Patent 1,304,156, 2003, to Ford Global Techn. Inc., U.S.A.
(446) Centi, G.; Perathoner, S. *Catal. Today* **2006**, *112*, 174.
(447) Palomares, A. E.; Uzcategui, A.; Corma, A. *Catal. Today* **2008**, *137*, 261.
(448) Park, S. J.; Ahn, H. A.; Heo, I. J.; Nam, I.-S.; Lee, J. H.; Youn, Y. K.; Kim, H. J. *Top. Catal.* **2010**, *53*, 57.
(449) Palomares, A. E.; Lopez-Nieto, J. M.; Lazaro, F. J.; Lopez, A.; Corma, A. *Appl. Catal., B* **1999**, *20*, 257.

(450) Fornasari, G.; Trifiro, F.; Vaccari, A.; Prinetto, F.; Ghiotti, G.; Centi, G. *Catal. Today* **2002**, *75*, 421.
(451) Centi, G.; Fornasari, G.; Gobbi, C.; Livi, M.; Trifiro, F.; Vaccari, A. *Catal. Today* **2002**, *73*, 287.
(452) Li, J.; Theis, J.; Chun, W.; Goralski, C.; Kudla, R.; Ura, J.; Watkins, W.; Chattha, M.; Hurley, R. *SAE Tech. Pap.* **2001**No. 2001-01-2503.
(453) Parks, J.; Huff, S.; Pihl, J.; Choi, J.-S.; West, B. *SAE* **2005**No. 2005-01-3876.
(454) Olsson, L.; Persson, H.; Fridell, E.; Skoglundh, M.; Andersson, B. *J. Phys. Chem. B* **2001**, *105*, 6895.
(455) Dawody, J.; Skoglundh, M.; Olsson, L.; Fridell, E. *J. Catal.* **2005**, *234*, 206.
(456) Dawody, J.; Skoglundh, M.; Olsson, L.; Fridell, E. *Appl. Catal., B* **2007**, *70*, 179.
(457) Taga, J.; Yokota, K.; Kuji, Y. Jpn Patent 6672052, 2004, to Mazda Motor Co., Jpn.
(458) Yonekura, T.; Wachi, S.; Katashiba, H.; Ohuchi, H. U.S. Patent 6,345,498, 2002, to Mitsubishi Denki Kabushiki Kaisha, Jpn.
(459) Hirano, T.; Sato, Y.; Nomoto, K. U.S. Pat. 7,634,906, 2009, to Bosch Co., Jpn.
(460) Rohr, F.; Gobel, U.; Kattwinkel, P.; Kreuzer, T.; Muller, W.; Philipp, S.; Gelin, P. *Appl. Catal., B* **2007**, *70*, 189.
(461) Centi, G.; Perathoner, S. *Appl. Catal., B* **2007**, *70*, 172.
(462) Gao, A.; Zhu, X.; Wang, H.; Tu, J.; Lin, P.; Torimoto, Y.; Sadakata, M.; Li, Q. *J. Phys. Chem. B* **2006**, *110*, 11854.
(463) Li, X. G.; Meng, M.; Lin, P. Y.; Fu, Y. L.; Hu, T.; Xie, Y. N.; Zhang, J. *Chem. Eng. Res. Des.* **2002**, *80*, 190.
(464) Li, X. G.; Meng, M.; Lin, P. Y.; Fu, Y. L.; Hu, T.; Xie, Y. N.; Zhang, J. J. *Top. Catal.* **2003**, *22*, 111.
(465) Machida, M. *Catal. Surv. Jpn.* **2002**, *5*, 91.
(466) Takahashi, N.; Yamazaki, K.; Sobukawa, H.; Shinjoh, H. *Appl. Catal., B* **2007**, *70*, 198.
(467) Gomez-Garcıa, M. A.; Pitchon, V.; Kiennemann, A. *Appl. Catal., B* **2007**, *70*, 151.
(468) Yang, R. T.; Chen, N. U.S. Patent 5,456,892, 1995.
(469) Hodjati, S.; Petit, C.; Pitchon, V.; Kiennemann, A. *J. Catal.* **2001**, *197*, 324.
(470) Hodjati, S.; Vaezzadeh, K.; Petit, C.; Pitchon, V.; Kiennemann, A. *Top. Catal.* **2001**, *16*−*17*, 151.
(471) Kaupert, A.; Strauhs, J.; Wiesheu, N. U.S. Patent 6,810,658, 2004, to DaimlerChrysler Ag, DE.
(472) Oshima, Y.; Muraki, H.; Yokota, K.; Nakanishi, K. EP 0,537,968, 1996, to Toyota Jidosha K.K, Jpn.
(473) Lueders, H. EP 0 621 400, 2006, to Robert Bosch GmbH, DE.
(474) Law, H. Y.; Kung, M. C.; Kung, H. H. *Ind. Eng. Chem. Res.* **2007**, *46*, 5936.
(475) Law, H.-Y.; Kung, M. C.; Kung, H. H. *Catal. Today* **2008**, *136*, 40.
(476) Ueda, A.; Takayuki, N.; Masashi, A.; Kobayashi, T. *Catal. Today* **1998**, *45*, 135.
(477) Pieterse, J. A. Z.; Booneveld, S. *Appl. Catal., B* **2007**, *73*, 350.
(478) Jones, J. H.; Kummer, J. T.; Otto, K.; Shelef, M.; Weaver, E. E. *Environ. Sci. Technol.* **1971**, *9*, 791.
(479) Burch, R.; Millington, P. J.; Walker, A. P. *Appl. Catal., B* **1994**, *4*, 65.
(480) Heeba, N. V.; Saxer, C. J.; Forss, A.-M.; Bruhlmann, S. *Atmos. Environ.* **2006**, *40*, 3750.
(481) Frank, E.; Oguz, H.; Weisweiler, W. *Chem. Eng. Technol.* **2003**, *6*, 679.
(482) Frank, B.; Lubke, R.; Emig, G.; Renken, A. *Chem. Eng. Technol.* **1998**, *6*, 498.
(483) Macleod, N.; Lambert, R. M. *Appl. Catal., B* **2002**, *35*, 269.
(484) Macleod, N.; Lambert, R. M. *Appl. Catal., B* **2003**, *46*, 483.
(485) Costa, C. N.; Efstathiou, A. M. *Appl. Catal., B* **2007**, *72*, 240.
(486) Costa, C. N.; Savva, P. G.; Fierro, J. L. G.; Efstathiou, A. M. *Appl. Catal., B* **2007**, *75*, 147.
(487) Engelmann-Pirez, M.; Granger, P.; Leclercq, G. *Catal. Today* **2005**, *107*, 315.
(488) Nazimek, D.; Cwikla-Bundyra, W. *Catal. Today* **2004**, *90*, 39.
(489) Marques, R.; Mazri, L.; Da Costa, S.; Delacroix, F.; Djega-Mariadassou, G.; Da Costa, P. *Catal. Today* **2008**, *137*, 179.
(490) Marques, R.; Mazri, L.; Da Costa, S.; Delacroix, F.; Djega-Mariadassou, G.; Da Costa, P. *Catal. Today* **2008**, *137*, 185.
(491) Pieterse, J. A. Z.; Top, H.; Vollink, F.; Hoving, K.; W. van den Brink, R. *Chem. Eng. J.* **2006**, *120*, 17.
(492) Savva, P. G.; Efstathiou, A. M. *J. Catal.* **2008**, *257*, 324.
(493) Costa, C. N.; Stathopoulos, V. N.; Belessi, V. C.; Efstathiou, A. M. *J. Catal.* **2001**, *197*, 350.
(494) Costa, C. N.; Savva, P. G.; Andronikou, C.; Lambrou, P. S.; Polychronopoulou, K.; Belessi, V. C.; Stathopoulos, V. N.; Pomonis, P. J.; Efstathiou, A. M. *J. Catal.* **2002**, *209*, 456.
(495) Costa, C. N.; Efstathiou, A. M. *J. Phys. Chem. C* **2007**, *111*, 3010.
(496) Costa, C. N.; Savva, P. G.; Fierro, J. L.; Efstathiou, A. M. *Appl. Catal., B* **2007**, *75*, 147.
(497) Chiarello, G. L.; Ferri, D.; Grunwaldt, J.-D.; Forni, L.; Baiker, A. *J. Catal.* **2007**, *252*, 137.
(498) Schott, F. J. P.; Balle, P.; Adler, J.; Kureti, S. *Appl. Catal., B* **2009**, *87*, 18.
(499) Newton, M. A.; Dent, A. J.; Diaz-Moreno, S.; Fiddy, S. G.; Evans, J. *Angew. Chem., Int. Ed.* **2002**, *41*, 2587.
(500) Szailer, T.; Kwak, J.; Kim, D.; Hanson, J.; Peden, C.; Szanyi, J. *J. Catal.* **2006**, *239*, 51.
(501) Kouakou, A.; Dhainaut, F.; Granger, P.; Fresnet, F.; Louis-Rose, I. *Top. Catal.* **2009**, *52*, 1734.
(502) Stathopoulos, V. N.; Belessi, V. C.; Bakas, T. V.; Neophytides, S. G.; Costa, C. N.; Pomonis, P. J.; Efstathiou, A. M. *Appl. Catal., B* **2009**, *93*, 1.
(503) Mondragon Rodriguez, G. C.; Saruhan, B. *Appl. Catal., B* **2010**, *93*, 304.
(504) Williams, A.; Ratcliff, M.; Pedersen, D.; McCormick, R.; Cavataio, G.; Ura, J. *SAE Tech. Pap.* **2009**No. 2009-01-2777.
(505) Arve, K.; Eranen, K.; Snare, M.; Klingstedt, F.; Murzin, D. Y. *Top. Catal.* **2007**, *42*−*43*, 399.
(506) Theinnoi, K.; Tsolakis, A.; Houel, V.; Rajaram, R. *SAE Pap.* **2007**No. 2007-01-1917.
(507) Theinnoi, K.; Tsolakis, A.; Sitshebo, S.; Houel, V.; Rajaram, R. R. *Energy Fuels* **2008**, *22*, 4109.
(508) Theinnoi, K.; Tsolakis, A.; Sitshebo, S.; Cracknell, R. F.; Clark, R. H. *Chem. Eng. J.* **2010**in press.
(509) Sitshebo, S.; Tsolakisa, A.; Theinnoi, K.; Rodríguez-Fernández, J.; Leung, P. *Chem. Eng. J.* **2010**in press.
(510) Xiaoyan, S.; Yunbo, Y.; Hong, H.; Shijin, S.; Hongyi, D.; Rulong, L. *J. Environ. Sci.* **2008**, *20*, 177.
(511) Tham, Y. F.; Chen, J.-Y.; Dibble, R. W. *Proc. Combust. Inst.* **2009**, *32*, 2827.
(512) Cavataio, G.; Jen, H.-W.; Dobson, D. A.; Warner, J. R. *SAE Tech. Pap.* 2009No. 2009-01-2823.
(513) Jaaskelainen, H. Biodiesel Standards & Properties, www.dieselnet.com/tech/fuel_biodiesel_std.html.
(514) Dou, D.; Balland, J. *SAE Pap.* **2002**No. 2002-01-0734.
(515) Kling, A.; Andersson, C.; Myringer, A.; Eskilsson, D.; Jaras, S. G. *Appl. Catal., B* **2007**, *69*, 240.
(516) Zheng, Y.; Jensen, A. D.; Johnsson, J. E.; Thogersen, J. R. *Appl. Catal., B* **2008**, *83*, 186.
(517) Zheng, Y.; Jensen, A. D.; Johnsson, J. E. *Appl. Catal., B* **2005**, *60*, 253.
(518) Szybist, J. P.; Kirby, S. R.; Boehman, A. L. *Energy Fuels* **2005**, *19*, 1484.
(519) Li, X.; Huang, Z.; Wang, J.; Zhang, W. *Sci. Total Environ.* **2007**, *382*, 295.
(520) Rodriguez-Fernandez, J.; Tsolakis, A.; Cracknell, R. F.; Clark, R. H. *Int. J. Hydrogen Energy* **2009**, *34*, 2789.
(521) Faiz, A.; Weaver, C. S.; Walsh, M. P. *Air Pollution from Motor Vehicles - Standards and Technologies for Controlling Emissions*; World Bank: Washington, D.C., 1996.

(522) Kato, K.; Inoue, T.; Nohira, H.; Nakanishi, K.; Iguchi, S.; Kihara, T.; Muraki, H. Jpn Pat. 5746989, 1991, to Toyota Jidosha Kabushiki Kaisha, Jpn.
(523) Pischinger, S.; Schon, C.; Weibel, M.; Krutzsch, B.; Pfaff, R.; Boegner, W. U.S. Patent 5,771,686, 1995, to Mercedes-Benz AG, DE.
(524) Katare, S. R.; Patterson, J. E.; Laing, P. M. *Ind. Eng. Chem. Res.* **2007**, *46*, 2445.
(525) Cavataio, G.; Jen, H.-W.; Warner, J. R.; Girard, J. W.; Kim, J. Y.; Lambert, C. K. *SAE Int. J. Fuels Lubr.* **2009**, *1*, 477.
(526) Cavataio, G.; Jen, H.-W.; Warner, J. R.; Girard, J. W.; Kim, J. Y.; Lambert, C. K. *SAE Tech. Pap.* **2008**, *SP-2154*, 451.
(527) Cavataio, G.; Girard, J.; Patterson, J. E.; Montreuil, C.; Cheng, Y.; Lambert, C. K. *SAE Tech. Pap.* **2007**, *SP-2080*, 455.
(528) Cheng, Y.; Xu, L.; Hangas, J.; Jagner, M.; Lambert, C. *SAE Tech. Pap.* **2007**, *SP-2080*, 499.
(529) Ura, J. A.; Girard, J.; Cavataio, G.; Montreuil, C.; Lambert, C. *SAE Tech. Pap.* **2009**, *2254*, 223.
(530) Johnson, T. V. *SAE Tech. Pap.* **2009**, *SP-2254*, 1.
(531) Joo, K.; Jo, J.-H.; Kim, C. D.; Lee, J.-h.; Kim, H.-j. *SAE Tech. Pap.* **2008**, *SP-2154*, 507.
(532) Sluder, C. S.; Storey, J. M. E.; Lewis, S. A.; Lewis, L. A. *SAE Tech. Pap.* **2005**, *SP-1942*, 373.
(533) Watanabe, M.; Yoshida, S.; Sawaki, T.; Hashimoto, S.; Miyamoto, T. *J. Soc. Automot. Eng. Jpn.* **2006**, *60*, 40.
(534) Levin, M. B.; Baker, R. E. *SAE Tech. Pap.* **2002**, *SP-1674*, 35.
(535) Lambert, C.; Hammerle, R.; McGill, R.; Khair, M.; Sharp, C. *SAE Tech. Pap.* **2004**, *SP-1860*, 357.
(536) Lambert, C.; Hammerle, R.; McGill, R.; Khair, M.; Sharp, C. *SAE Tech. Pap.* **2004**, *SP-1835*, 672.
(537) Twigg, M. V.; Wishart, I. C. UK Patent GB 2458994, 2009, to Johnson Matthey Public Limited Company.
(538) Tatur, M.; Nanjundaswamy, H.; Tomazic, D.; Thornton, M. *SAE Int. J. Fuels Lubr.* **2009**, *1*, 119.
(539) Tatur, M.; Nanjundaswamy, H.; Tomazic, D.; Thornton, M. *SAE Tech. Pap.* **2008**, *SP-2169*, 71.
(540) Tatur, M.; Nanjundaswamy, H.; Tomazic, D.; Thornton, M.; McCormick, R. L. *SAE Tech. Pap.* **2009**, *SP-2254*, 67.
(541) Kim, C. H.; Qi, G.; Dahlberg, K.; Li, W. *Science* **2010**, *327*, 1624.
(542) Mathisen, K.; Stockenhuber, M.; Nicholson, D. G. *Phys. Chem. Chem. Phys.* **2009**, *11*, 5476.